FACULTY OF SCIENCE

Charles University

DOCTORAL THESIS

Mgr. Vladimir Sincari

Self-assembled polymer systems responsive to external stimuli for biomedicine

Samouspořádané polymerní systémy citlivé na vnější podněty pro biomedicínu

Supervisor of the doctoral thesis: RNDr. Petr Štěpánek, DrSc.

Study program: Macromolecular Chemistry

Department of Physical and Macromolecular Chemistry

Prague
2022

Acknowledgment

Dedicated to my grandmother.

I would like to give my sincere and deepest gratitude to RNDr. Petr Štěpánek, DrSc for the all invaluable support and for the great opportunity and honor to work under his guidance.

Also, I would like to thank Mgr. Martin Hrubý, Ph.D., DSc for his advices, motivation and possibility to work in international projects, and as well for his kindness and vision of science.

My special thanks to Jäger brothers. I'm very grateful to Dr. Eliézer Jäger for his patience, delicacy, attitude and for the ability to grow in professional way under his supervision. Thanks for all help, fruitful discussion and great time during experiments and outside of work. I would like to thank Dr. Alessandro Jäger for his nerves of steel during my training in fields of self-assembly and microfluidics. As well as for his intelligence, insights, enthusiasm and deep understanding of science and for making pleasant environment to achieve the set goals.

I am grateful to my colleagues from IMC, especially Dr. Peter Černoch for his help, advices and kind conversations. Mrs. Martina Hlavničková for help in understanding of Czech life, multiple discussions, eco products and hearty cheerfulness. Dr. Rafal Konefał for decoding of NMR samples, and his positivity. Dr. Lukáš Petrova Svetlana for her enthusiasm and great synthesis skills. Dr. Lindomar Albuquerque, as a good friend and master of order, my very big thanks, in Vietnamese restaurant orders still are going wrong.

And especially big thanks to my family and wife, that support me in everything.

Contents

List of abbreviations

^{1}H NMR	proton nuclear magnetic resonance
AIBN	2,2'-azobis(2-methylpropionitrile)
ATRP	atom transfer radical polymerization
bocAPMA	*N*-(3-Boc-aminopropyl)methacrylamide
BSA-FITC	albumin from bovine serum conjugated with fluorescein
CK	creatine kinase
CLRP	controlled/"living" radical polymerization
CMC	critical micelle concentration
cryo-TEM	cryogenic electron microscopy
CTA	chain transfer agent
CVD	cardiovascular disease
DADMAC	diallyldimethylammonium chloride
DBCO	dibenzocyclooctyne
DDS	drug delivery systems
DLS	dynamic light scattering
DNA	deoxyribonucleic acid
DOX	doxorubicin

DPA	2-(diisopropylamino)ethyl methacrylate
EE	encapsulation efficiency
EMA	European medicines agency
EPR	enhanced permeability and retention
FDA	food and drug administration
FRET	Forster resonance energy transfer
FTIR	Fourier-transform infrared spectroscopy
HEI	high-energy intermediates
HPMA	*N*-(2-hydroxypropyl) methacrylamide
IF	inner flow
LC	loading content
LDH	lactate dehydrogenase
MABH	*N′*-methacryloyl *tert*-butyl carbazate
mAbs	monoclonal antibodies
MALS	multiangle light scattering
mCTA	macro-chain transfer agent
MDR	multiple drug resistance
MF	middle flow
MOF	metal-organic framework
MPS	mononuclear phagocytic system
MWI	microwave irradiation
NC	nanocarrier
NP	nanoparticle
NSCLC	non-small cell lung cancer
PBS	phosphate-buffered saline
PCL	polycaprolactone
PDC	polymer-drug conjugate
PDEA	poly[(2-diethylamino)ethyl methacrylate]

PDI	polydispersity index
PDMS	polydimethylsiloxane
PDPA	poly(2-(diisopropylamino)ethyl methacrylate)
PEG	polyethylene glycol
PLA	polylactic acid
PLGA	poly(lactic-*co*-glycolic acid)
PMeOx	poly(2-methyl-2-oxazoline)
POXs	polyoxalates
PPO	polypropylene oxide
PR	photoresist
PS	polymersome
PTX	paclitaxel
PVA	poly(vinyl alcohol)
PVP	polyvinylpyrrolidone
RAFT	reversible addition−fragmentation chain-transfer
RI	refractive index
rMSCs	rat mesenchymal stem cells
RNA	ribonucleic acid
RNS	reactive nitrogen species
ROMP	ring-opening metathesis polymerization
ROS	reactive oxygen species
Rp	polymerization rate
RRMM	relapsed/refractory multiple myeloma
RT	room temperature
SANS	small-angle neutron scattering
SAXS	small-angle X-ray scattering
SEC	size-exclusion chromatography
siRNA	small interfering RNA

SLS	static light scattering
STEM	scanning TEM
TEM	transmission electron microscopy
TEOS	tetraethyl orthosilicate
TME	tumor microenvironment
UAc	uranyl acetate
W/O/W	water-in-oil-in-water

Abstract

The first work[1] in my doctoral thesis described a novel rapid and eco-friendly reversible addition-fragmentation chain transfer (RAFT) polymerization reaction of the *N*-(2-hydroxypropyl) methacrylamide (HPMA) monomer under microwave irradiation (MWI). Optimal conditions for the polymerization such as reaction time, solvents, monomer stoichiometry and RAFT agents was determined. The polymerization kinetics demonstrated the linear increase in the number-average molecular weight (*Mn*) with monomer conversion. Good agreement between the theoretical and experimental *Mn* values was verified with pseudo-first-order kinetic plots, with low dispersities ($Đ \leq 1.04$). Furthermore, this publication demonstrated the ability of MWI to facilitate copolymer formation by the preparation of relevant copolymers, such as poly(HPMA-*b*-bocAPMA), poly(HPMA-*b*-MABH) and poly(HPMA-*b*-PDPA) which were used as a base for the following work in the thesis.

The second[2,3] and third[4] study are devoted to delivery of therapeutic molecules by using cargo-delivery self-assemblies in the form of polymersomes (PS). Such drug delivery systems (DDS) potentially minimize the premature degradation of drug, fast clearance from bloodstream and dosing frequency which leads to lower toxicity. The main advantage of DDS is the controlled manner of drug release at a specific site via active or passive targeting strategies. Passive targeting is a preferential accumulation of nanocarriers (NCs) in tumor tissue based on pathophysiological features (*i.e.*, leaky tumor vasculature and poor lymphatic drainage) of the growing solid tumor. For passive targeting, suitable particles size (from 10-100nm), surface charge and surface modification can promote effective extravasation as well as reduced liver capture and renal clearance. Active targeting refers to ligands' affiliation to receptors or with physicochemical engineering of structure for recognition by specific antigen/receptor of targeting cell. More novel stimuli-responsive programmed specific targeting in combination with previously mentioned strategies could achieve higher accumulation in tumor and enhance cellular internalization.

Stimuli-responsive drug-loaded polymersomes can respond to the inherent features of tumor microenvironments (TME), such as extracellular acidosis or higher levels of reactive oxygen species (ROS) in tumor sites. In this thesis novel TME-responsive amphiphilic block copolymers

(BCs) based on HPMA were synthesized by a reversible addition-fragmentation chain transfer (RAFT) polymerization and characterized by standard techniques (^{1}H NMR and SEC). Hydrodynamic flow-focusing nanoprecipitation microfluidics (MF) was used in the preparation of well-defined ROS or pH-responsive PSs. The obtained PSs with desired size (hydrodynamic diameter - D_H ~ 100 nm) were evidenced by dynamic light scattering (DLS), static light scattering (SLS), transmission electron microscopy (TEM), and cryogenic electron microscopy (cryo-TEM). PSs loaded with doxorubicin (DOX) were evaluated by the cellular uptake and cytotoxicity in EL4 lymphoma cancer cells. The *in vivo* biodistribution studies were performed in nude mice using covalently attached fluorescent dye (DBCO-Cyanine7) to the polymersomes by copper-free, strain promoted alkyne azide cycloaddition "click chemistry". The obtained results demonstrated PSs circulation for a longer time (~ 144h). and accumulation to a greater extent compared to the free fluorescent probe. *In vivo* antitumor efficacy was analyzed in mice bearing EL4 lymphoma tumor. The results evidenced enhanced suppression of tumor cell growth and extended survival rate compared to the administration of free DOX. Side-effects characteristic of therapeutic treatments based on DOX, such as hair loss and cardiotoxicity, were remarkably reduced.

The final part of the thesis reports about giant stimuli-responsive PS. Polydimethylsiloxane (PDMS) microfluidic device casted with sol-gel process with a coating rendered hydrophilic on selected junction channels was used for preparation of giant non-responsive and stimuli-responsive PS by w/o/w double emulsion method. The pH-responsive behavior was studied in detail by confocal microscopy and the results demonstrated the spatial and temporal pH-controlled PS disruption under simulated relevant physiological conditions. Cytotoxicity studies demonstrated excellent biocompatibility of produced PS. The giant PS could find application in pH-responsive drug and gene delivery, microreactors and as a model of artificial cell studies.

Keywords: polymersomes, self-assembly, ROS, drug delivery, stimuli-responsive, microfluidics, DOX.

List of publications and contributions at conferences

Publications included into this thesis:

Sincari, V.; Lukáš Petrova, S.; Konefał, R.; Hruby, M.; Jäger, E. Microwave-assisted RAFT polymerization of *N*-(2-hydroxypropyl) methacrylamide and its relevant copolymers. Reactive and Functional Polymers **2021,** 162, 104875.
https://doi.org/10.1021/acs.biomac.9b01748. [1]

Sincari, V.; Jäger, E.; Cavalcante, K.; Vragovic, M.; Hofmann, E.; Shlenk, M.; Štěpánek, P.; Hrubý, M.; Förster, S.; and Jäger, A. pH-dependent disruption of giant polymer vesicles: A step towards biomimetic membranes.

RSC Chemical Science **2022,** manuscript under review.

Albuquerque, L. J. C.; **Sincari, V.**; Jäger, A.; Konefał, R.; Pánek, J.; Černoch, P.; Pavlova, E.; Štěpánek, P.; Giacomelli, F. C.; Jäger, E. Microfluidic-Assisted

Engineering of quasi-monodisperse pH-responsive polymersomes toward advanced platforms for the intracellular delivery of hydrophilic therapeutics. *Langmuir* **2019**, 35, 8363–8272. https://doi.org/10.1021/acs.langmuir.9b01009. [2]

Albuquerque, L. J. C.; **Sincari, V**.; Jäger, A.; Kucka, J.; Humajova, J.; Pankrac, J.; Paral, P.; Heizer, T.; Janouškova, O.; Davidovich, I.; Talmon, Y.; Pouckova, P.; Štěpánek, P.; Šefc, L.; Hruby, M.; Giacomelli, F. C.; Jäger, E. pH-responsive polymersome-mediated delivery of doxorubicin into tumor sites enhances the therapeutic efficacy and reduces cardiotoxic effects. *Journal of Controlled Release,* **2021,** 332, 529-538. https://doi.org/10.1016/j.jconrel.2021.03.013. [3]

Jäger, E.; **Sincari, V**.; Albuquerque, L. J. C.; Jäger, A.; Humajova, J.; Kucka, J.; Pankrac, J.; Paral, P.; Heizer, T.; Janouskova, Konefał R.; Pavlova, E.; Sedlacek, O.; Giacomelli, F.C.; Pouckova, P.; Sefc, L.; Stepanek, P.; Hruby. M. Reactive oxygen species (ROS)-responsive polymersomes with site-specific chemotherapeutic delivery into tumors via spacer design chemistry. *Biomacromolecules* **2020**, 21 (4), 1437–1449. https://doi.org/10.1021/acs.biomac.9b01748. [4]

Publications not included into this thesis

Černoch, P.; Jäger, A.; Černochová, Z.; **Sincari, V**.; Albuquerque, L. J. C.; Konefał, R.; Pavlova, E.; Giacomelli, F. C.; Jäger, E. Engineering of pH-triggered nanoplatforms based on novel poly(2-methyl-2-oxazoline)-*b*-poly[2-(diisopropylamino)ethyl methacrylate] diblock copolymers with tunable morphologies for biomedical applications. *Polymer Chemistry*, **2021,** 19. https://doi.org/10.1039/D1PY00141H

Pandya, A. D.; Jäger, E.; Bagheri Fam, S.; Höcherl, A.; Jäger, A.; **Sincari, V.**; Nyström, B.; Štěpánek, P.; Skotland, T.; Sandvig, K.; Hrubý, M.; Mælandsmo, G. M. Paclitaxel-loaded biodegradable ROS-sensitive nanoparticles for cancer therapy. *International journal of nanomedicine*, **2019,** 14, 6269–6285. https://doi.org/10.2147/IJN.S208938

Operti, M.C.; Bernhardt, A.; **Sincari, V.;** Jager, E.; Grimm, S.; Engel, A.; Hruby, M.; Figdor, C.G.; Tagit, O. Industrial Scale Manufacturing and Downstream Processing of PLGA-Based Nanomedicines Suitable for Fully Continuous Operation. *Pharmaceutics* **2022**, *14*, 276. https://doi.org/10.3390/pharmaceutics14020276

Operti, M.C.; Bernhardt, A.; Pots, J.; **Sincari, V.;** Jager, E.; Grimm, S.; Engel, A.; Benedikt, A.; Hrubý, M.; De Vries, I.J.M.; Figdor, C.G.; Tagit, O. Translating the Manufacture of Immunotherapeutic PLGA Nanoparticles from Lab to Industrial Scale: Process Transfer and In Vitro Testing. *Pharmaceutics* **2022**, *14*, 1690. https://doi.org/10.3390/pharmaceutics14081690

1. Introduction

1.1 Smart cancer nanomedicine

Nowadays, cancer is one of the leading causes of deaths worldwide [5], with increase of new cases up to 70% for next 20 years. Nanomedicine is a rapidly developing emerging field in cancer treatment. Contrary to conventional treatment such as chemotherapy, surgery or radiation, which affects not just the tumor tissue but also healthy tissues, with other collateral damage to human organism, nanomedicine promises to improve the abovementioned disadvantages. In the field of nanomedicine, multidisciplinary science combines the knowledge for development of novel biomedical technologies that are more effective in treating cancer. Effectiveness could be achieved through solving the current issues that include rapid drug liver/renal clearance, ineffective response and limited targeting. Multidrug resistance (MDR) [6] is another major obstacle that reduces the efficacy of cancer treatment which can be reversed by nanomedicine.

The specifically engineered particle "nanocarriers" with size from 10 to 100 nm, high surface-to-volume ratios, more homogeneous biodistribution and coupled with targeting modifications may lead to better targeting to tumor tissue. Submicron size of nanocarriers could also provide accumulation in tumor trough leaky vasculature, with longer intratumoral retention and better biodistribution. In addition, the ability to release loaded drug from nanocarriers in a controlled manner should sufficiently reduce the toxicity to healthy tissue. The drug release could be triggered by external or internal stimuli. To the external stimuli we attribute the temperature change due to heating, light, electric field, ultrasound or magnetic field exposure [7]. While, Internal stimuli may include temperature change, the presence of enzymes, pH changes and concentration of ROS, which are significantly different in diseased tissues, for example in tumor microenvironment [8]. Various materials can be used for preparation of nanotherapeutic platforms based on lipids, polymers, viruses or drug-conjugates, the most common systems are represented in Figure 1. Some of such platforms are already approved by the United States Food and Drug Administration Agency (FDA) or the European Medicines Agency (EMA) and used in clinical medicine.

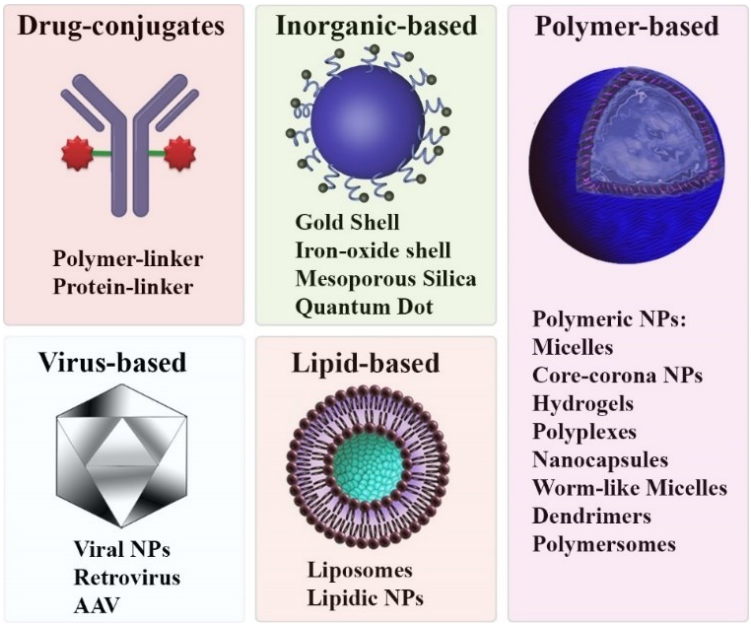

Figure 1. Schematic representation of conventional nanotherapeutic platforms.

For instance, superparamagnetic iron oxide nanoparticles are a common class of market - authorized metallic nanomaterials with applications in DDS, diagnostics, imaging and photothermal therapies. Other examples of inorganic nanoparticles based one silver, gold and silica, could be engineered with various sizes, geometry and structures like nanospheres, nanorods, nanoclusters, nanodiscs and nanoshells. Moreover, the nature of such materials provides special physical, magnetic, and opto-electrical properties. However, inorganic NPs still remain a challenging issue, since they have unfavorable accumulation in human body, low solubility and toxicity caused by chemical composition.

Another successful example of nanomedicine is soft matter, which differs from inorganic NPs by its “softness” that gives alternative drug loading/release mechanisms.
Furthermore, soft matter offers a range of advantages including improved pharmacokinetic and pharmacodynamic profiles of biopharmaceuticals, protection of drug from different types of degradation, and biodegradability. Typical representatives of soft matter are lipids and polymers. Due to the natural origin and ability to self-assemble lipids are desirable materials for use in nanotechnology medicine. Lipids can undergo self-assembly into various nano-objects: films, micelles, reverse micelles and liposomes. Naturally, lipids are biocompatible and amphiphilic, thus a cargo could be loaded in the hydrophobic biomembrane or in the aqueous core.
Liposomes nanomedicine (usually phospholipids) are approved by FDA and EMA.
One of the most commercially successful liposomal anticancer formulation - Doxyl®/Caelyx® (the first approved liposomal product by FDA in the US) was a pioneer in cancer nanomedicine treatment. Doxyl® (nanosized liposomal Doxorubicin) demonstrates extended circulation in blood with higher uptake by tumor, and reasonably reduced cardiotoxicity. Even though, lipid nanoparticles still have drawbacks like low drug loading, chemical instability, and fast clearance (by liver or spleen uptake).

Polymeric nanomaterials are another class in soft matter that was intensively studied in last decades, due to their ability to encapsulate without chemical interaction almost all types of compounds like drugs, proteins, contrast agents and antibodies, for biomedical uses. The other main characteristics of polymers is their versatility and adjustable functionality, that could provide better stability, controlled drug release, and more specific targeting into tumor sites.

Polymer-drug conjugates (PDCs) are a current group of polymeric nanomedicines that successfully translated to clinical practice. Block copolymer nanoparticles are next highly perspective candidate for clinical approval. Their unique feature is the aforementioned response to external and internal stimuli. The formation of polymeric vesicles – polymersomes is the main area of research in this thesis.

Despite the exponential growing impact that nanomedicine brought to cancer treatment, only few products went to the authorized market. Nanoparticle science requires deeper understanding of processes concerning vehicle/physiological barriers, interactions with liver, spleen and kidneys, tumor uptakes by specific targeting, and other long-term consequences. These limitations will be discussed below.

1.1.2 Biological and physical barriers

For effective cancer treatment nanotherapeutics must overcome various bio-physical barriers (Figure 2).

The first significant biological barrier driven by mononuclear phagocytic system (MPS) is phagocytic capture by macrophages of the NPs – the opsonization process. Since, nanocarriers are intravenously injected, they start to interact with thousands of biomolecules, in particular lipids, proteins and nucleic acids. These interactions may lead to protein corona effect, triggered by electrostatic contact between charge on nanocarrier and opposite charge of serum protein. In protein corona state, NPs lose their targeting properties, and after marking them with opsonins (the protein for phagocytic recognition that is present in blood serum), NPs undergo rapid clearance within seconds by phagocytic cells (Kupffer cells and hepatocytes) typically from liver, lymph nodes or spleen. To minimize protein absorption on the surface of nanoparticles these may be coated with highly hydrophilic *N*-(2-hydroxypropyl)methacrylamide (HPMA) polymer, that forms a hydration layer with antifouling properties[9] [10].

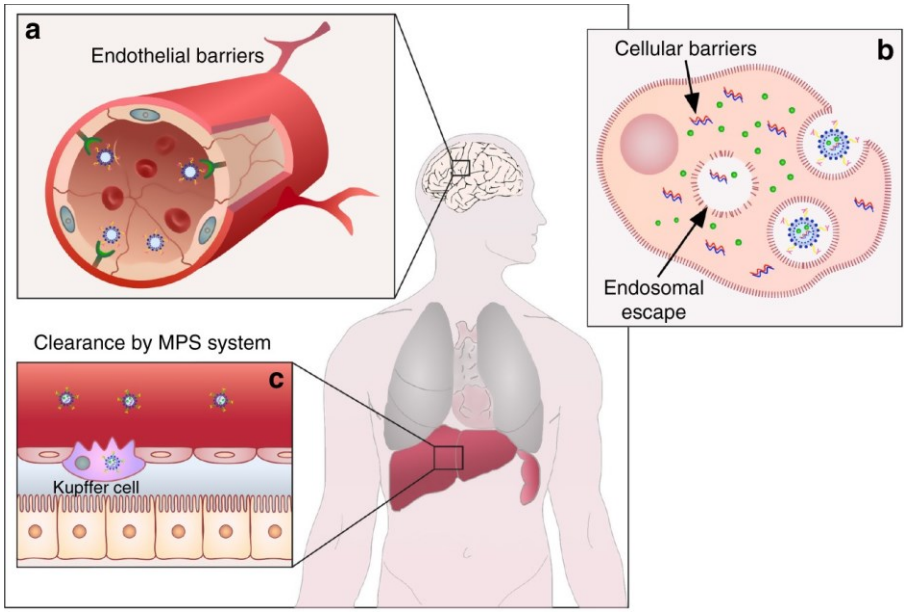

Figure 2. Schematic representation of main physiological barriers faced by passively and actively targeted NCs. **a** in the process of extravasation into tumor tissue, NCs encounter endothelial barriers; the blood–brain barrier is an example. **b** the major cellular barrier is the uptake of NCs by the target cells and their escape from the endo-lysosomal system into the cytosol. **c** clearance of systematically administered NPs by Kupffer cells as an example of mononuclear phagocytic system (MPS) [11].

The next barrier is tumor vasculature, in cancer sites the accelerated development of tumor cells generates new blood vessels for transportation of oxygen, sugar and other nutrients. Abnormal and irregularly developed blood vessels form gaps between endothelial cells through which nanosized particles can pass and presumably accumulate. Also, tumor tissue has a less tight lymphatic drainage than healthy tissue, so the fluid dynamics is different. The combination of "leaky" vasculature and less efficient lymphatic drainage permit the permeation and retention of nanoparticles within tumor sites, the so-called EPR effect firstly described by Maeda and colleagues. [12]

To overcome the tumor vascular barrier and improve NPs accumulation various strategies can be utilized. For enhancing tumor permeability physical action of ultrasound or hyperthermia might allow increased local vascular permeability. Another strategy is to use EPR enhancers, such as nitric oxide donors which work as vasodilators that increase blood flow and open tight endothelial cells-cell junctions [13].

1.1.3 Targeting strategies

Targeted delivery is an advantageous system for drug-loaded nanocarriers that is more specifically oriented to cancer cells, thereby healthy cells are more protected from cytotoxic drugs [14]. The cell targeting could be achieved by passive, active or programmed targeting strategies.

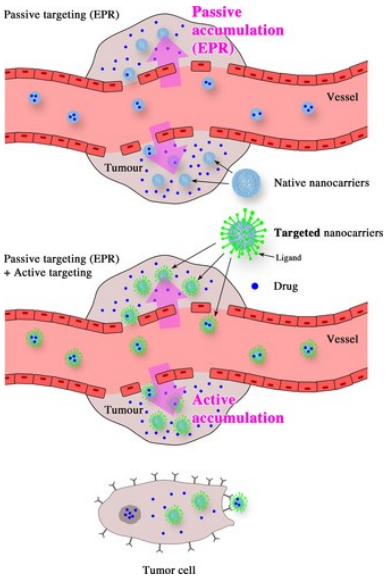

Figure 3. Scheme illustrating the passive targeting (EPR) and the active targeting into a tumor [14].

Passive targeting is the most systematically studied strategy, refers to NPs designed for diffusion into tumor cell and accumulation with enhanced permeation by the above-mentioned EPR effect. The size of particles is the key factor in passive targeting; depending on the type of tumor the fenestrations can reach a size up to 2 μm however, the common size for nanocarriers is in a range of $D_H < 100$ nm. The biodistribution studies revealing the enhanced tumor-accumulation of sub-micron particles were performed by Matsumura and Maeda, who observed a time-dependent accumulation of SMANCS, a conjugate of neocarzinostatin and ^{51}Cr -labeled poly(styrene-*co*-maleic acid) with molecular weight higher than 60kDa. Additionally, injection of labeled albumin-dye complex (69 kDa) demonstrated the retention of complex only in tumor tissue. This principle became a basis for the further development of cancer nano-therapies. Nevertheless, the EPR effect now is questioned in clinical studies, due to its moderate efficiency [15]. It could be explained by a heterogeneity of the EPR effect in humans comparing to animal models for biological experiments. In mice models' tumors growth is faster with many endothelial fenestrations, contrary to human tumors that grow slowly with moderate or even absent fenestrations. Type and size of tumor are also important factors, it is known that in large tumors blood flow is often obstructed, while small tumors are less heterogenous with more uniform EPR effect. Such knowledge contributes to development and use of EPR enhancers, for instance vascular mediators and vasodilators [16]. Recent studies of EPR effect revealed more complicated mechanisms such as vascular burst in blood vessels, or extravasation that happens by trans-endothelial pathways [17][18].

Active targeting is a complementary strategy which can work synergistically with passive targeting for improved overall tumor accumulation and prolonged retention with increased targeting efficiency. In active targeting the NPs surface is functionalized with targeting ligands, which favors cell recognition and targeting cell uptake. The ligand-mediated targeting is used for intracellular delivery of active compounds like high molecular weight proteins, RNA and DNA

that cannot cross cell membranes to reach required active site by themselves. For successful binding of nanocarrier decorated with ligands the receptors must be overexpressed on target cells. The binding affinity of nanoparticles also depends on its architecture and type of receptor-ligand binding mechanism. Other parameters such as size, shape, molecular weight, concentration and ligand density can also influence efficacy of treatment [19]. The internalization of nanoparticles is another important aspect that can be improved by specific ligands that may provide efficient endocytosis, since endosomal escape of NPs still is a very challenging task, various strategies that facilitate escape of nanoparticles in cytosol are currently investigated.

The standard principle of choosing target in active targeting is based on disease distinctive biomarkers, such as CD19 B-lymphocyte antigen (the most targeted marker), or BCMA B-cell maturation antigen (for multiple myeloma therapy) *etc* [20]. Other possibility is to use strong ligand/receptor mechanisms for targeting arduous sites. As example, transferrin ligands that bind the acetylcholine receptors allow passing of blood-brain barrier for delivery into brain tumors. Peptides are another potential model, recently it was found that arginylglycylaspartic acid (RGD) peptides bind $\alpha v\beta 3$ integrin, a receptor that is highly present in glioblastoma and in TME; F3 peptide is found to bind the nucleolin receptor which is expressed in glioma and endothelial cells, folic acid binds the folate receptor that is also presented in TME.

The most investigated ligands for surface functionalization of nanoparticles are: antibodies (monoclonal antibodies – mAbs, bispecific mAbs or antibody fragments – scFv), proteins, nucleic acids, carbohydrates, folates and aptamers [21].

1.1.4 Specific programmed targeting

Targeting properties of nanocarriers can be combined with the stimuli-responsiveness which could trigger drug release in a controlled manner at the targeted site. Such targeting stimuli-responsive nanocarriers possessing mutual properties with enhancement in bioavailability of drug and reduction of side effects are highly desirable. Stimuli-responsive nanomaterials exhibit chemical or physical changes in response to external signals; such changes include shift in macromolecular structure, swelling and dissociation, solubility, fragmentation, and changes in surface properties. The types of stimuli-responsive NCs are classified by triggers that are either physical or biological. Physical (external) stimuli are heat, light, ultrasound, magnetic or electrical fields as mentioned above.

The biological stimuli that might trigger the delivery of active or diagnostic agents are widely available in nature. The biological or endogenous stimuli are enzymes, ions, and tumor microenvironment. The last-mentioned tumor microenvironment is a promising target as the triggering factor is due to its bio-physical differences with normal homeostatic environments.

1.1.5 Tumor microenvironment targeting

Tumor microenvironment consists of a cellular part that includes tumor cells, stromal cells like fibroblast, endothelial cells, immune cells, T cells, macrophages, and extracellular matrix (ECM) components. It is a known fact that extracellular and subcellular compartments of tumor tissue are more acidic than healthy ones, the reason for it is a dynamic metabolism in tumor with high glucose consumption and lactic acid accumulation (the Warburg effect [22]). The

extracellular pH (pHe) in solid tumor sites is 6.0 to 6.8, even lower pH is possible in more aggressive cancer phenotypes. This knowledge has been considered for engineering pH-responsive systems. Typically, nanoparticles with size range from 20 to100 nm undergo cellular internalization *via* endocytosis, where they face compartments with concrete different pH values. Values of pH drop from the extracellular media (pH ~ 7.4), to early endosomes (pH ~ 6.0), late endosomes (pH ~ 5.5) and lysosomes (pH < 5.0), so the kinetics of drug release may be guided by acidification. These pH gradients were used for the design of pH-responsive drug delivery systems that can selectively release the cargo at specific tumor site.

Another approach of using TME as a stimuli trigger is the elevated levels of reactive oxygen species present there. ROS is a class of chemically reactive molecules that are generated intracellularly in human body by oxygen reduction in mitochondria. ROS mainly includes the superoxide anion (O_2^-) and hydrogen peroxide (H_2O_2), other derived species are singlet oxygen (O_2), hypochlorous acid (HOCl), hydroxyl (•OH), and peroxyl (ROO•) radicals. The role of reactive oxygen species can be beneficial since they act as signaling molecules in metabolic pathways. The concentrations of ROS are adequately regulated by homeostasis mechanism. A number of studies report that overproduction of ROS as a result of oxidative stress was found in pathological disorders including inflammatory, diabetes, cardiovascular, neurological diseases and cancer. High level of ROS is persistently exhibited in many types of cancer cells, since they play a vital role in cancer progression. [23] Therefore, high levels of ROS in cancer tumor make it more distinctive than the surrounding. The importance of these findings has driven new promising strategies of smart drug delivery vehicles utilizing ROS as a stimulus in TME. Considering the abovementioned, the thesis was focused on preparation of nano-assemblies in form of polymersomes sensitive to unique features of TME such as pH or ROS.

1.2 Soft matter for cancer drug delivery

1.2.1 Liposomes

Liposomes are self-assembled spherical vesicles produced from amphiphilic phospholipids (Figure 4). The first were prepared from ovolecithin by Bangham *et al*. in 1965 [24], who initially named them bangosomes. These swollen phospholipid systems - liposomes lately found application in drug delivery. Liposomes have a hydrophilic aqueous core which can accommodate proteins, hydrophilic drugs and siRNA/DNA. The lipid hydrophobic membrane allows the entrapment of hydrophobic agents. Naturally produced liposomes are the multilamellar vesicles; more desired unilamellar liposome vesicles (with one lipid bilayer) can be obtained by different techniques (freeze-thaw, extrusion). The other parameters of liposomes such as charge, size or morphology can be controlled by modification of physicochemical and biophysical properties of selected lipids. Lipids can be of natural origin, or synthesized from diverse library of compounds, the synthesis includes hydrophilic head groups, specific linkers and hydrophobic moieties. The conventional method for liposomes preparation is film-rehydration[25], followed by sonication or electroformation; the drug loading can be achieved *via* active or passive techniques.

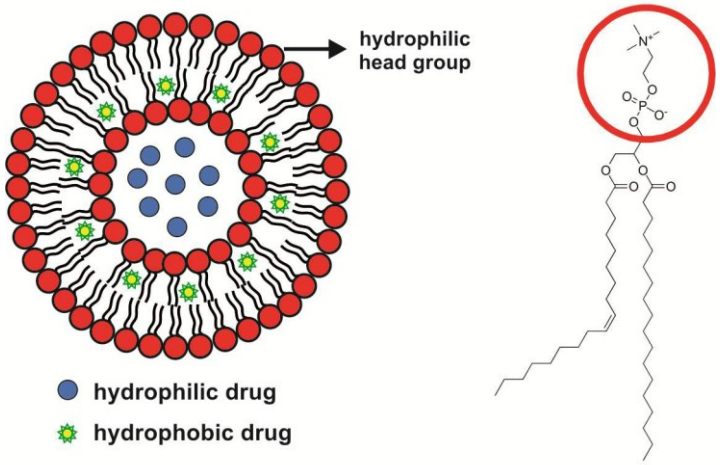

Figure 4. Schematic representation of a drug-loaded liposome and the molecular structure of a phosphatidylcholine related phospholipid.

In nanomedicine field liposomes are widely represented in delivery of drugs, vaccines and imaging agents. As a delivery platform liposome demonstrate several advantages like biodegradability and biocompatibility, non-immunogenicity and ability to carry various active agents, stimuli-responsiveness, and surface functionalization for ligand mediating targeting.

However, liposomes are associated with several disadvantages such as low solubility, short stability during blood circulation, drug leakage and possible phospholipid oxidation (hydrolysis).

The stability and prolonged-circulation in blood can be improved by PEGylation (grafting of PEG on liposome surface). PEGylated lipids (Doxyl®) are the first clinically approved nanomedicine by FDA for cancer therapy. Incorporation of small molecules can enhance the solubility and reduce overall toxicity. Increased cohesiveness and reduction of permeability in lipid membrane could be achieved using cholesterol, that helps to increase packing of phospholipids.

1.2.2 Polymer nanoparticles

Polymer nanoparticles drug delivery systems received great attention in terms of improving conventional chemotherapies. Polymers for intravenous drug delivery must be biocompatible and biodegradable (by erosion, enzymes, dissolution, fragmentation or by hydrolysis of labile bonds in backbone/crosslinker). The saturated hydrocarbon chains of polymers were found to be not biodegradable in most living organisms, therefore polymers must be removed from the body to prevent bioaccumulation. Natural polymers like polysaccharides or proteins and some synthetic polymers *e.g.*, polyacrylamides, polyoxazolines or polyethylene glycol, can be cleared through the kidneys (renal clearance). However, kidneys renal filtration has a threshold for molecular weight ranging from 30kDa to 50kDa for polymers, macromolecules with higher M_w have either slower renal elimination or even extended retention in body. Polymer chemistry, charge, molecular conformation, flexibility or rigidity also affects the passing threshold.

First reports about biodegradable polymeric NPs appeared few years after liposomes. The major type of biodegradable polymers are synthetic polyesters, or their derivatives such as

poly(lactic acid) (PLA), poly(lactic-*co*-glycolic acid) (PLGA) and poly(ε-caprolactone) (PCL) [26] which are already FDA approved. For example, PLA and PLGA, the most commonly used nanoformulations for encapsulation of chemotherapeutics, degrade into small biocompatible molecules which are also by-products of several metabolic pathways, that are easily metabolized and cleared by liver or kidneys with minimal toxicity.

The rapid uptake and fast clearance are still the largest issue for polyester NPs, so stabilizers are needed. The stabilizing outer shell is basically achieved by grafting, conjugating or adsorbing of highly hydrophilic polymers like poly(ethylene glycol) (PEG), polyvinyl alcohol (PVA) or poly(*N*-vinyl-2-pyrrolidone) (PVP) and polysaccharides (usually dextran or chitosan). Such shell covers extend the circulation time by reducing the opsonization (adsorption of plasma proteins on surface that interact with MPS), but bring another limitation, for instance PEG and PVP can undergo thermal/oxidative degradation, PVA has a drawback with associated toxicity. Essential efforts should be directed to development of new bioinert polymers for improving of long-term drug delivery applications.

Natural-based polymeric nanoparticles also received a tremendous attention in delivery of bioactive agents. Natural based polymers include mainly polysaccharides (chitosan, dextrin or hyaluronic acid) and proteins (keratin, collagen or silk fibroin). Their essential advantages are high biocompatibility, accessibility, controlled enzymatic degradation, and versatile functionalization of reactive groups on the native material. Hybrid materials can be prepared by incorporation of natural based polymers into other native or synthetic materials. Additionally, adjustment of physico-chemical properties endows them with stimuli-triggered or targeted motifs. The natural based nanocarriers loaded with small molecules, DNA or proteins found application in tissue engineering, wound healing, antibacterial therapy and cancer treatment.

Polymer-drug conjugates are macromolecular constructs covalently bound with pharmacologically active agents, several systems are already applied in clinical practice. The first synthesis of a polymer-drug conjugate was done in 1955 by Jatzkewitz who prepared a copolymer of *N*-vinylpyrrolidone and acrylic acid conjugated with psychedelic alkaloid mescaline using a dipeptide (GL) spacer. His purpose was to increase the residence time of mescaline *in vivo* by using a dipeptide linker for an enzymatic cleavage with release of active agent. [27] In the 1970s polymer conjugates were promoted by the work of Ringsdorf, Kopecek and Duncan and in 1990 for the first time a polymer-conjugate Adagen was approved for the treatment of severe combined immunodeficiency disease (SCID). Up to now the field of polymer-conjugates is displaying a remarkable growth in the development of a variety of engineered materials and responsive linkers.

Indisputably, optimization of polymer-conjugates linkers is a challenging issue since they should be stable in bloodstream circulation and provide controlled release of the conjugated drug at a target site. Primary choice for linkers is peptides, hydrazine, azo, acetal, and disulfides. [28]

Polymer conjugates combined with drug and imaging agent are called theranostic agents, because of the ability to provide diagnosis or imaging simultaneously with therapy. Imaging can provide information about the state of the target site, and about the localization/biodistribution of drug simultaneously with treatment.

Most investigated polymers for PDCs are highly hydrophilic polymers: PEG, PHPMA, PVP, poly(amino acids) and polysaccharides. Systems based on these polymers demonstrate higher solubility and stability of conjugated drug, enhanced half-life in blood circulation, potential stimuli triggered release, and biocompatibility. PEG and HPMA conjugates represent a wide repertoire of available architectures and functionalities, the simplest linear conjugates are the most investigated but limited with the numbers of conjugation sites; branched, star-like, multi-armed, or forked configurations have much more hydroxyl functional groups, with more unique biomedical properties which in turn expands the scope of application. Several low M_w multi-arm PEG drug conjugates enter clinical trials and are under different development status, such as EZN-2208 (40kDA PEG-SN38), NKTR-102 (PEG-Irinotecan) or NKTR-105 (PEG-Docetaxel) [29]. PHPMA-drug conjugates are also in demand for PDCs formulations, the first PDC that reached clinical trials was HPMA conjugated with DOX [30]. The chemotherapeutic drug doxorubicin was bound to HPMA via peptidyl spacer, for treatment of solid tumors. Multiple reactive groups of HPMA copolymers were used for attachment of various drugs, several successfully reported are PHPMA- doxorubicin-aminoglutethimide [31], PHPMA-DOX-dexamethasone [32], PHPMA-DOX-gemcitabine [33], and PHPMA-DOX-Mitomycin C[34].

1.3 Block copolymer nanoparticles

Block copolymers are widely employed in drug delivery field, especially in delivery of DOX and PTX. By definition, a block copolymer is a linear macromolecule where the blocks are distinct polymers that are linked by covalent bond. Block copolymers originated from the discovery of termination-free anionic polymerization, which is still the best method for production of highly monodisperse block-copolymers. Typically, block-copolymers are not branched structures, however various architectures with branches composed of blocks are possible *i.e.,* starblock copolymer with a junction of blocks to one single point, which creates three-dimensional branched architecture. Usually the synthesis of block copolymers is done by living polymerization, its starts with the synthesis of the first block (homopolymer A), with following addition of a second monomer (B), which reacts with living active center with growth of the chain that form a second block (A-B block copolymer). A triblock copolymer can be obtained by addition of one more monomer.

Currently, block copolymer drug-loaded micelles are under different phase stages in clinical trials. The well-studied Genexol®-PM a formulation of PTX loaded in monomethoxy poly(ethylene glycol)-*block*-poly(D,L-lactide) (mPEG-PDLLA) block copolymer, was approved in South Korea, Bulgaria and Hungary in 2001, the superiority of this product is high drug solubilizing capacity (~25%), and higher maximum tolerated doses (MTD) than in the case of Taxol® (paclitaxel). In clinical phase II, Genexol®-PM tests have been conducted in patients with breast cancer, pancreatic cancer and with cisplatin for advanced non-small cell lung cancer (NSCLC). In patients was observed neutropenia, sensory neuropathy and myalgia [35], however acute hypersensitivity reactions [36] which are common adverse effect for Taxol treatment were not observed. Currently Genexol®-PM is in Phase IV clinical trials in recurrent breast cancer [37], and more therapies combined with anticancer drugs are being investigated.

The PEG-poly(aspartic acid) copolymer, known as NK105with PTX physically entrapped in micelles with ~23% loading, is an example of poly(amino acids)-based block copolymer micelles. PEG corona and small size about ~85 nm prolong the circulation time and demonstrate linear pharmacokinetics (PK) behavior in Phase I for solid tumors [38]. Phase II study of NK105 was done for previously treated advanced or recurrent gastric cancer [39], the result demonstrates modest activity and tolerability. Phase III clinical study[40] for metastatic or recurrent breast cancer patients, showed better PK profile.

NK911 is a micellar formulation of DOX conjugated to PEG-P(Asp), with ~ 45% loading efficiency. The Phase I study revealed prolonged half-life comparing to free DOX, however NK911 demonstrated poor stability in bloodstream, and 400-fold higher plasma clearance compared to Doxil®.

Also, NC-6300 a conjugate of epirubicin (4′-epimer of DOX), which is favored over DOX by reduced toxicity, and PEG-P(Asp) via an acid-labile hydrazone bond. The anticancer efficacy is similar to NK911, but with significant decrease in cardiovascular toxicity, which was demonstrated in pre-clinical studies on mice xenograft models bearing Hep3B liver orthotopic tumors. [41] Phase I/II trials are ongoing in Japan for advanced solid tumors or soft tissue sarcoma.

The micelles of copolymer of PEG-poly(*L*-glutamic acid) with SN38 water insoluble metabolite of irinotecan hydrochloride identified as NK012, have a size of ~20 nm and ~20 % loading efficiency. SN38 is an extremely water insoluble compound which was restricted for market use, encapsulation in micelles of PEG-P(Glu) was the first successful approach for clinical therapies.

The NK102 demonstrates slow clearance and high tumor accumulation and no sever dose dependent toxicity in two independent Phase I studies. A Phase I study also was conducted between NK102 combined with 5-fluorouracil [42] for advanced solid tumors, the therapy was well tolerated. NK102 is ongoing Phase II in patients with relapsed/refractory multiple myeloma (RRMM), in some cases long-term disease control was observed.

NC-4016 is another micellar system composed of PEG-P(Glu) stabilized by dichloro(1,2-diaminocyclohexane) platinum (II) developed for delivery of oxaliplatin for reduced neurotoxicty. The phase I study was done in US for advanced solid tumor or lymphoma.

Cisplatin antineoplastic drug was also incorporated in PEG-P(Glu) micelles *via* polymer-metal complex-formation in NC-6004 (Nanoplatin™), with drug loading ~39 % and ~30 nm size. In 2006 UK and USA conducted Phase I where NC6004 demonstrated superior anti-tumor activity in colorectal cancer. Phase II was conducted in Singapore and Taiwan with advanced or metastatic pancreatic cancer; the NC-6004 safety, tolerability and efficiency was examined in combination with gemcitabine. Combination of gemcitabine and NC-6004 and gemcitabine alone currently are on Phase III for treatment of pancreatic cancer, higher overall survival rate is expected [43].

The major challenge in cancer treatment is MDR, only one copolymer has been reported that can significantly reduce the drug resistance, the PEO–PPO–PEO copolymers (Pluronic ^{TM}).

SP1049C is a nanocarrier formulation of Pluronic and DOX, prepared by reconstituting DOX with a 0.9% sodium chloride solution containing Pluronic L61 (0.25% w/v) and F127 (2% w/v) with final DOX concentration of 2.0 mg/mL. The Pluronic L61 inhibits the P-glycoprotein efflux mechanism that modulates the activity of drug in MDR cell, and non-ionic Pluronic F127 provides increased stability with no changes in cytotoxicity. Increased efficacy of SP1049C was investigated in brain tumor, suggesting its promising use in brain solid tumors. Phase I trial initiated in Canada 1999, treatment confirmed linear PK profile. The achieved promising preclinical and Phase I data prompted the Phase II investigations in patients with advanced adenocarcinoma of esophagus and gastroesophageal junctions in 2002. Trials were performed for 19 patients, 9 patients had a partial response, 8 patients had a minor response or stable disease, overall objective response rate was 47%.

Block copolymer nanoparticles come a long way to become a promising target delivery therapy against cancer.

1.4 Giant Polymer Vesicles

Giant polymer vesicles are a novel class of larger scale (1-100 μm) self-assembled structures, that possess structural properties of nanosized polymersomes (1-100 nm) - a polymeric membrane of amphiphilic diblock copolymer, that can be used for encapsulation of hydrophobic agents, and an aqueous core for hydrophilic compounds (Figure 5). The polymeric membrane promotes semi-permeability and by tuning the thickness and overall size of vesicle the permeability and mechanical stability can be modified, which is a critical parameter for biomedical controlled release applications. Another distinction of giant PSs is their ability to encapsulate more various types of cargo such as cells, artificial organelles and nanoparticles. The trigger mechanisms for release of payload, in addition to those existing for nano-polymersomes (such as temperature, magnetic field, ultrasound, ROS and pH) are added hypo-osmotic shock, hypertonic shock or light by encapsulation of photo-cleavable dyes or molecules, that can increase the internal osmotic pressure by irradiation. Also, giant PSs could serve as an artificial bioreactor for application in biotechnology and medicine[44].

Another attractive feature of Giant PSs is their use as a biomimetic model, for studying cellular membranes properties and as an environment for complex biochemical reactions.

Considering the aforementioned, we designed a giant smart functional biomimetic vesicle sensitive to pH-cellular imbalances for mechanical and biological studies.

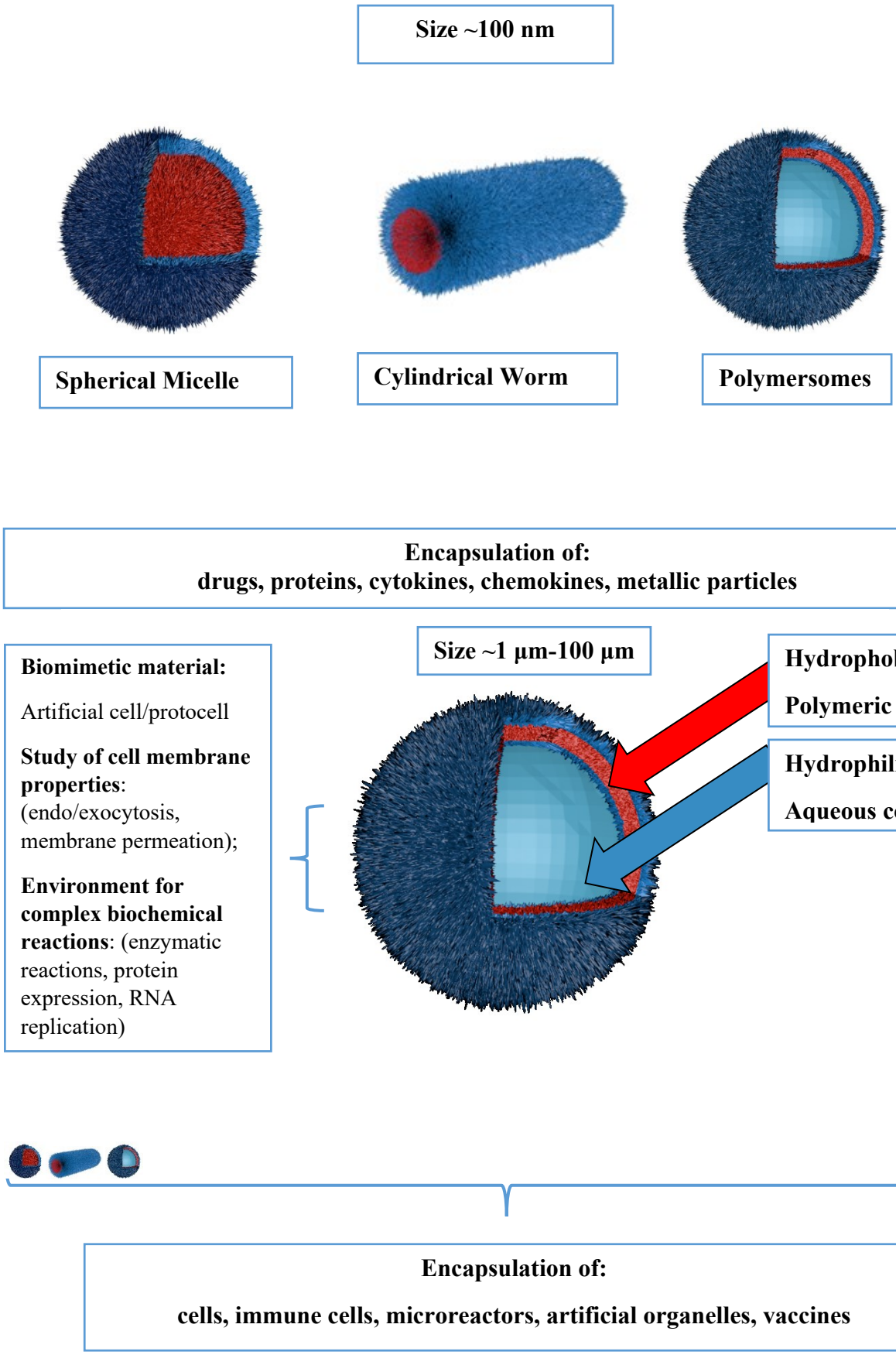

Figure 5. Comparison of nano-sized structures and giant self-assembled polymersome.

1.5 RAFT Polymerization

The living polymerization is a general method for preparation of well-defined polymers with low polydispersity ($Đ$), control over M_w (chain length), initiating and end functional groups. In living polymerization chain termination and chain transfer reactions are essentially eliminated, which results in constant rate of polymer chains growth which makes chain lengths very similar (low polydispersity index), leaving only initiation and propagation steps. The precision and control over molecular weight is of importance for engineering of polymer nanoparticles. Techniques employed in living polymerization are atom transfer radical polymerization (ATRP), living cationic/anionic polymerizations, ring-opening metathesis polymerization (ROMP), reversible addition fragmentation chain transfer (RAFT) polymerization and several other controlled radical polymerization techniques. Despite the fact that disulfides and sulfides were used as polymerization initiators in the 50s, and addition-fragmentation mechanism in organic synthesis was known in the 70s, RAFT polymerization was first described by Thang et al. in 1998 [45], as the combination of the knowledges accumulated in novel living polymerization. RAFT is distinguished from other methods by a wide range of compatible monomers and more tolerant required conditions. The polymerization is based on a reversible chain transfer equilibrium between active and dormant chains.

The method starts with thermal decomposition of radical initiators, similarly to traditional radical polymerization, where we obtain the active species $P_n^{\bullet}$. The most common initiators are 2,2'-azobis(2-methylpropionitrile) (AIBN) and 4,4'-azobis(4-cyanovaleric acid) (V501) with the half-lives typically hours at temperatures between 60 and 80 °C. The propagating species $P_n^{\bullet}$ react with RAFT agent species **(**polymeric chain containing the CTA group) which enables equilibrium between active and dormant species, followed by fragmentation of the generated intermediate and a new radical $R^{\bullet}$. Typical chain transfer agents comprise a thiocarbonylthio group, Z-C(=S)-S-R *i.e.* dithioesters or trithioesters, where the Z group (phenyl, dodecyl) stabilize the radical intermediate, while the R group (cyanopentanoic acid, *iso*-propylcarboxylic acid) must be stable enough to be fragmented as radical and reactive enough to reinitiate the polymerization; also, the R group can be used for future functionalization. The next step is re-initiation, where the radical $R^{\bullet}$ reacts with another chain transfer agent and forms new propagating agent $P_m^{\bullet}$. Afterwards main RAFT equilibrium is established between active propagating species and the dormant species, fast exchange reactions and equally shared radicals lead to equally growing polymer chains with well-controlled M_w and narrow PDI. Termination of polymerization is achieved by quenching the reaction mixtures by exposure to air or liquid nitrogen. The whole RAFT polymerization mechanism is depicted in Figure 6. The retention of thiocarbonylthio groups is responsible for the living character of polymerization, which makes this polymerization suitable for the formation of diblock copolymers. The removal or transformation of thiocarbonylthio group can be achieved by various methods. [46]

Typically, RAFT polymerization is very sensitive to nucleophiles like oxygen, moisture, or amines, even traces of nucleophilic agents could scavenge radicals, which will result in broader molar mass distribution, so it is carried on in inert atmosphere with degassed liquids.

The macroCTA could be prepared not just by RAFT but also by modifying prepared polymers with CTA molecule (PEG, PMeOx, etc). [47]

The RAFT polymerization was herein used to synthesize well-defined PHPMA-based ROS and pH responsive block copolymers and their corresponding self-assembled structures were produced by microfluidics. Microwave irradiation was employed for RAFT polymerization to overcome some of the drawbacks existing in the conventional heating process.

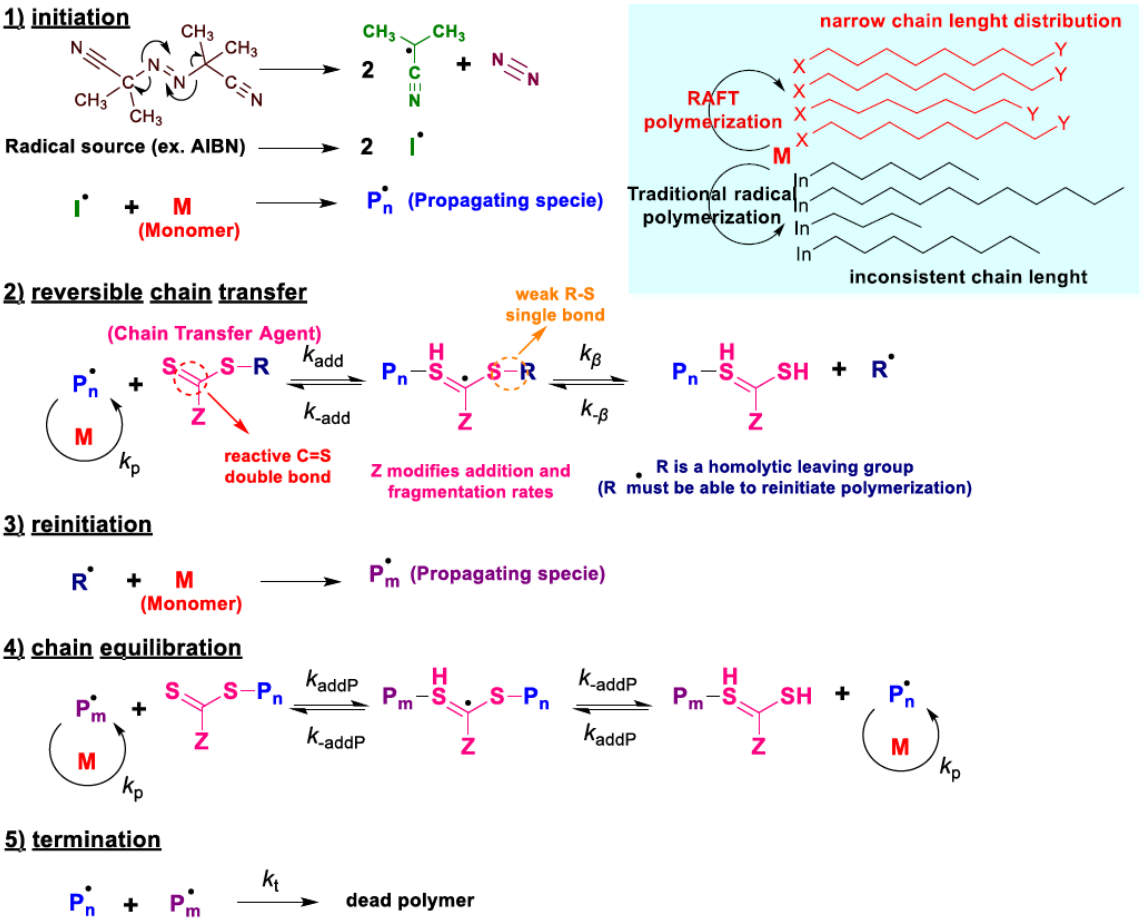

Figure 6. Mechanism of RAFT polymerization.

1.5.1 Microwave-assisted RAFT polymerization

Microwave irradiation is a widely employed technique for synthesis in inorganic, organic and polymer chemistry. The MWI synthesis with rapid and homogenous heating lead to enhanced rates, yields and purities comparing with conventional heating. [48] Upon optimized conditions the reactants directly absorb microwave irradiation compared to conventional heating cases where the heterogeneous thermal energy transfer is conducted via solvent. Vinylic polymers such styrene, acrylates and (meth)acrylamides polymerized by MWI radical polymerization demonstrates faster conversion and much faster Rp. Typical conventional RAFT polymerization reaction times of HPMA range from several hours to days, utilizing the effect of microwave

irradiation this drawback can be overcome. The attempts to control the HPMA polymerization was firstly reported by Matyjaszewski using atom transfer radical polymerization (ATRP), the group of Scales et al. reported the aqueous RAFT polymerization of HPMA with the use of 4-cyanopentanoic acid dithiobenzoate and 4,4‘-azobis(4-cyanopentanoic acid) as CTA and initiating species in the presence of an acetic acid buffer solution at 70 °C [49,50]. Herein, we utilized microwave-enhanced RAFT to perform aqueous polymerization of HPMA and its relevant copolymers for clinical applications.

1.6 Self-assembly of block copolymers

Block copolymers self-assemble to nanoparticles in aqueous solutions due to poor dispersibility of the hydrophobic moieties. The hydrophobic blocks tend to avoid their contact with water hiding into hydrophilic block, which generally lead to creation of a spherical object with a hydrophobic core and hydrophilic shell. The balance between attractive and repulsive forces guides the molecules to form an ordered structure - micelles. [51]. Concentration of block copolymer above which micelles are formed is in surface and colloidal chemistry named critical micelle concentration (CMC). The size of micelles ranges from 10 to 100 nm. The hydrophobic core of micelles can be used for solubilization of lipophilic drugs, thus to increase its concentration in hydrophilic media. The drug loading efficiency depends on many parameters, such as solubility parameters of drug and polymer and their interaction, block copolymer length, shape, and volumetric size of the carrier. Also, active agents can be attached to the hydrophobic block by environmentally responsive chemical bonds, which will trigger the release of the compound in the target site and it will simplify the renal clearance afterwards.

By tuning or modifying the M_w of hydrophobic/hydrophilic blocks several stable self-assembled morphologies can be obtained. The packing parameter (p) that is related to the size of both blocks can be used for prediction of self-assembled structure to some extent (Figure 7). Larger hydrophilic chains in block copolymer will usually lead to assembly into micelles, by increasing the length of the hydrophobic part wormlike micelles (filomicelles) and polymersomes (vesicles) will occur.

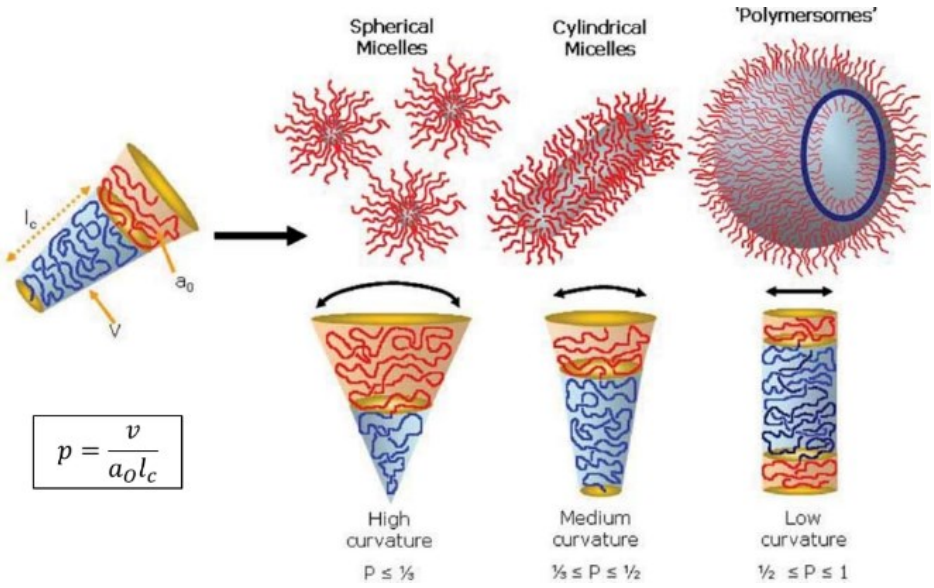

Figure 7. Self-assembled structures formed by amphiphilic block copolymers. The type of structure formed depends on the dimensionless packing parameter, *p* [52].

The micelles and filomicelles are capable of integrating only the hydrophobic molecules in the core, while polymersomes are capable of accommodation of hydrophobic compounds in membrane and hydrophilic in the aqueous lumen. Polymersomes are newer platforms than liposomes, and they are characterized by increased stability compared to lipid vesicles.

The typical hydrodynamic radius (R_H) of polymersomes ranges from 50 nm to a few μm, the size can be tuned by modifying the parameters such as amphiphilicity of polymer and by the methods of preparation. Methods that are used for preparation of PS are thin-film hydration, nanoprecipitation (solvent-shifting), pH-switch when the block copolymer is pH-sensitive and more novel PRINT templates, polymer-induced self-assembly (PISA), and microfluidic assisted nanoprecipitation. By using microfluidics technique highly monodisperse particles with higher encapsulation efficiency could be obtained, due to precise micromixing control. Moreover, well-defined polymersomes might provide enhanced chemotherapeutic effects due to more homogenous biodistribution. This approach was straightforwardly used in this thesis, the PS was prepared via microfluidic-assisted nanoprecipitation and tested *in vitro* and *in vivo.*

An advantage of polymersomes is their ability to deliver a protected payload into intracellular environment with triggered release, compartmentalization properties, and increased stability which made them a promising platform for vesicular drug delivery of drugs, genes, for a relevant clinical application.

Herein, polymersomes responsive to ROS and pH-cellular imbalances were produced by microfluidics technique and characterized.

1.7 Stimuli-responsive polymersomes for cancer targeted drug delivery

1.7.1 Polymersomes responsive to pH-cellular imbalances.

As was mentioned before, in tumor tissues due to vigorous metabolism the pH status in cellular and sub-cellular levels is more acidic (*vide* section **Tumor microenvironment targeting**), so sensitivity to pH could be efficiently used for targeting tumor tissues and the intracellular well-defined compartments with strong pH differentiation as well (the pH value in endosomes may typically drop to ca 5). As an example of extracellular pH change, pH_e of adenocarcinoma and soft tissue sarcoma is ~6.94, thus adenocarcinoma cell lines are the most reported models for investigation of pH-responsive therapeutic effect. [53]

The pH differences have been widely utilized in formulation of acidic sensitive platforms, that have three forms of responsive mechanisms: bond cleavage, protonation and gas generation.

Bond cleavage is a system where pH-sensitive chemical bond can be disrupted in presence of acid with subsequent drug release and it is the most common class of biomaterials with acidic triggered release. This type of biomaterials preserves the therapeutic payload at normal pH and effectively releases the drug at acidic pH conditions. In such systems drugs can be attached via acid labile linker or encapsulated in acid labile nanocarrier. The pH sensitive linkers must be stable at physiological pH (~7.4) and hydrolyzing at acidic pH (4.5-6.5). The typical organic pH-sensitive bonds are imines, hydrazones [54], oximes, acetals, coordination metal-organic frameworks (MOFs), and amides (Figure 8). The polymersomes prepared using these pH-linkers are widely reported [55].

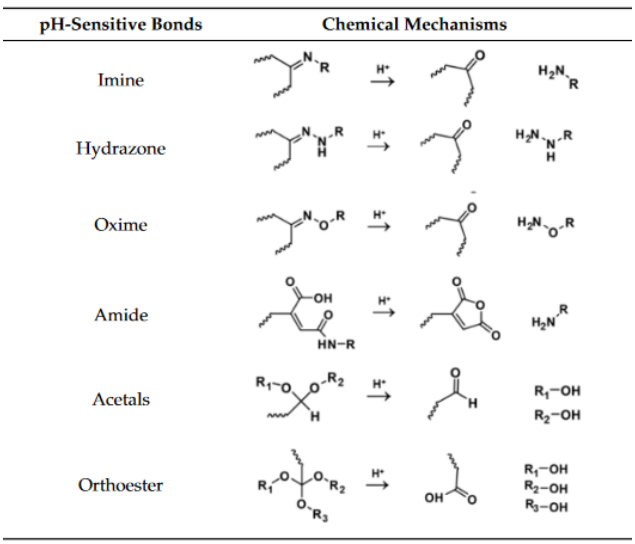

Figure 8. pH-sensitive chemical bonds and release mechanisms in the acidic conditions [55].

pH-sensitive polymers based on bond cleavage are promising biomaterials for acid-responding drug delivery systems, however, there are still many challenges that need to be solved,

such as biocompatibility of pH-sensitive linkers, stable mass production, and toxicity of nanocarriers.

Protonation of chemical groups such as carboxylic, phosphoric or sulfonic acids and/or amines can be utilized for the preparation of pH-sensitive drug delivery systems. The weakly acidic or basic pendant groups (Table 1) are capable for accepting or donating of protons depending on their pK_a, which in turn cause conformational changes. This ionization and deionization transitions have a polyelectrolyte nature and allow for tuning the hydrophilicity, that regulates the precipitation and solubilization, swelling or deswelling and surface hydrophobic/hydrophilic changes of nanocarriers in aqueous solution.

Table 1. pH-responsive acidic and basic pendant groups.

pH-responsive acidic polymers pendant groups	**pH-responsive basic polymers pendant groups**
Carboxylic groups	Morpholino groups
Sulfonic acid	Pyrrolidine
Phosphonic acid	Piperazine
Boronic acids	Imidazole
	Pyridine
	Imine
	Tertiary amine

Dendritic polymers with amine groups and a natural polymer with suitable chemical modifications are also a group of widely used pH-responsive systems.

Vinylic polymers, (meth)acrylates and (meth)acrylamides containing tertiary amine groups were extensively investigated in past decade. Most popular weak basic polymers with tertiary amine group are poly[(2-diethylamino)ethyl methacrylate] (PDEA) and poly[(2-diisopropylamino)ethyl methacrylate] (PDPA). In physiological conditions the diisopropylamino group of the PDPA have $pK_a = 6.8$, which is similar with pH of tumor microenvironment, which makes it particularly useful in anticancer therapy. Moreover, PDPA-based polymers prepared by various techniques are commercially available, and can be used in many fields covering the imaging, diagnostics, theranostics, antibacterial coatings, bio-separations and catalysis.

Herein, PDPA was used for preparation of pH-responsive part in diblock copolymer based on hydrophilic HPMA, extra and intracellular pH gradients will be used as a trigger for drug delivery system which will selectively release the transported drug at the specific site of action.

1.7.2 Polymersomes responsive to reactive oxygen species (ROS) imbalances

Reactive oxygen species (ROS) and reactive nitrogen species (RNS) are two types of oxidative species, that are formed under physiological conditions in living systems. ROS including H_2O_2, O^2•, •OH, $ONOO^-$, $HOCl^-$ etc., play a double role in human body that is harmful and beneficial, since they can cause oxidative stress and inflammation events and serve as a signal molecule in cell metabolic pathways. Imbalances of ROS production are often associated with various diseases including diabetes, cardiovascular disease (CVDs), neurodegeneration and cancer

(*vide* section **Tumor microenvironment targeting**). Cancer cells due to abnormal proliferation has increased levels of ROS, especially H_2O_2 (one of the main components of intracellular oxidate) with concentration 50–100 μM, while in normal tissue it is 1-5 μM. The H_2O_2 is less reactive than superoxide anion and is involved in many physiological processes including hypoxic signal transduction, cell differentiation, proliferation, and in mediating immune responses, therefore H_2O_2 could act in either the growth or apoptosis of cancer cells. Aberrant production of H_2O_2 in tumors which make TME more distinctive for surrounding encourages the construction of ROS-specific detections systems, ROS-responsive prodrugs, pro-chelators, theranostic agents, and intelligent nanocarriers [56].

Delivery systems that demonstrate the leverage ROS sensitivity are capable for targeted release of therapeutic payloads at sites with high ROS concentrations. The nanoparticles with ROS triggered response could be prepared by incorporation of sensitive linkers or side groups into the polymer (Figure 9).

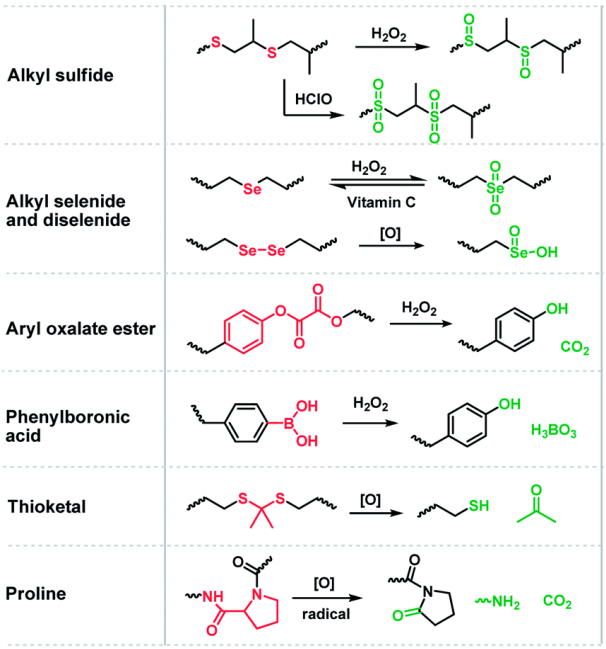

Figure 9. Oxidation-responsive motifs and their oxidation products [56].

Sulfide groups were the first reported ROS-responsive moiety which was utilized in drug delivery systems, the first report was done in 2004, with polymersomes of triblock copolymer of PEG-PPS-PEG [57]. The sulfide hydrophobic moieties could be converted in presence of ROS into more hydrophilic sulfoxides and sulfones. Currently, sulfur(II)-containing polymers are systematically studied including synthesis, self-assembly, ROS triggered response, and biological activity [58].

Selenium belongs to group of chalcogens (16 in the periodic table), the same group as the sulfur, which makes them similar in many aspects, such as oxidative transformation of hydrophobic selenium to hydrophilic selenoxide or/and selenone. Together with redox sensitivity selenium-based materials also possess the γ-irradiation sensitivity, with possible dual response by

oxidation changes. Even more, the advantage of selenium-based materials is a higher sensitivity than sulfur or thioethers and faster response, since the C–Se bond (244 kJ mol^{-1}) is weaker than that of the C–S bond (272 kJ mol^{-1}), and the bond energy of the Se–Se bond (172 kJ mol^{-1}) is smaller than the S–S bond (240 kJ moL^{-1}), which makes it more labile. The diselenide bonds are very attractive motifs for redox-sensitive polymers. Synthesis of selenium-containing polymers was known since early 1972, with step-growth polymerization as the predominant method. As example, polymers based on polyselenide hydrophobic block and two hydrophilic PEG blocks loaded with DOX were prepared for possible biomedical applications. [59] The main limitation of selenium-based systems is possible toxicity.

Thioketals are another ROS-cleavable moiety, which can be oxidized by hydroxyl radical or superoxide into ketones and organic thiols. The incorporation of thioketal as linker is used for fabrication of prodrugs for improvement of drugs selectivity and efficiency. Thioketal-based polymers were synthesized by various techniques, and used for oral delivery of RNAs, gene delivery, anticancer drug delivery and ROS-responsive scaffolds [60–62].

The aliphatic polyoxalates (POXs) were firstly reported in early 1930s; they can be prepared by ROP of cyclic oxalates of 1,2 glycols or by polycondensation of small molecules with diol group (*i.e.,* 4-hydroxybenzyl alcohol, diethylstilbestrol or curcumin) with oxalyl chloride or oxalic diesters. Aryl oxalates have been extensively investigated from the 1960s, due to their peroxide-based chemiluminescence properties [63]. In the presence of H_2O_2 oxalates oxidize and produce 1,2-dioxetanedione or other kinds of high-energy intermediates (HEI), which could interact with a fluorophore to form an activated complex. The decomposition of complex with subsequent CO_2 release leads to decay into ground state of excited fluorophore with emitted fluorescence. Furthermore, oxalate bonds are highly specific to H_2O_2. Recent studies that were done in murine models demonstrate interesting properties such as antioxidant-theranostic agents, [64] ischemia/reperfusion-targeted nanotherapeutics,[65] and as nanoreactor systems for *in vivo* imaging of H_2O_2. Attractive properties of oxalate-based polymers are ROS-induced luminesce with tunable emission by the encapsulation of specific dyes, exceptional sensitivity to H_2O_2 among other ROS species, deep-tissue imaging capabilities, and continuous detection of *in situ* produced H_2O_2 for long times. Oxalate-based system demonstrated a promising perspective for effective therapeutic delivery to disease sites, however more *in vivo* studies are necessary in the future.

Boronic acids are a unique class of ROS responsive biomaterials because of their reactivity toward H_2O_2. The phenylboronic acid and it's derivates used as a building blocks in construction of functional polymers, prodrugs and networks with great potential in catalysis, sensing, separation, imaging and drug delivery. The mechanism of oxidation was proposed by Kuivila *et al.* in the 1950s. The phenylboronic acid or ester is exclusively sensitive towards H_2O_2, with cascade reaction in which phenol and boronic acid as the oxidation products are formed. Arylboronic acid or arylboronic ester-based polymers can be prepared via polymer post-modification methods, step-growth polymerization of the phenylboronic ester-based monomers, and RAFT polymerization of the phenylboronic ester-containing vinyl monomers. Upon exposure to H_2O_2 such ROS-responsive polymers undergo the subsequent self-immolative elimination, where they either degrade totally or the properties are changing significantly.

The sensitivity only to H_2O_2 of which the levels are highly elevated in tumor microenvironment, has a great potential for the effective delivery of antitumor agents into specific cancer sites. Considering the aforementioned, the thesis was driven for the preparation of novel phenylboronic based polymersomes for the delivery of chemotherapeutic drugs into TME sites, the H_2O_2 scavenging ability was evaluated, and the deprotection/degradation mechanisms were studied by various techniques. The system was prepared taking advantages based on the biological and physical barriers. Since biocompatibility is a key factor for biomaterials, *in vitro* and *in vivo* studies were performed.

1.8 Preparation methods of polymeric nanoparticles by self-assembly

1.8.1 Nanoprecipitation (Solvent displacement technique)

The nanoprecipitation is an essential example of one of the most commonly used techniques for the preparation of self-assembled polymer nanoparticles for biomedicine. It is characterized by mild procedural conditions, simplicity, high encapsulation efficiency, low number of possible contaminants and good reproducibility. For the preparation of nanoparticles amphiphiles and non-amphiphiles with surfactant can be used. Nanoparticles formation proceeds from polymers than are not toxic as monomers or solvents, which makes it more preferable for clinical translation.

Nanoprecipitation is a low-energy mixing process based on self-diffusion, where solvent and nonsolvent phases must be miscible. The solvent phase contains organic solvent with polymer. The nonsolvent phase consist of water or buffer solution, which can be supplemented with surfactants such as PVA, Pluronic™ F-127, etc. The addition of solvent phase into stirred nonsolvent phase can be immediate, stepwise or dropwise by controlled rate. The self-assembly of nanoparticles occurs by precipitation due to their decrease of solubility in aqueous solution. The removal of solvent from the system is achieved by evaporation, dialysis or lyophilization with finalization of particles formation.

Varying the parameters such as type of solvent, speed of phase mixing, the organic/aqueous phase ratio, temperature and concentration of polymer can be used to tune the final size distribution of the nanoparticles. The nanoprecipitation technique is very straightforward, facile, and a fast process which is crucial for the biomedical applications.

1.8.2 Hydrodynamic flow focusing nanoprecipitation microfluidics (MF)

Microfluidics is an emerging field for the production of particles, droplets, capsules and multiple emulsions. Among other common techniques such as nanoprecipitation, film-rehydration and electroformation, microfluidics allows more controlled and precise way for the production of highly monodisperse polymeric structures including micelles, worms and vesicles.

Microfluidics nanoparticle preparation systems with high shear micromixing and hydrodynamic focusing methods give precise particle sizes in the range of ~20 nm to 500 nm. The microfluidics use continuous and controllable laminar flow for the production of high-yield and high-quality nanoparticles. The superior control over the size, shape and morphology of particles enables greater reproducibility and scalability. These substantial improvements in nanoparticle generation are highly valued in pharmaceutical industry compared to conventional batch methods. In this thesis, for production of well-defined nanosized polymersomes was used the commercial microfluidic chip from Dolomite company (Figure 10).

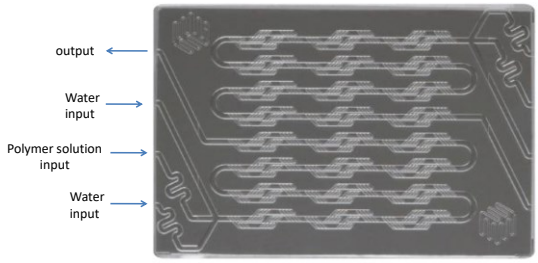

Figure 10. Dolomite setup of the micromixing chip with two water inputs and one polymer solution input.

The mixing time (τ_{mix}) for the hydrodynamic flow focusing using a two-dimensional model is estimated according to equation 1:

$$\tau_{mix} = \frac{w^2}{9D} \frac{1}{(1+1/R)^2} \quad (1)$$

where D is diffusivity of the solvent, w is channel width, and R is the ratio of flow rate of the polymeric stream to the total flow rate of water. For $D \sim 10^{-9}$ $m^2 \cdot s^{-1}$ and $w = 125$ µm equation 1 predicts a mixing time in the range of 0.6 to 7 ms for typical flow ratios ($R = 0.04$ - 0.8) in this device. Particles sizes can be finely tuned by changing the flow ratios between the organic and the aqueous phase, the slowest flow gives the smallest particles which was explained by the decrease in the τ_{mix}. Furthermore, besides the lower particle sizes a decrease in the width of the particle size distribution is observed compared with the bulk nanoprecipitation process. The NPs produced using this microfluidic device always presented size distributions with dispersity below 0.1 when measured by dynamic light scattering.

Superior properties of microfluidics open wide frontiers for applications in the field of drug delivery, small bio-reactors, organ-on-chips, etc.

1.9 Preparation methods of giant polymer vesicles by self-assembly

1.9.1 Water-In-Oil-In-Water (W/O/W) Double Emulsions by Microfluidics

Giant polymer vesicles are a novel class of self-assembled particles, giant PS possess the same properties as polymersomes like hydrophobic membrane and aqueous core, but with enlargement of compartments, since the overall size of giant PS size ranges from 1 µm to 500 µm. Thus, giant PS could be used for encapsulation of micron-size cargo such as: lysosomes, cells, immune cells, microreactors, and artificial organelles. Moreover, incorporation of pH-sensitive polymers in formation of giant PS allows the triggered release of loaded cargo at specific pH sites. In such pH-responsive giant polymersomes the release in acidic environment occurs due to rupture of membrane wall.

Another unique perspective for giant PS is the use of its biomimetic properties as artificial cell/protocell, to study the cell membrane properties (endo/exocytosis, cell adhesion, membrane permeation) and for artificial living simulation of complex biochemical reactions (RNA expression, protein expression and selective catalytic transformation).

Traditional methods for preparation of micron-sized giant PS are electroformation and thin-film rehydration, however these methods due to spontaneous assembly of diblock copolymers have a large size distribution and poor drug encapsulation profiles.

Microfluidics offers a highly controlled and reproducible way to produce giant polymersomes on chip. This method involves forming water-in-organic solvent-in-water double-emulsion droplets (Figure 11), followed by slow evaporation of organic solvent to let the diblock copolymer form a membrane [66].

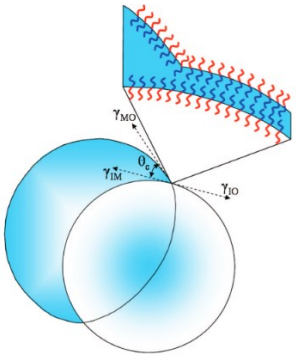

Figure 11. Scheme of double emulsion drop with partial wetting of the organic phase on a polymeric layer of block copolymer. [67]

Microfluidic devices for production of giant PS are glass capillary devices, 3D-printed devices, and poly(dimethylsiloxane) (PDMS) systems based on soft-lithography process. Glass capillary systems have difficulties in channel design and customization. Devices which are done by 3D printing up to now have another properties limitation, such as material properties, precision of channel lengths, but they are promising candidate for the future of microfluidics. PDMS devices fabricated by soft lithography can be performed with wide ranges of sophisticated channel designs with high accuracy. However, PDMS can be used directly only with a limited range of solvents such as alcohols and oils. Since PDMS has poor chemical resistance and swells in contact with many organic solvents, additional cover of the channel must be applied involving, e.g., methyltriethoxysilane (MTES), (3-aminopropyl)triethoxysilane (APTES) or tetraethoxysilane (TEOS). In this work was used TEOS-modification which produced durable glass-like layer, which significantly increased the resistance of PDMS channel wall. For the production of giant PS also should be modified the wettability of downstream channels for this purpose PVA was used for rendering of selected channels in spatially controlled way.

Herein, the poly[2-(diisopropylamino) ethyl methacrylate-*b*-poly(ethylene-glycol) prepared by RAFT in combination with poly(1,2-butadiene)-*b*-poly(ethylene oxide) was used for the production of homogeneous pH-responsive giant PSs.

1.10 Methods for characterization of polymers and their assemblies

1.10.1 1D and 2D NMR measurements

^{1}H or ^{13}C NMR measurements are a straightforward method for determination of the polymer composition and its purity. NMR spectroscopy involves three main steps: first the sample is placed inside of the instrument, where magnetic nuclear spins are aligned in constant magnetic field, then the sample is exposed to a powerful short-term RF pulse, finally the emission of absorbed RF energy is transferred to computer where it is processed with the Fourier transform in order to obtain the spectrum. Therefore, the NMR analysis determines the molecular structure by interaction of nuclear spins when they are placed in powerful magnetic field. ^{1}H-NMR spectroscopy has been employed as one of the most important techniques for studying the molecular weights of polymers and copolymer composition.[68–70]

^{1}H-NMR spectroscopy has been successfully used for the kinetic study of RAFT polymerization. To obtain the kinetic information, data of the overall monomer and copolymer conversions versus time of reaction is used.

1.10.2 Size exclusion chromatography (SEC)

Gel-permeation chromatography (GPC) or SEC is a separation technique that is commonly used to separate macromolecules by their hydrodynamic size. In SEC, effective separation is achieved inside of a column packed with beads with pores of a given size, which retain small molecules by diffusion and exclude the large molecules. The first approach to separate high molecular weight polymers was proposed by J.C. Moore in 1964, with the use of porous cross-linked polystyrene material with controllable pore sizes. Later on, this material was replaced with more advanced gels like dextran polymers (Sephadex) or agarose (Sepharose) etc.

Thus, SEC has also the possibility to evaluate dispersity by determining of molar mass and polymer size which made SEC a very advantageous technique for polymer chemistry. The SEC measurements are based either on a calibration curve with known standards, or alternatively absolute molecular weight can be detected with appropriate detectors such as RI detector, light scattering and/or viscosimetry detectors without a known calibration standard.

1.10.3 Dynamic light scattering (DLS)

Dynamic light scattering is a technique which determines the size distribution of nano- and micron-sized particles in a solution [71]. The principle of measurement is based on the fluctuation of the intensity of scattered light on optical inhomogeneities in solution due to volume elements with polymer and without. The fluctuations occur due to Brownian motion of small particles which is a random motion of the particles suspended in the solution as a result of their collisions with the solvent molecules of the fluid. When a source of light is applied which interferes with particles causing scattering in all direction directions (Rayleigh scattering) the resulting fluctuations in scattering intensity are recorded in short time intervals, collected and analyzed.

The recorded information is analyzed by an autocorrelator, which compares changes of light intensity over time (Figure 12).

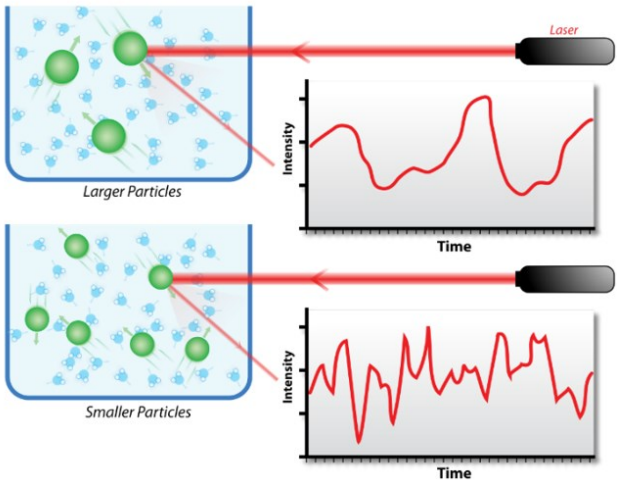

Figure 12. Hypothetical dynamic light scattering intensity for two different samples with different particle sizes [72].

The dynamic information of the particle size is obtained from the autocorrelation function of the recorded intensity fluctuations by various algorithms. The rate of Brownian motion is related to the translation diffusion coefficient D_t that can be determined from a first-order autocorrelation function. The autocorrelation function with subtracted baseline is a simple exponential decay according to equations (2), (3), and (4).

$$g^1(q;\tau) = \exp(-\Gamma\tau) \tag{2}$$

$$\Gamma = q^2 D_t \tag{3}$$

$$q = \frac{4\pi n_0}{\lambda}\sin\frac{\theta}{2} \tag{4}$$

where $g^1(q;\tau)$ is the field autocorrelation function for wave vector q and delay time τ, and Γ is the decay rate (the inverse of the correlation time), n_0 is the refractive index, λ is laser wavelength, and θ is scattering angle of the detector relative to the incident beam.

The described equations correspond to the simplest monodisperse and diluted system (to suppress the collision between particles). The value of the diffusion coefficient is then used to determine the hydrodynamic radius R_H of the spherical particles using the Stokes-Einstein equation (5),

$$D_t = \frac{k_B T}{6\pi\eta R_h} \tag{5}$$

where k_B is the Boltzmann constant, T is the absolute temperature of the solution and η is the viscosity of the solution.

1.10.4 Static light scattering (SLS)

Static light scattering is a technique that measures the intensity of the scattered light of macromolecules or proteins in solution to obtain the average molecular weight M_w. Comparing

with DLS the SLS is not monitoring the Brownian motion of particles, instead it involves recording the amount of light scattered either at one or many of angles and/or for different sample concentrations. By measuring the scattering intensity at different angles, it is possible to calculate of the root mean square radius of gyration, also called R_G. By varying the concentration, the second virial coefficient A_2 can be calculated. For the full characterization of M_w from the light scattering intensity in solution many parameters must be known: the laser intensity, the quantum efficiency of the detector, full scattering volume, refractive index (RI) of the sample, RI increment and solid angle of the detector. However, all commercial instruments are calibrated with a strong scatterer typically toluene and the refractive index increment can be measured by a differential refractometer.

For monodisperse polymer particles the common way for calculation of parameters is the Zimm equation.

$$\frac{Kc}{\Delta R(\theta,c)} = \frac{1}{M_w}\left(1 + \frac{q^2 R_g^2}{3} + O0(q^4)\right) + 2A_2 c + O(c^2) \tag{6}$$

where q is the scattering vector for polarized light, c is the solution concentration and $\Delta R(\theta, c)$ is the difference between the scattering intensity of the analyte and the scattering intensity of the solvent.

During SLS, the sample is usually measured at least at 4 concentrations and for several angles (multiangle light scattering - MALS). The obtained results are used for the so-called Zimm plot (double extrapolation of the Zimm equation to zero angle and zero concentration), from which we can derive the radius of gyration (R_G), second viral coefficient (A_2) and molecular mass (M_w).

By combining dynamic and light scattering measurements it is possible to obtain the structural parameter or the so-called ρ-ratio that provides the indication of the scattering particle topology and is simply defined as:

$$\rho = \frac{R_G}{R_H} \tag{7}$$

For spherical objects like micelles the $\rho < 1$, for vesicles it is $\rho \geq 1$ and for coils $\rho > 1.7$

1.10.5 Electrophoretic Light Scattering (ELS)

In polymer chemistry the ELS measurements are used to determine the average zeta potential (ζ) of the self-assemblies in dispersion. For ELS measurements a dispersion with particles is introduced in the cell with two electrodes, afterwards an electrical field is supplied to the electrodes, particles or molecules having a net charge, or more precisely, a net zeta potential, migrate towards the oppositely charged electrode at a velocity linked to their zeta potential. The ELS instrument measures the electrophoretic mobility (U_E) and converts the value to ζ-potential (mV) through the Henry's equation:

$$U_E = \frac{2\,\varepsilon\,\zeta\,f(ka)}{3\,\eta} \tag{8}$$

where ε is the dielectric constant of the medium and η its viscosity. Furthermore, $f(ka)$ is the Henry's function that involves Smoluchowski assumption that $f(ka) = 1.5$.

1.10.6 Small-angle X-ray scattering (SAXS)

SAXS is a type of small angle scattering techniques, that is used for investigation of various substances structures including macromolecules and self-assembled aggregates. That technique measures the small deflection with angle of 0.1-10° of a collimated beam after occurring collision with macromolecules in the size range of mesoscopic scale (1 - 100 nm). Advantages of these technique are possibility to get unique information in real time regarding the size, shape, and the spatial relationship of macromolecular self-assemblies (such as micelles, worms, vesicles or aggregates). SAXS utilizes X-ray beams which are scattered by sample, X-ray beam sources are widely available but not very suitable for thermo-unstable samples due to the heat that me be induced by the X-ray beam. Despite that, SAXS is a powerful technique for structural characterization, however, only R_G could be extracted as a direct data, for other characteristics a modeling approach is required.

1.10.7 Transmission electron microscopy (TEM)

A transmission electron microscopy is a technique that uses a beam of electrons to visualize the specimen to form an image. TEM has significantly stronger magnification then light microscopes (thousands of times smaller objects) owing to the smaller de Broglie wavelength of electrons. Transmission electron microscope is an instrument that is commonly used for analysis of morphology and structure at nanoscale level in fields of physical, biological and polymer chemistries. The first TEM was created by Max Knoll and Ernst Ruska in 1931[73], their merits were awarded the Nobel Prize in physics. TEM instruments have an enormous array of operating modes that are conventional imaging (with various contrast settings), scanning TEM (STEM), diffraction, spectroscopy, and their combinations. TEM is a primary tool for visualization of the macromolecular assemblies. Sample preparation is a crucial step in TEM, firstly sample is deposited onto TEM grid (made from carbon, copper or polymer) and upon fast drying (*e.g.*, evaporated in a heated oven, freeze-dried) the solvent is removed. Drying is a risky technique of soft matter, since images of a dried sample are not representing the sample in liquid environment. In order to increase the contrast which is preferable for soft matter staining techniques are used. A staining usually performed with heavy metals, the most popular choice for polymers is negative staining with uranyl acetate (UAc) and phosphotungstic acid (PTA). The negative staining is useful for identification of hollowness or solidness of an object, measuring of membrane-thickness and better contouring. However, fast drying and staining are not precise methods since the properties of the analyzed sample may have changed during the process. Visualization of a sample in its native state can be performed with cryo-TEM. [74–76] In this technique the sample is deposited onto on a lacey or holey carbon coated grid, and vitrified in a thin layer of solvent by freezing in liquid ethane or liquid nitrogen. Since vitrification is a very fast process in which the sample is fixed in current state without dehydration, it is the most similar conditions to macromolecules assemblies in aqueous solution. Cryo-TEM images could suffer from low rates of sample freezing, low contrast of the sample (size result does not contain the solvation layer of the particles), and contamination by hexagonal and vitreous ice. However, it is the most advantageous and suitable technique to study soft matter systems. As assumption, TEM and cryo-TEM are the mostly used techniques for the direct structural information of nano-objects as a supplement to data from light scattering methods.

1.10.8 Förster Resonance Energy Transfer (FRET):

The FRET principle considers the non-radiative energy transfer between a fluorescent donor and an acceptor. This method is used for studies related to nanoparticle-based systems,[77] drug-drug carrier compatibility [78] or membrane fusion processes[79]. The energy transfer efficiency (E) is highly dependent on the distance between the donor and acceptor in the FRET fluorophore pair, as well as lifetime of the dyes. In fact, since the energy transfer depends on the inverse sixth power of the intermolecular distance the pair distance should be in the range of 1-10 nm.

The FRET efficiency is mathematically described by equation 9 where R_o is the Förster distance between donor and acceptor at which the FRET efficiency is 50 % and R is the donor-to-acceptor separation distance. The FRET efficiency can also by determined using equation 10 where τ_{DA} and τ_D are respectively the fluorescence lifetime of the donor in the presence and in the absence of an acceptor.

$$E = \frac{R_0^6}{R_0^6 - R^6} \quad (9)$$

$$E = 1 - \frac{\tau_{DA}}{\tau_D} \quad (10)$$

2. Aims of the thesis

The aims of the thesis involve several consequent partial tasks leading to polymersomes and giant vesicles with advantageous properties for biomedical uses:

1) Development of more rapid and eco-friendly RAFT polymerization of [*N*-(2-hydroxypropyl)methacrylamide] HPMA by microwave irradiation. Preparation of relevant PHPMA copolymers by RAFT MWI with possible application in clinical medicine as high-potential hydrophilic alternatives to polyethylene oxide.

2) Preparation of pH-responsive poly([*N*-(2-hydroxypropyl)] methacrylamide)-*b*-poly[2-(diisopropylamino)ethyl methacrylate] polymer system to respond to the inherent features of tumor microenvironments, such as extracellular acidosis. Manufacturing of the pH-responsive self-assemblies by microfluidics loaded with DOX and testing *in vitro* and *in vivo*.

3) Synthesis of different ROS-responsive polymers based on hydrophilic PHPMA and hydrophobic phenylboronic acid pinacol ester methacrylates with following characterization and degradation studies. Production of ROS-responsive monodisperse polymersomes by microfluidic flow-focusing method, with subsequent *in vitro* and *in vivo* experiments.

4) Manufacturing of pH-Responsive giant polymer vesicles based on a polyethylene glycol-*b*-poly[2-(diisopropylamino)ethyl methacrylate] via polydimethylsiloxane (PDMS) microfluidics for biomedical applications.

3. Microwave-assisted RAFT polymerization of *N*-(2-hydroxypropyl) methacrylamide and its relevant copolymers

The PHPMA is a water-soluble (highly hydrophilic), nonimmunogenic and nontoxic polymer which is frequently used as a macromolecular carrier for low molecular weight drugs, especially anticancer chemotherapeutic agents. PHPMA drug conjugates are under intense research with applications in different treatment delivery systems, while PHPMA copolymers are considered as a perspective alternative with higher composition variability and enhanced targeting delivery. Also, PHPMA is a good candidate for replacing poly(ethylene oxide) (PEG), because of the immunogenic reactions reported for PEG. [80,81]

The PHPMA and its copolymers is mainly synthesized by CLRP. As was mentioned in chapter 1.5.1 the first attempt of controlled PHPMA polymerization was done by Matyjaszewki et al. [49] using ATRP, however the resulting copolymers had high molecular weight distributions and low conversions. The optimization of HPMA polymerization by ATPR with improved conversion, product dispersity and M_w control was recently reviewed by [82]. RAFT aqueous polymerization of PHPMA copolymer with defined molecular weight and low $Đ$ was reported in 2005 by McCormick et al. [83] In 2013 Özdemir et al. [84] reported on RAFT of PHPMA and its copolymers in DMF and MeOH by conventional MWI at 70C° using 4-cyano-4-(((ethylthio)carbonothioyl)thio)pentanoic acid as chain transfer agent and AIBN as an initiator. Nevertheless, in this study the homopolymerization was investigated only in MeOH with relatively low conversions ~40 %.

Although to date, the RAFT technique has been widely employed for the polymerization of PHPMA and its copolymers [85–87], the polymerization times are still relatively long, from several hours to almost a day. In order to improve this issue microwave irradiation was applied.

Microwave irradiation has presently been successfully applied to organic synthesis, material science, polymer chemistry, and other disciplines. During the past decades, the microwave-assisted synthesis has been effectively used for CRLP as an alternative to conventional thermal heating methods. Results demonstrated a higher conversion of monomers, faster Rp, and excellent control over molecular weight distributions. [88–90] Microwave assisted RAFT polymerization in addition to aforementioned advantages, sufficiently accelerates the process and thus leads to reduction of overall time of reaction, to minutes or hours depending on the target weight-average molecular weight (M_w). The favorable effect of MWI on RAFT polymerization was demonstrated for styrene [91,92], methyl methacrylate [93], methyl acrylate [92], *N*-isopropylacrylamide [94], diallyldimethylammonium chloride (DADMAC) [95], vinylcyclicsilazane [96] and vinyl pyridines [84] monomers.

Herein, we investigate the preparation of PHPMA homo- and copolymers by microwave-assisted RAFT polymerization. For the microwave-assisted RAFT polymerization of HPMA in various solvents we used the commercial and commonly used 4-cyano-4-(phenylcarbonothioylthio)pentanoic acid (named CTA1) and the synthesized 4-cyano-4-(((ethylthio)carbonothioyl)thio)pentanoic acid (named CTA2) in the presence of 4,4′-azobis(4-

cyanovaleric acid) (V-501) as an initiator (Scheme 1). We investigated various stoichiometric ratios between the monomer, CTA and initiator.

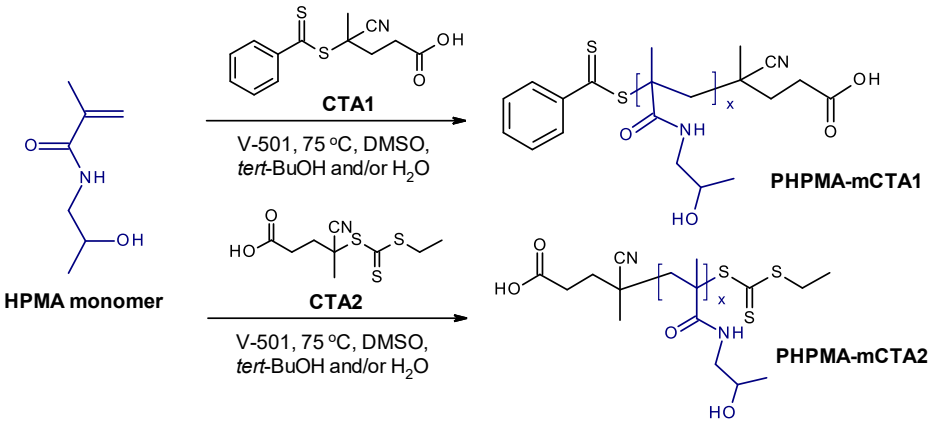

Scheme 1. General synthetic procedure for MWI-assisted RAFT polymerization of the monomer HPMA to produce PHPMA-mCTAs using 4-cyano-4-(phenylcarbonothioylthio)pentanoic acid (CTA1) and 4-cyano-4-(((ethylthio)carbonothioyl)thio)pentanoic acid (CTA2) as RAFT agents.

In addition, we produced several copolymers, thus illustrating the "livingness" of the system. MWI-RAFT homopolymers and copolymers were compared with standard preparation by a conventional heating method. Optimal conditions for the preparation of PHPMA homopolymers (named PHPMA macroCTAs – PHPMA-mCTA) and PHPMA-based copolymers using MWI-assisted RAFT polymerization were established.

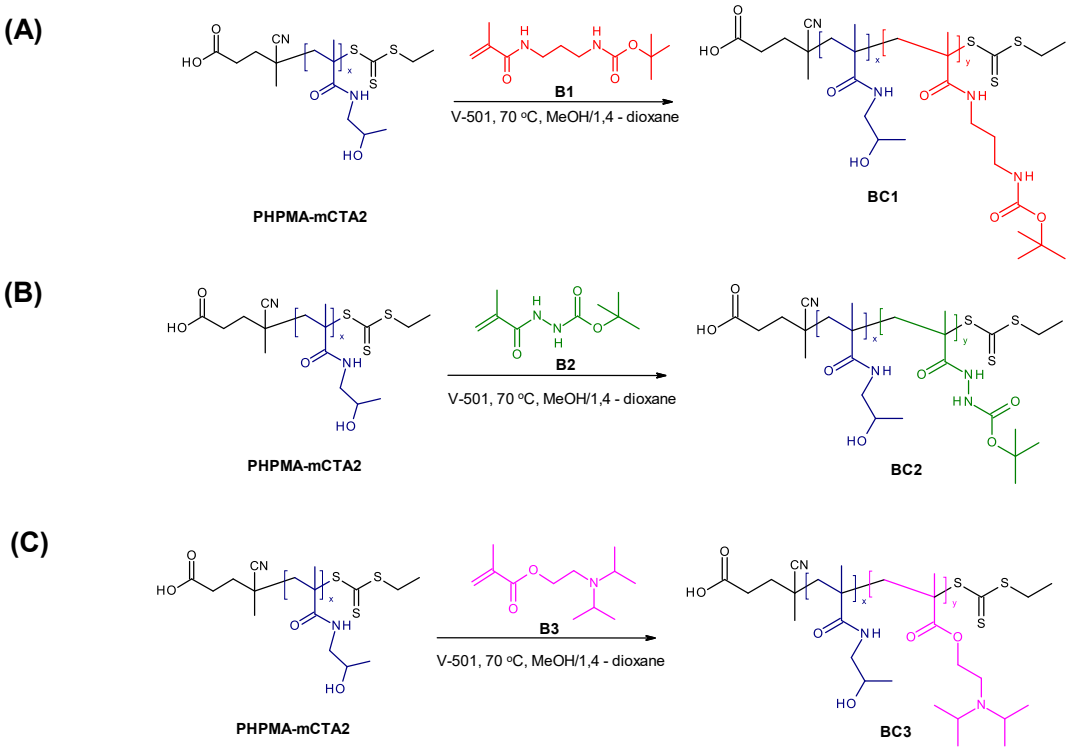

Scheme 2. RAFT-mediated synthesis of diblock copolymers via MWI. (A) PHPMA-*b*-bocAPMA (BC1), (B) PHPMA-*b*-PMABH (BC2) and (C) PHPMA-*b*-PDPA (BC3).

3.1 Synthesis of monomers and RAFT agent.

The monomer HPMA was synthesized according to reference [97]. *N*-(3-Boc-aminopropyl)methacrylamide (boc-APMA) was obtained commercially. *N′*-Methacryloyl *tert*-butyl carbazate with a protected hydrazide bond (MABH) was synthetized according to reference. [98] The RAFT agent 4-cyano-4-(((ethylthio)carbonothioyl)thio)pentanoic acid (CTA2) was synthesized according to reference. [99]

3.2 Instruments and analyses

Microwave-mediated RAFT polymerizations were done on a Biotage Initiator Sixty microwave system. The CTA, monomers, PHPMA homopolymers and their copolymers were evaluated by ^{1}H NMR (Bruker Avance 600 MHz spectrometer with $CDCl_3$, methanol-d_4 or D_2O (acidified with DCl; pH ~ 3.0) as the solvent at 295 K. The molecular weight characterizations were performed by SEC using an HPLC Ultimate 3000 system (Dionex, USA).

3.3 Results and discussion

3.3.1 Kinetic study of microwave-assisted RAFT polymerization of HPMA

Several parameters must be evaluated and optimized for the preparation of well-defined PHPMA homo- and copolymers via MWI RAFT polymerization. It is necessary to carefully select the CTA for successful RAFT polymerization in microwave. The chosen CTAs (based on dithiobenzoates and trithiocarbonates**)**, are known to be compatible and generally work well in the polymerization of methacrylates and methacrylamides [87,99]. Targeted molecular weight was 25,000 $g \cdot mol^{-1}$ for PHPMA (due to threshold of renal clearance and avoiding polymer accumulation) envisaging further biological applications. [100]

For the kinetic studies we used a stock solution of HPMA (1.2 g, 3.99×10^{-5} mol at DP 175), CTA and initiator V-501 ([CTA]/[I] 1/0.5 and 1/0.2) in certain amounts of DMSO, *tert*-BuOH and/or DI water. An aliquot (1 mL) from a stock solution was transferred to several glass vials equipped with a magnetic stir bar and purged for 30 minutes with Argon. The MWI-RAFT experiments were conducted at 70 °C, with a reaction time ranging from 60 min to 12 h. At different time points, the polymerization was stopped and reaction mixture was quickly quenched in liquid nitrogen. The sample solution (20 µL) was directly analyzed by ^{1}H NMR spectroscopy. By comparing the remaining monomer concentration to the initial monomer feed, the monomer conversion was calculated. The remaining fraction of the sample solution was precipitated into cold acetone or an acetone/ether mixture 3/1 (*v*/v), dried, and analyzed by SEC.

In the first series, for the MWI-RAFT polymerization of HPMA, DMSO (aprotic solvent) was chosen due to its solubility properties. The selected molar ratio was: [M]/[CTA]/[I] = 175/1/0.5 with quite high initiator concentration, the resulting conversion data, *Mn* and dispersity (*Đ*) are summarized in Table 2.

As can be seen, for the CTA1 the maximum conversion was only ~25%, no linear increase of molecular weight in time, and poor dispersity. From the third hour of kinetic study, the *Mn* values were closer to each other, indicating that longer polymerization times are not required for these selected reaction conditions. Slightly better situation was observed for CTA2, the monomer conversions reached were ~75%, however, low-quality control over the molecular weight and relatively low dispersity ($Đ \leq 1.2$) were reached. As observed for CTA1, the similar molecular weights obtained within 4 h and 5 h for CTA2 demonstrate that conversion reached its maxima for these selected reaction conditions, and no longer polymerization time is needed. A possible reason for the limited conversion and obtained dispersity could be the selected solvent that might cause negative impact on the polymerization process.

Table 2. Conversion data, number-average molecular weight (*Mn*) and dispersity (*Đ*) for MWI-assisted RAFT polymerization of HPMA. DMSO was used as a solvent in the presence of CTA1 and CTA2 with V-501 as initiator at molar ratio [M]/[CTA1]/[I]=175/1/0.5 and [M]/[CTA2]/[I]=175/1/0.5 for target *Mn* ~ 25 000 g·mol^{-1}.

	Time (h)	**Conv.[a] (%)**	***Mn*,th[b] ^{1}H NMR (g·mol^{-1})**	***Mn*, SEC (g·mol^{-1})**	***Đ***
CTA 1	1	11	3 065	5 550	1.1
	2	20	5 340	7 100	1.08
	3	25	6 600	8 200	1.08
	4	24	6 350	8 500	1.07
	5	25	6 610	8 400	1.06
CTA 2	1	12	3 155	5 220	1.18
	2	30	7 490	6 140	1.14
	3	50	12 300	11 120	1.15
	4	75	18 340	15 330	1.09
	5	70	17 130	16 700	1.1

[a] Determined by ^{1}H-NMR analysis.

[b] Theoretical $Mn = [M]_0/[CTA]_0 \times \text{conv.} \times M_{w\,HPMA} + M_{w\,CTA}$

Newly, Thang et al. investigated the effect of solvents on the conventional thermal RAFT polymerization of HPMA [101]. The authors conclude that the intra- and inter-molecular hydrogen bonding between polymer chains in aprotic solvents has a negative influence (poor controllability) on the RAFT polymerization process (Figure 13). The deviation from linearity in aprotic solvents like DMSO might be attributed to radical loss, which is most likely due to radical-radical termination, which results in dead chains and hence low conversions.

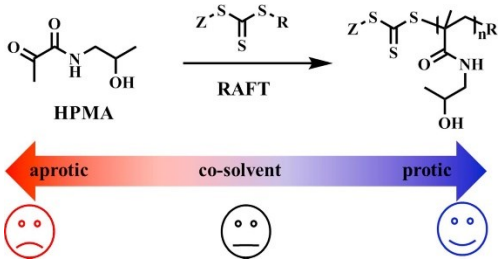

Figure 13. Influence of the protic and aprotic solvents for the RAFT polymerization of HPMA. [101]

It should also be noted that MWI absorbed by the solvents may have an impact on polymerization. The ability of solvents to convert MW energy into heat is determined by the so-called loss tangent (tan δ), where for DMSO, tan $\delta = 0.825$, that is classified as ultrahigh MW absorption [102]. High MW absorption solvents have been observed to cause considerable chain-end loss during RAFT polymerization, possibly as a result of accidentally high starting temperatures in the reaction medium, which leads to chain transfer or other side reactions during polymerization [103]. Indeed, during first kinetic experiments with DMSO, it was not possible to achieve good control (in particular, low $Đ$) for both CTAs. In order to find appropriate reaction conditions other solvent with less microwave absorption were investigated for achievement of better control (*i.e.*, low $Đ$, predictable molar mass, faster polymerization times) over the polymerization of HPMA.

For the next kinetic study we selected *tert*-BuOH, a moderately polar solvent with a slightly lower ability to convert MW energy into heat (tan $\delta = 0.80$) comparing to DMSO; this makes it very attractive for use in MWI synthesis which might provide faster reaction rate. Moreover, *tert*-BuOH is a nontoxic and relatively inexpensive solvent that was never used in MWI-RAFT HPMA polymerization. Therefore, we tested the efficiency of *tert*-BuOH at the same molar ratios as those used for DMSO - [M]/[CTA]/[I] = 175/1/0.5. The results are shown in Table 3. Despite that for the CTA1 the conversion was increased to ~52 % and up to 80 % for CTA2, the molecular weight was not controlled during the first 5 h of polymerization in both cases. As before, there was no consistently good agreement between theoretical and experimental molecular weights, however, the obtained $Đ$ values obtained were slightly improved.

Table 3. Conversion data, number-average molecular weight (*Mn*) and dispersity (*Đ*) for MW-assisted RAFT polymerization of HPMA. *Tert*-BuOH was used as solvent in the presence of CTA1 and CTA2 with V-501 as initiator in molar ratio [M]/[CTA]/[I]=175/1/0.5 for target *Mn* ~ 25 000 g·mol^{-1}.

	Time (h)	**Conv.[a] (%)**	***Mn*,th[b] ^{1}H NMR (g·mol^{-1})**	***Mn*, SEC (g·mol^{-1})**	***Đ***
CTA 1	1	38	9 900	9 999	1.03
	2	44	11 415	9 700	1.20
	3	48	12 940	11 000	1.10
	4	52	13 440	14 145	1.03
	5	50	12 930	12 460	1.04
CTA 2	1	25	6 270	9 340	1.05
	2	80	19 480	20 490	1.13
	3	68	16 600	18 380	1.05
	4	71	17 321	20 000	1.07
	5	70	17 080	19 000	1.11

[a] Determined by ^{1}H-NMR analysis.

[b] Theoretical $Mn = [M]_0/[CTA]_0 \times \text{conv.} \times M_{w\,HPMA} + M_{w\,CTA}$

Still the targeted *Mn* (~ 25,000 g·mol^{-1}) was not reached within a short time, indicating a slow rate of polymerization (Rp). This problem might be related to inappropriate ratios between CTA and initiator, [CTA]/[I] = 1/0.5. Indeed, it is a well-known fact that concentration of active species influences the Rp in RAFT polymerization, whereas decrease of total active species concentration has a positive impact on Rp. Due to fast propagation rate for acrylamide monomers such as HPMA with use of initiators with high efficiency or decomposition rate the Rp might be fast with even low initiator concentration [104,105].

The amount of initiator, V-501 was reduced by 2.5 times in relation to CTAs, with all the other parameters kept constant. At this molar ratio Rp was still quite slow, with highest M_w at 12 h; however, the HPMA dispersity and conversion in case of both CTAs proceeded in a controlled fashion, producing polymers with low *Đ*, as seen in Table 4.

Table 4. Conversion data, number-average molecular weight (*Mn*) and dispersity (*Đ*) for MW-assisted RAFT polymerization of HPMA. *Tert*-BuOH was used as solvent in the presence of CTA1 and CTA2 with V-501 as initiator in molar ratio [M]/[CTA]/[I]=175/1/0.2 for target *Mn* ~ 25 000 g·mol^{-1}.

	Time (h)	**Conv.[a] (%)**	***Mn*,th[b] ^{1}H NMR (g·mol^{-1})**	***Mn*, SEC (g·mol^{-1})**	***Đ***
CTA 1	1	16	4 330	4 400	1.13
	2	20	5 340	6 410	1.11
	3	29	7 620	7 700	1.10
	4	40	10 390	9 100	1.07
	5	49	12 666	10 000	1.10
	12	88	22 540	22 760	1.03
CTA 2	1	15	3 870	2 900	1.16
	2	22	5 450	6 133	1.10
	3	34	8 430	7 400	1.13
	4	49	12 035	12 890	1.04
	5	60	14 680	15 000	1.11
	12	91	22 125	26 320	1.04

[a] Determined by ^{1}H-NMR analysis.

[b] Theoretical $Mn = [M]_0/[\mathrm{CTA}]_0 \times \mathrm{conv.} \times M_{w\,\mathrm{HPMA}} + M_{w\,\mathrm{CTA}}$

For the CTA1 and CTA2 with molar ratio [*M*]/[CTA]/[I] = 175/1/0.2 in *tert*-BuOH, the controlled living character of polymerization was demonstrated by plotting the natural logarithm of the total monomer conversion versus time. The pseudo-first-order kinetic plot showed a linear trend in the increase of M_n with conversion and low dispersity ($Đ$ ~ 1.03 to 1.04 at the 12 h time point), however, CTA2 exhibits more controlled behavior (red lines, Fig. 14B) than that observed for the polymerization using CTA1 (blue lines, Fig. 14A and Table 4). Good agreement between theoretical and experimental molecular weights was achieved, as well (Figure 14).

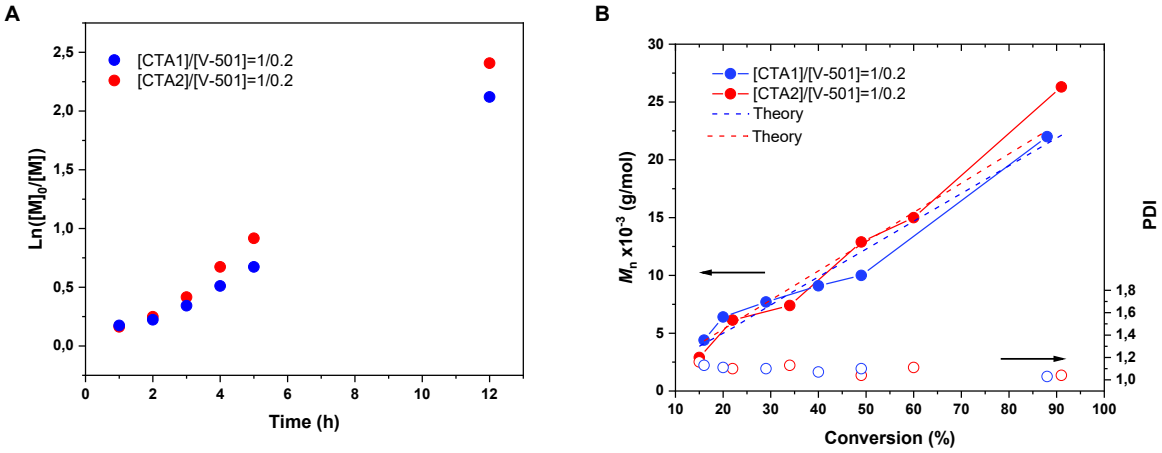

Figure 14. (A) Semilogarithmic plots and (B) molecular weight and dispersity *vs* conversion of microwave-assisted RAFT polymerization of HPMA in *tert*-BuOH.

The obtained SEC chromatograms of homopolymers PHPMA-mCTA1 (Figure 15A) and PHPMA-mCTA2 (Figure 15B) demonstrate a monomodal distribution, as indicated by the overlap of the SEC traces. SEC traces showed a shift to lower retention time as a function of polymerization time, indicating an increase in molecular weight (Table 4). These results proposed that MWI- RAFT polymerization of HPMA in *tert*-BuOH at selected stoichiometry proceeds in a controlled manner, with exceptional results for CTA2.

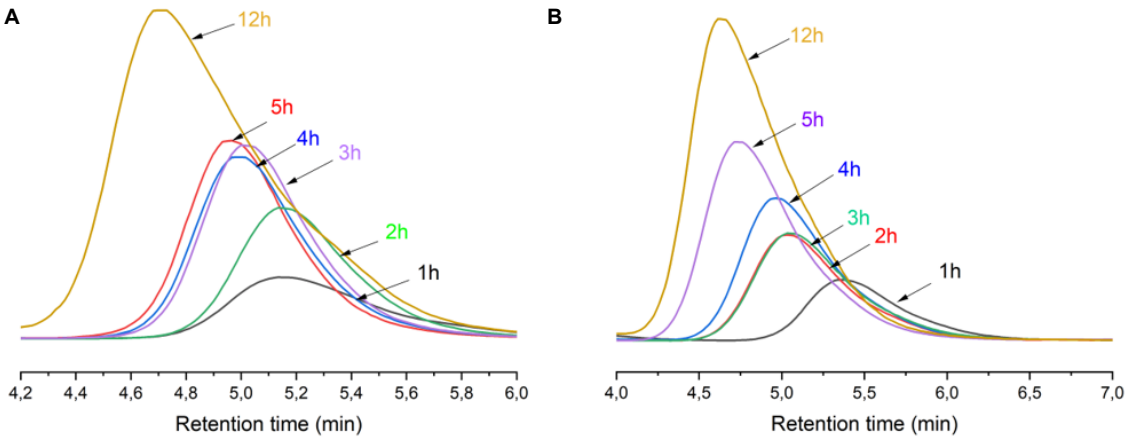

Figure 15. SEC chromatograms in MeOH/acetate buffer of the PHPMA-macroCTA1 (A) (CTA1, in Table 4) and (B) PHPMA-macroCTA2 (CTA2, in Table 4) with molar ratio ([M]/[CTA]/[I] = 175/1/0.2) at varying polymerization times.

We next explored the opportunities for using water as a solvent for clean process and to prevent pollutions. Numerous publications report the use of water as an environmentally benign solvent for chemical reactions with the application in MWI as a solvent. [106,107] Water is readily available, nontoxic, and nonflammable solvent for use in organic synthesis. Moreover, water is a medium MW-absorbing solvent with a loss tan δ of 0.123 [102], that makes it very suitable for MW-assisted synthesis. Additionally, HPMA monomer is highly soluble in aqueous medium, that makes water an excellent solvent for MWI-RAFT polymerization of HPMA. Therefore, the same set of experiments with molar ratio [M]/[CTA]/[I] = 175/1/0.2 for both CTAs was performed but with water as a solvent. The polymerization was carried out for different times (0.5–4 h). The kinetic plots of $Ln([M]_o/[M]_t)$ for both CTAs versus polymerization time, demonstrates excellent linearity for CTA2 (Figure 16A). The conversion of the HPMA monomer versus molecular weight and dispersity was also linear, indicating that polymerization proceeded in a well-controlled manner (Figure 16B).

Table 5. Microwave-assisted RAFT polymerization of HPMA in water. Conversion data, number-average molecular weight (*Mn*) and dispersity (*Đ*) for MWI-assisted RAFT polymerization of HPMA. V-501 as the initiator in a molar ratio of [M]/[CTA]/[I] = 175/1/0.2 for the target *Mn* ~ 25000 g·mol^{-1}.

	Time (h)	Conv.[a] (%)	*Mn* $_{th}$[b] ^{1}H NMR (g·mol^{-1})	*Mn*, SEC (g·mol^{-1})	*Đ*
CTA1	0.5	20	5 340	2530	1.95
	1	28	7 295	10420	1.08
	1.5	36	7 796	14950	1.05
	2.0	47	12060	17950	1.04
	3.0	58	14810	22040	1.04
	4.0	56	12810	22750	1.05

CTA2	0.5	12	3 150	4300	1.19
	1	40	9 875	9000	1.16
	1.5	50	12280	12400	1.13
	2	61	14920	15600	1.09
	3.0	71	18970	19200	1.08
	4.0	80	21080	24200	1.09

[a] Conversion data determined by ^{1}H NMR analysis. [b] Theoretical Mn = $[M]_0/[CTA]_0 \times$ conv. $\times$ $M_{w\,HPMA} + M_{w\,CTA}$.

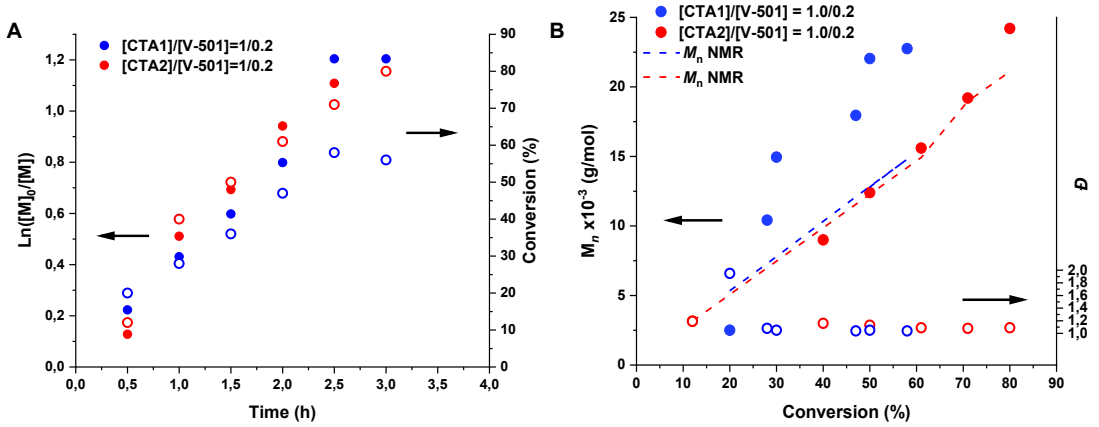

Figure 16. (A) Semilogarithmic plots and (B) molecular weight and dispersity versus conversion of microwave-assisted RAFT polymerization of HPMA in water.

As seen, PHPMA-mCTA prepared in water was obtained with a higher conversion, and the polymerization time was four times reduced (Table 5) comparing with that in DMSO (Table 2) or *tert*-BuOH (Table 3 and 4). At this reaction conditions, we finally obtained the desired target *Mn* (~ 25,000 g·mol^{-1}) within a comparatively short period of time (4.0 h, CTA2).

SEC measurements were performed for all samples from the kinetic study by MWI in water. The variations in the elution profiles of PHPMA-mCTA1 and PHPMA-mCTA2 are depicted in Figure 17 (A) and (B), respectively, and the maxima of the different peaks (*Mn*) are presented in Table 5.

The unimodal SEC traces of homopolymerization in corresponding ratios proceeds in a controlled manner; similar results were obtained with *tert*-BuOH for both CTAs and in water for CTA2, shifts towards higher molecular weights in SEC traces indicates good livingness and control during the synthesis of the macroCTA RAFT agents (Figure 17B).

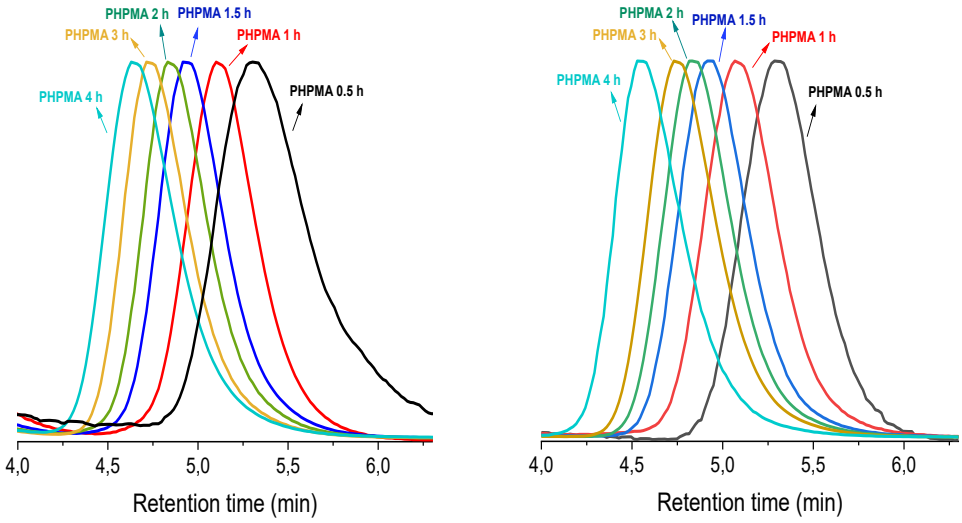

Figure 17. SEC traces in MeOH/acetate buffer of PHPMA-mCTA1 (a) (CTA1, Table 2) and PHPMA-mCTA2 (b) (CTA2, Table 2) at varying polymerization times.

Although the *Mn* values acquired by SEC for CTA1 are reasonable, pseudo-first-order kinetic plots were not reached, and the *Mn* values obtained by NMR differed significantly from those obtained by SEC. This difference could happen due possible degradation of CTA1 in water at 70 °C (due to its aromatic moiety) [108], and the chain-end functionality of the growing chain might have been compromised. The UV and RI traces would be similar for samples with low dispersity (UV reflects terminal dithiobenzoate and therefore number of molecules while RI reflects mass of molecules, which is dependent not only on number, but also molecular weight of the molecules) and if almost all the polymer chain would contain dithiobenzoate group, however, if the fraction of dead chains is increased (*i.e.*, those not containing a dithiobenzoate moiety at their end), then deviation between UV and RI traces would appear. Such deviation could be evaluated by observing discrepancies among the SEC-UV, SEC-RI and SEC-LS data [104]; truly, discrepancies especially among the SEC-UV and SEC-RI were observed for the CTA1 hinting that the growing chain from CTA1 could be compromised (Figure 18 A).

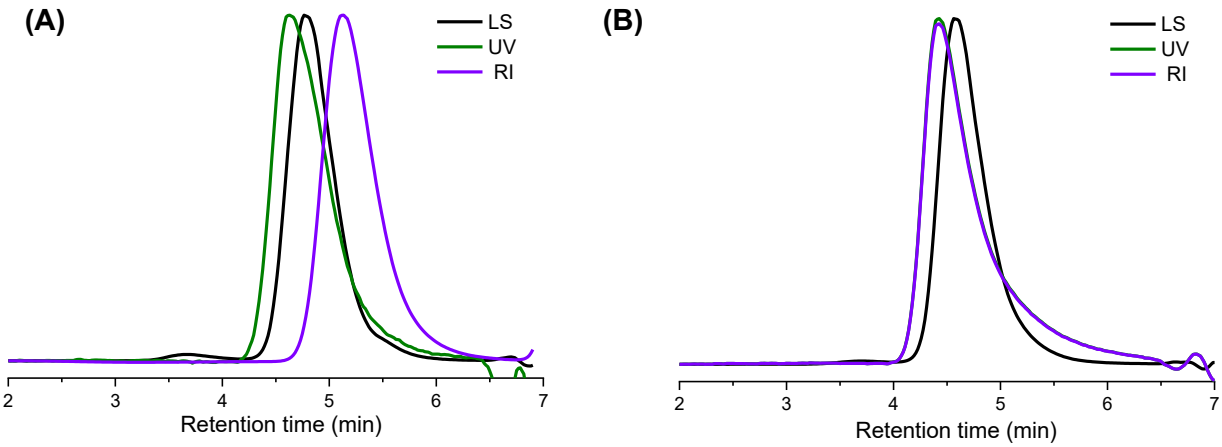

Figure 18. SEC chromatograms (LS - black, UV - green and RI - magenta) in MeOH/acetate buffer of the PHPMA-macroCTA1 (A) (CTA1, in Table 5) and (B) PHPMA-macroCTA2 (CTA2, in Table 5) at polymerization time of 4h.

As comparison, the same experimental set ([M]/[CTA]/[I] = 175/1/0.2) was performed by the conventional heating method, with water as a solvent (Table 6).When compared to MWI (Table 5), the acquired results reveal a slightly slower reaction rate, broader dispersities, and homopolymer conversion (~48 % for CTA1; ~65 % for CTA2, Table 6), indicating that MWI via RAFT in water is a preferable solution for obtaining HPMA homopolymers.

Table 6. Conventional thermal heating RAFT polymerization of HPMA in water. Conversion data, number-average molecular weight (*Mn*) and dispersity (*Đ*) for MWI-assisted RAFT polymerization of HPMA. V-501 as the initiator in a molar ratio of [M]/[CTA]/[I]=175/1/0.2 for the target *Mn* ~ 25 000 g·mol^{-1}.

	Time (h)	Conv.[a] (%)	$Mn_{,th}$[b] ^{1}H NMR (g·mol^{-1})	*Mn*, SEC (g·mol^{-1})	*Đ*
CTA1	0.5	3	1 030	-	-
	1	14	3 800	6 045	1.39
	1.5	25	6 540	9 866	1.17
	2.0	25	6 540	12 210	1.08
	3.0	38	9 800	16 880	1.08
	4.0	48	12 310	16 610	1.09
CTA2	0.5	10	2 900	4 756	1.55
	1	25	6 850	7 910	1.25
	1.5	35	9 500	12 350	1.10
	2	45	12 120	14 800	1.09
	3.0	59	16 100	19 300	1.07
	4.0	65	17 400	17 860	1.11

[a] Conversion data determined by ^{1}H NMR analysis. [b] Theoretical $Mn = [M]_0/[CTA]_0 \times \text{conv.} \times M_{w\,HPMA} + M_{w\,CTA}$

3.4 Synthesis of PHPMA-*b*-bocAPMA, PHPMA-*b*-PMABH and PHPMA-*b*-PDPA copolymers via MWI.

3.4.1 Microwave-assisted block copolymerization.

Finally, by growing a second block via MWI-assisted RAFT polymerization, the livingness and end-group functionality of the previously synthesized PHPMA-mCTA2 were demonstrated. Several monomers were selected such as *N*-(3-Boc-aminopropyl)methacrylamide (bocAPMA) (B1, Scheme 2), *N´*-methacryloyl *tert*-butyl carbazate (MABH) (B2, Scheme 2) and 2-(diisopropylamino)ethyl methacrylate (DPA) (B3, Scheme 2). These monomers can readily polymerize with other vinylic monomers and already have been tested in several biological *in vitro* and *in vivo* experiments. Thus, B1 and B2 contain *tert*-Boc protected multifunctional groups in

their composition that could be deprotected to a free amine with several reagents including HCl/MeOH, Me3Sil, or heat (185 °C) for subsequent "universal" post-reaction modifications for a variety of applications, such as small interfering RNA (siRNA) delivery [109] or for imaging and diagnostics by functionalization of B1 [110]; B2 is a successful pH-labile hydrazone linkage-based copolymer of HPMA that can be functionalized with various drugs for pH-controlled activation [111]. B3 is an highly-pH-sensitive monomer that undergoes a hydrophobic/hydrophilic transition within a small pH window of 6.30 < pH < 6.95, which is similar to the pH of tumor cell microenvironment and makes the block copolymer useful for supramolecular self-assembly towards several structures for numerous applications [2,112–115].

The mCTA2 was chosen because it produced best results in the kinetic studies. The BCs were successfully obtained (Table 7) with desirable *Mn* values, as determined by the SEC traces towards lower elution volumes, indicating an increase in molecular weights (Figure 19). ^{1}H NMR spectroscopy was used to determine the composition of each BC copolymer. The ^{1}H NMR spectra of the diblock copolymers (BC1 – Figure 19) show a singlet signal at chemical shift 4.8 ppm corresponding to the protons of −OH group from the HPMA repeating units. The peak is overlapped by the signal corresponding to residual methanol-d_4. The broad singlet signal at δ = 3.9 ppm (**d**) is attributed to the methine proton from the −C*H*–(OH) group. Furthermore, the signal corresponding to methylene protons from the pendant group (−C(O)–NH–CH_2−) at δ = 2.9-3.3 ppm, marked as (**c**), overlaps with signals from -NHCH_2- (f and h) methylene protons of bocAPMA monomer repeat units. The spectrum also demonstrated a broad characteristic signal for methylene protons from the main polymer chain at δ = 1.70 ppm, labeled (**a**) ((CH$_3$)C–CH_2−), which is overlapped by -CH$_2$-CH_2-CH$_2$- (**g**) methylene protons at δ= 1.55-2.1 ppm and signals in the range δ = 0.8-1.3 ppm (**b** and **e**) typical of methyl groups from the PHPMA backbone ((CH_3)C–CH$_2$−) and the pendant group (CH_3–CH(OH)), respectively. Strong signal at δ= 1.45 ppm is related to methyl protons (CH_3)$_3$- (**i**) of bocAPMA side-chain. Moreover, a broad signal was also detected at 7.3-7.7 ppm (−C(O)–N*H*−) for the amide groups in the composition of both blocks.

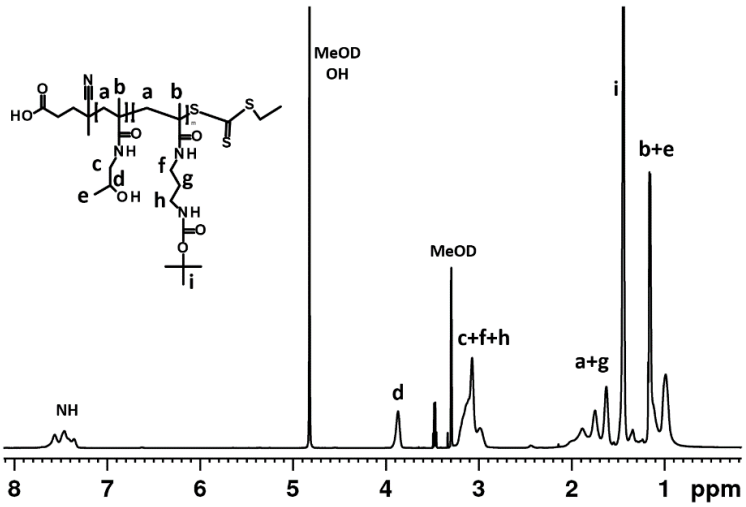

Figure 19. ^{1}H-NMR spectrum of PHPMA-*b*-bocAPMA diblock copolymer (BC1) in methanol-d$_4$.

For BC2 – the characteristic proton signals corresponding to the monomer repeating units from the PHPMA-*b*-PMABH diblock copolymer are assigned in the ^{1}H NMR spectra given in Figure 20. As can be seen, no big difference was observed in comparison to the Figure 19, due to the similar chemical structure. The number-average molecular weight *Mn* (NMR) of the corresponding BC1 is shown in Table 7.

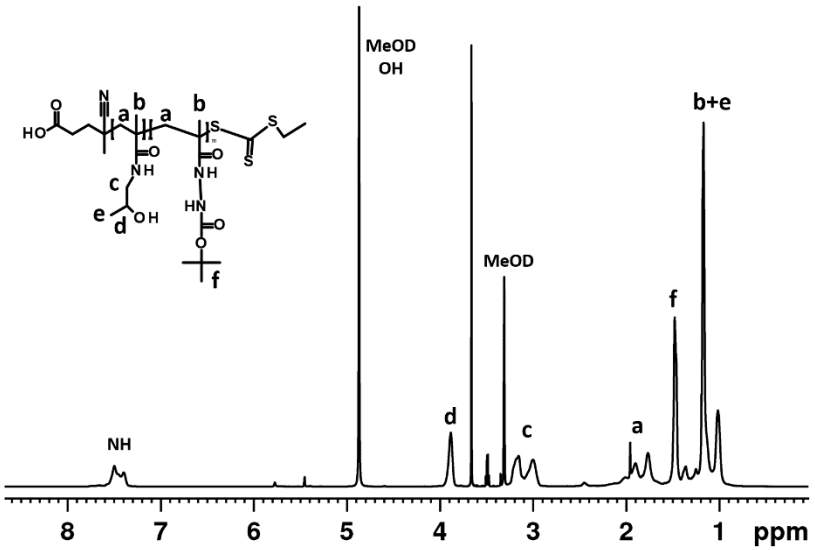

Figure 20. ^{1}H-NMR spectrum of PHPMA-*b*-PMABH diblock copolymer (BC2) in methanol-d_4.

The characteristic proton signals corresponding to the monomer repeating units from the PHPMA-*b*-PDPA diblock copolymer (BC3) are assigned in the ^{1}H NMR spectra given in Figure 21. The number-average molecular weight *Mn* (NMR) of the correspond BC2 is represented in Table 7.

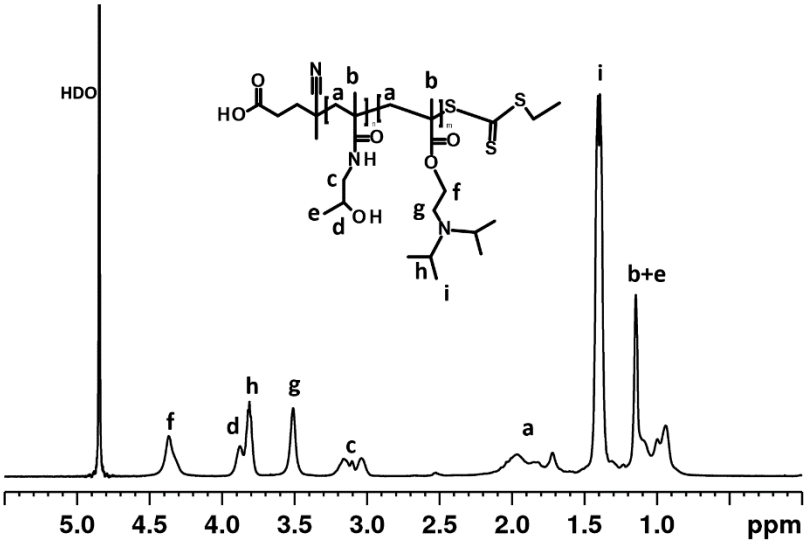

Figure 21. ^{1}H-NMR spectrum of PHPMA-*b*-PDPA diblock copolymer (BC3) in acidic D_2O.

Along with NMR, was performed SEC measurements in order to evaluate *Mn* (Figure 22).

Table 7. Experimental conditions and macromolecular characteristics of the block copolymers prepared via microwave-assisted RAFT polymerization.

Sample	$[M]_0/[CTA]_0/[I]_0$	Time (h)	Conv. (%)	*Mn*, NMR[c] ($g \cdot mol^{-1}$)	*Mn*, SEC ($g \cdot mol^{-1}$)[d]	*Đ*
$PHPMA_{29}$-mCTA2	100/1/0.2	3	93[a]	4130	4410	1.04
$PHPMA_{29}$-*b*-$bocAPMA_{47}$ (BC1)	75/1/0.5	6	96[a]	15500	25000	1.06
$PHPMA_{29}$-*b*-$PMABH_{44}$ (BC2)	75/1/0.5	6	30[a]	12208	22200	1.38
$PHPMA_{29}$-*b*-$PDPA_{34}$ (BC3)	75/1/0.5	6	45[b]	11851	13720	1.14

[a]Determined by ^{1}H NMR spectroscopy in methanol-d_4 or using end-group analysis.
[b]Determined by ^{1}H NMR in acidic D_2O using end-group analysis.
[c] *Mn* was calculated via ^{1}H NMR spectroscopy according to $Mn = (n\text{MU} \times M_w \text{ HPMA}) + (n\text{MU} \times M_{w\ \text{monomer}}) + M_{w\ \text{CTA}}$.
[d]Determined by SEC in MeOH/acetate buffer, pH 6.5, 80/20 vol%.

It is noteworthy that lower conversion was observed for BC2 and BC3 for the growth of the second block. Since the same PHPMA-mCTA was used for the growth of BC1 (~ 96% conversion), we hypothesized that this result could not have been caused by low reinitiation efficiency of the macroRAFT agent nor by decreased reinitiation efficiency due to the molecular weight of the macroRAFT agent (hindrance effect); the cause of low conversion remains unclear, and still is a subject for investigation.

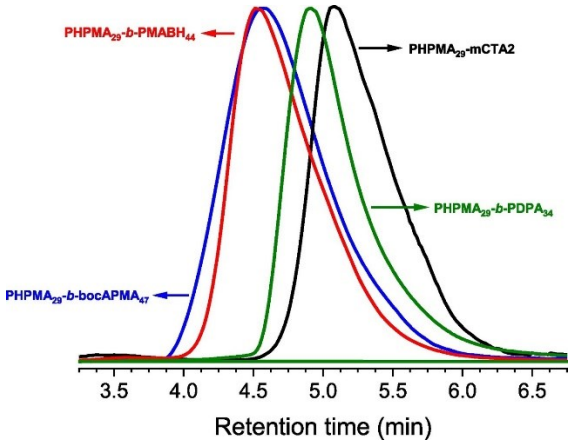

Figure 22. SEC chromatograms in MeOH/acetate buffer of the $PHPMA_{29}$-mCTA2 (black lines) $PHPMA_{29}$-*b*-$bocAPMA_{47}$ (blue lines), $PHPMA_{29}$-*b*-$PMABH_{44}$ (red lines) and $PHPMA_{29}$-*b*-$PDPA_{34}$ (green lines) diblock copolymers (Table 7).

By way of comparison, the block copolymers were made using the conventional heating method under identical conditions. The obtained results demonstrated the obtention of the BCs with generally broader dispersities and lower or similar conversions (~30% for BC1; 20% for BC2; 50% for BC3, Table 8) if compared with synthesis via MWI (Table 7). The observed differences between theoretical molecular weight (NMR) and experimental molecular weight (SEC) could be due to SEC's strong dependence on the calibrant, solvent, and column, as well as the fact that it is a relative method requiring a molecular weight detector, as opposed to NMR, which is an absolute primary method requiring no calibration [116].

Table 8. Experimental conditions and macromolecular characteristics of the block copolymers prepared via conventional thermal heating RAFT polymerization.

Sample	$[M]_0/[CTA]_0/[I]_0$	Time (h)	Conv.[a] (%)	Mn ,NMR[b] ($g \cdot mol^{-1}$)	Mn ,SEC ($g \cdot mol^{-1}$)	$Đ$
$PHPMA_{29}$-mCTA1	100/1/0.2	3	93	4 130	4 410[c]	1.04
$PHPMA_{29}$-*b*-$bocAPMA_{47}$ (BC1)	75/1/0.5	6	30	4 850	10 600[c]	1.11
$PHPMA_{29}$-*b*-$PMABH_{44}$ (BC2)	75/1/0.5	6	20	8 140	10 300[c]	1.44
$PHPMA_{29}$-*b*-$PDPA_{34}$ (BC3)	75/1/0.5	6	50	10 582	12 190[c]	1.32

[a]Determined by ^{1}H NMR spectroscopy in methanol-d_4 and acidic D_2O using end-group analysis; [b] Mn was calculated via ^{1}H NMR spectroscopy according to $Mn = (n\text{MU} \times M_{w\ \text{HPMA}}) + (n\text{MU} \times M_{w\ \text{monomer}}) + M_{w\ \text{CTA}}$; [c]Determined by SEC in MeOH/acetate buffer, pH 6.5, 80/20 vol %.

4. Preparation of pH-responsive poly([*N*-(2-hydroxypropyl)] methacrylamide)-*b*-poly[2-(diisopropylamino)ethyl methacrylate] polymer system to respond to the inherent features of tumor microenvironments, such as extracellular acidosis.

4.1 Introduction

As was mentioned, cancer causes 1 in 6 deaths worldwide, according to most recent survey by the International Agency for Research on Cancer reported that the global mortality caused by cancer is approximately 9.6 million in 2018 (21% higher than in 2008) [117]. This number is predicted to be 19.3 million by 2025 [118], calling for immediate improvements in cancer therapies [119].

The current cancer treatments include surgery, radiation and chemotherapy, however, these procedures cause side-effects that damage healthy tissues.

Chemotherapeutic therapies are still one of the most important cancer treatments, but developing novel techniques to improve efficacy while reducing side effects remains a challenge.

Anthracycline doxorubicin (DOX), one of the most often used chemotherapeutic drugs, is effective in the treatment of lymphoma, acute myeloid leukemia, and breast cancer.

The main limitation of this chemotherapeutics is short blood circulation time, cardiotoxicity, and unavoidable exposure to normal tissues that kills healthy cells [120]. Recent efforts have embraced the construction of nanoparticles that can navigate in the body and deliver anticancer medications to tumor locations, improving therapeutic efficacy while lowering overall toxicity. Therefore, DOX-based nanoparticles are currently considered as a promising candidate for overcoming such noteworthy drawback. Mainly, DOX-loaded nanoparticles are administrated intravenously, upon intravenous injection nanomaterials quickly covered on their surface by biomolecules that are present in body fluids leading to formation of "protein corona" (vide section biological and physical barriers). This adsorption influences the nanoparticle's physicochemical properties, including hydrodynamic size, surface charge and aggregation behavior, which leads to rapid clearance. This undesired barrier could be overcome by using a coating with highly hydrophilic polymer such as *N*-(2-hydroxypropyl)methacrylamide (HPMA). Another obstacle is the preferred accumulation, which can be solved by passive tumor targeting strategy which utilized previously mentioned EPR effect (vide section **Biological and physical barriers**), typically nanocarriers with D_H < 100 nm can diffuse across cancer tissues resulting in enhanced permeation and retention (Figure 23).

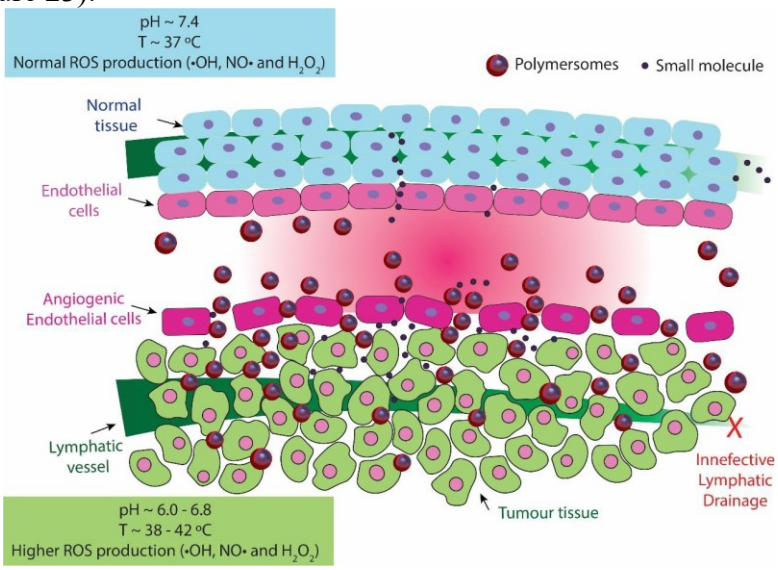

Figure 23. Schematic representation of the accumulation of polymersomes in tumor sites due to the EPR effect.

Advances in controlled-living polymerization processes have recently encouraged the preparation of a wide range of macromolecules with controllable architecture, functionality, composition, and topology, allowing the engineering of self-assemblies with controllable membrane thickness, flexibility, size, permeability, and, most importantly, responsiveness [121–123].

As was discussed earlier the polymersomes (PSs) can be made responsive to pH of tumor microenvironment which has a slightly acidic pH (6.5~6.8), depending on the tumor type (vide section 1.1.5 Tumor microenvironment targeting). [124,125].

Therefore, the DOX-loaded pH-responsive polymersomes are capable of transporting the cargo while navigating through healthy tissues (pH ~ 7.4), and rapidly releasing the payload in tumor microenvironment (the slightly acid pH), which is presumably a suitable strategy to enhance the therapeutic efficacy, with reduction of DOX side effects. For this goal we used a design of the amphiphilic diblock copolymer prepared by RAFT, based on hydrophilic PHPMA and hydrophobic pH-responsive poly(2-(diisopropylamino)ethyl methacrylate (PDPA) as building units for polymersomes. The PDPA completely dissociates when the pH drops below its pKa ~ 6.8 in less than a second [112]. As was mentioned, the polymer poly(*N*-(2-hydroxypropyl) methacrylamide (PHPMA) was chosen as the hydrophilic stabilizing segment due to its protein-repelling characteristics (which presumably restricts protein adsorption) and prolonged blood circulation lifetime. [126,127].

Although the utility of pH-responsive polymersomes for cancer treatment is obvious, current polymeric vesicle manufacturing techniques typically result in polydisperse assemblies with poor control over average size. [128]. Moreover, the presence of multiple morphologies is often observed. This problem can be avoided by producing the assemblies via microfluidics. The control over the mixing conditions enables high reproducibility, narrow size distribution and the precise tuning of the nanostructures size [129]. Encapsulation of drugs into size-defined and monodisperse PSs can improve cellular uptake due to a more consistent biodistribution of the therapeutic agent in the target site. The herein prepared DOX-loaded pH-responsive polymersomes were characterized by DLS, SLS, small-angle X-ray scattering (SAXS), and imaged by cryo-TEM. The effectiveness of the DOX-loaded PSs was tested *in vitro* by the cellular uptake analysis and cytotoxicity study, and *in vivo* by assessing the biodistribution of the assemblies and their antitumor efficacy in mice bearing EL4 lymphoma model.

We aimed at fundamentally contributing to cancer nano-therapy by designing DOX-loaded, stimuli-responsive polymeric vesicles (polymersomes) capable of responding to the inherent features of tumor microenvironments, with possible enhancement of the therapeutic outcomes, and reduction of the side-effects of the widely used DOX (Figure 24).

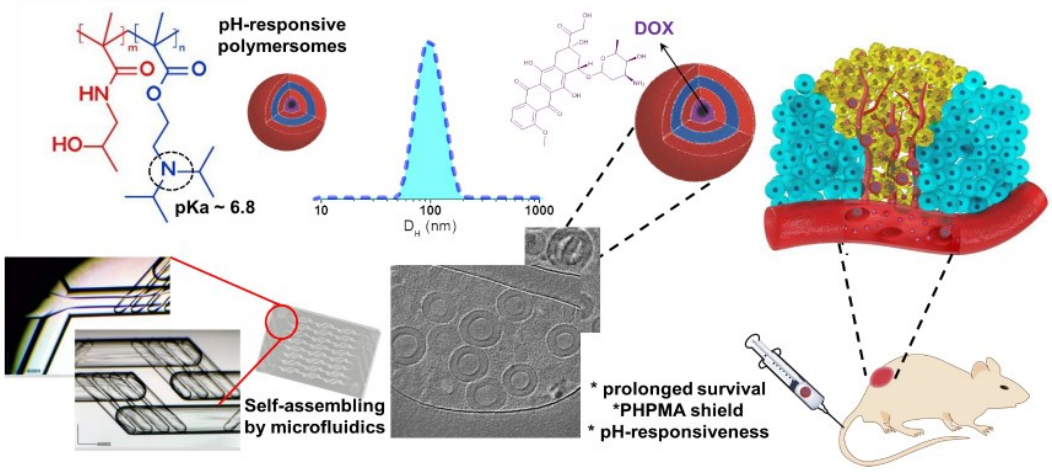

Figure 24. Schematic illustration of the preparation of pH-responsive polymersomes based on PHPMA-*b*-PDPA block copolymers loaded with DOX by microfluidics and the *in-vivo* approach for a treatment with prepared formulation of a lymphoma tumor of a mouse.

4.2 Synthesis of monomers and RAFT agent

Firstly, the HPMA was synthesized as previously mentioned (Figure 25), secondly, the CTA-Azide was synthesized from the derivatization of the 4-cyano-4-(phenylcarbonothioylthio)pentanoic acid (CTA-OH) with 3-azido-1-propanol according to the chemical route given in Figure 26.

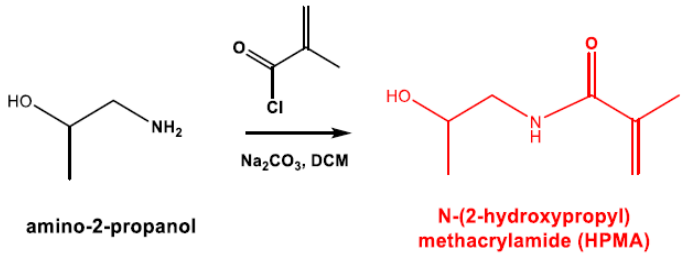

Figure 25. Synthetic approach used to synthesize HPMA.

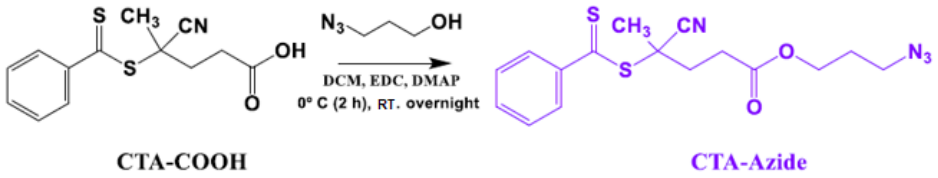

Figure 26. Synthetic route used in the synthesis of the CTA-Azide.

FTIR (Figure 27) revealed the existence of the azide group in the CTA-Azide, and it was used as a chain transfer agent to generate the first segment of the block copolymers.

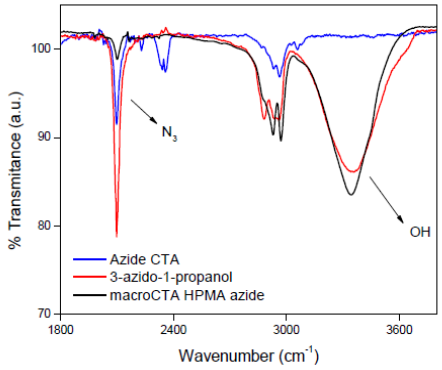

Figure 27. FTIR spectra of 3-azido-1-propanol (precursor) and CTA-azide. The arrows indicate the corresponding chemical groups.

Afterwards, the azide-terminated PHPMA macroCTA was synthesized (Mn = 5000 g·mol^{-1}, M_w/Mn = 1.06), purified, characterized by ^{1}H NMR and SEC (Figure 28), and further used as chain transfer agent for polymerization.

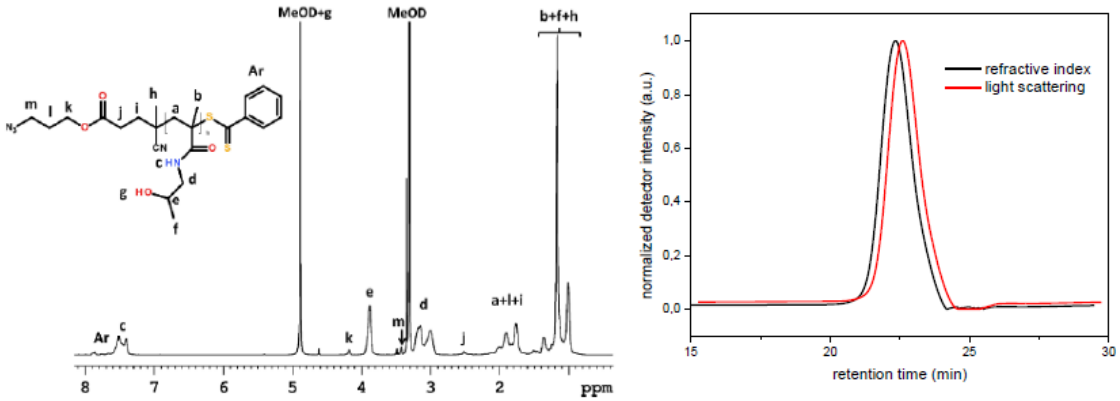

Figure 28. ^{1}H NMR spectrum of PHPMA macroCTA acquired in MeOH-d4 (left) and SEC traces for PHPMA macroCTA synthesized *via* RAFT in MeOH/acetate buffer pH 6.5 (80/20 *v*/*v*) (right).

At higher temperatures (~ 70 ºC), the azido group is known to undergo 1,3-cycloaddition to carbon double bond, which should be avoided in the polymerization process. [130–132]. However, this problem could be diminished in methacrylamide monomers (such as HPMA) because of their low reactivity and the presence of a methylene group on the monomer's double bond, resulting in steric hindrance and preventing undesirable side reactions. [132–134] In the obtained final products azide groups were proven by FTIR and by ^{1}H NMR where methylene (CH_2) groups (m, l, k) were visible next to the azide group. (Figure 28). Furthermore, the azide group functionality was also validated by the successful coupling of the DBCO-cyanine dyes by a copper-free click chemistry (see below).

The second block was then produced by RAFT using the PHPMA macroCTA, as illustrated in Figure 29. The molecular weight characteristics were evaluated by SEC (Table 9, Figure 30). The hydrophilic-to-hydrophobic weight ratios were determined using ^{1}H NMR (representatively available for PHPMA35-*b*-PDPA75 in Figure 30).

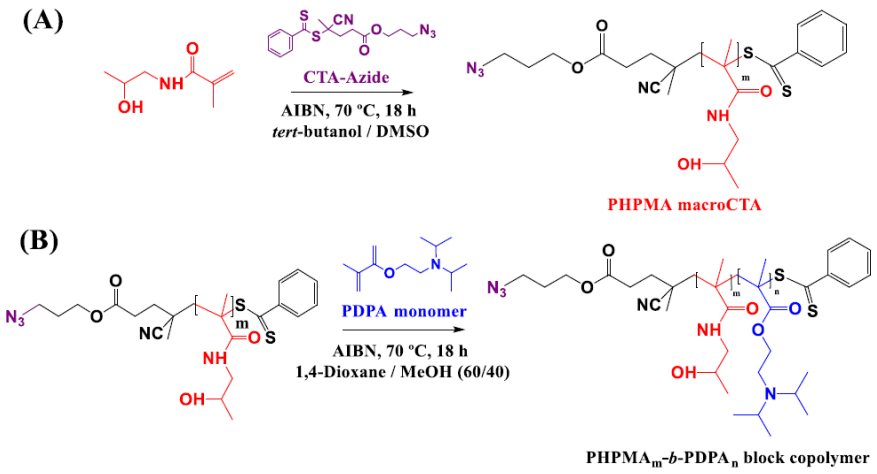

Figure 29. Synthetic route used in the synthesis of azide-terminated PHPMA macroCTA (A) and of N3-PHPMAm-*b*-PDPAn diblock copolymers (B).

Table 9. Synthetic parameters and molecular weights of the synthesized PHPMA$_m$-*b*-PDPA$_n$ block copolymers.

Block Copolymer	[M]$_0$/[CTA]$_0$/[I]	*Mn* SEC (g.mol^{-1})	Đ	Conversion (%)	Yield (%)	*wt* (%) PHPMA
PHPMA$_{35}$-*b*-PDPA$_{26}$	50 / 2 / 1	10600	1.25	69	53	53
PHPMA$_{35}$-*b*-PDPA$_{43}$	100 / 2 / 1	14200	1.09	68	58	35
PHPMA$_{35}$-*b*-PDPA$_{75}$	150 / 2 / 1	21000	1.05	72	56	24

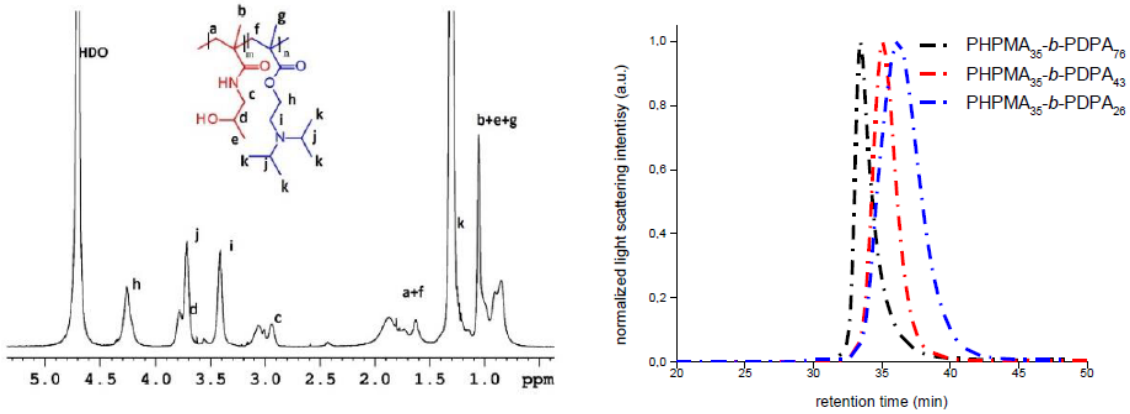

Figure 30. ^{1}H NMR spectrum of PHPMA$_{35}$-*b*-PDPA$_{75}$ diblock copolymer obtained in D$_2$O/DCl (pH ~ 2) (left) and SEC traces in DMF for PHPMA$_m$-*b*-PDPA$_n$ diblock copolymers synthesized *via* RAFT (right).

The summary of data in Table 9 shows the production of block copolymers with narrowly-distributed molecular weights (PDI ≤ 1.25) ranging from 10.6 to 21.0 kDa with various PDPA content for further preparation of thermodynamically stable polymersomes. The pH-responsive block copolymers behavior was assessed by ζ-potential titration and representative results are shown in Figure 31.

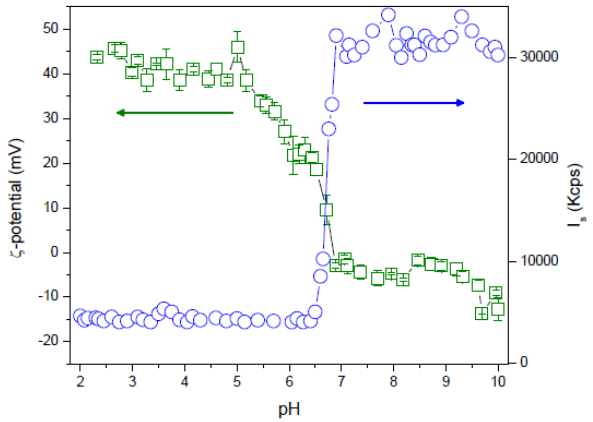

Figure 31. ζ-potential (squares) and light scattering intensity (spheres) as a function of pH for $PHPMA_{35}$-*b*-$PDPA_{75}$ block copolymer in water at initial copolymer concentration c = 1.0 $mg \cdot mL^{-1}$.

The obtained results clearly indicated that the pKa of the synthesized block copolymer ($PHPMA_{35}$-*b*-$PDPA_{75}$) is in the range 6.8-6.5, which agrees with data from literature. [135] Accordingly, PDPA chains are protonated at pH < 6.5, as suggested by the positive ζ-potential values and reduced light scattering intensity (open circles). Typically, the degradation of $PHPMA_m$-*b*-$PDPA_n$ nanoparticles leads to the appearance of two populations of scattering objects: free molecularly dissolved block copolymer chains, and a very small number of large aggregates. [135]

4.3 Manufacturing and Characterization of the Polymersomes

Polymersomes are efficient active agent carrier particles that are used as a clever platform for drug, gene and protein delivery. [136] The control over particles size and polydispersity is critical for effective therapies. With the advent of the microfluidic technique, new opportunities for production of nanostructures with a number of advantages including non-excessive consumption of expensive chemicals and high, solid and fast throughput controlled by high-precision equipment. Additionally, by using micromixer platforms the encapsulation of hydrophilic and hydrophobic substances can be accomplished. [129] However, the approach was only seldom studied for the production of PDPA-based polymersomes. [128] Considering the aforementioned, the self-assembly of the diblock copolymers as polymeric vesicles was conducted using a microfluidic chip with a micro-mixing design (Figures 32 A-B) for the manufacturing of either DOX-free and DOX-loaded polymersomes. For proper dissolving of the amphiphilic diblock copolymer was selected THF/MeOH 80/20 *v*/*v* as the organic phase to dissolve the three block copolymers and PBS (pH 7.4) as the aqueous phase. The self-assembly of $PHPMA_{35}$-*b*-$PDPA_{26}$ (f ~ 53%) produced small particles (Figure 32 E) with average size that is incompatible with polymersomes (D_H = 30.6 nm).

Core-shell nanoparticles (micelles) were probably obtained due to the high content of hydrophilic PHPMA in the copolymer chains. With increase of hydrophobic content, the diblocks $PHPMA_{35}$-*b*-$PDPA_{43}$ (f ~ 35%) and $PHPMA_{35}$-*b*-$PDPA_{75}$ (f ~ 24%) predominantly produced polymersomes as confirmed by TEM (Figures 32 F and G, respectively).

Furthermore, the structure sensitive parameter value ($R_G/R_H \sim 1$) are trustable experimental evidence (Table 10) with the presence of the hollow spheres (polymersomes). However, self-assemblies made from PHPMA$_{35}$-*b*-PDPA$_{43}$ constantly form small particles together with the polymeric vesicles and therefore, we have decided to use the block copolymer PHPMA$_{35}$-*b*-PDPA$_{75}$ which demonstrated single morphology. In order to investigate the influence of the flow rates on the final properties, the aqueous flow rate was a chosen as a variable parameter (50, 100 and 200 µL.min^{-1}) while the flow rate of the organic phase (100 µL.min^{-1}) was kept constant (Table 10 and Figure 32.)

Table 10. Physicochemical characteristics of the PHPMA$_{35}$-*b*-PDPA$_{75}$ polymersomes produced by microfluidics.

Flow Rate (WP/OP)	D_H (nm)	D_G (nm)	$\rho = D_G/D_H$	PDI	ζ (mV)
50/100	179.2	168.2	0.94	0.05	-4.1
100/100	151.0	161.0	1.06	0.06	-3.5
200/100	113.8	123.4	1.08	0.06	-3.8

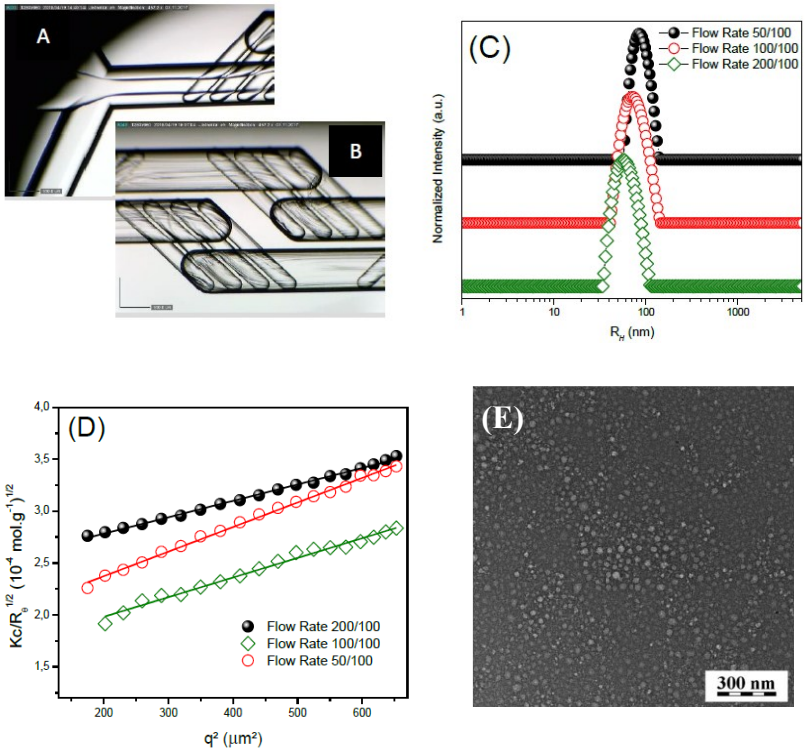

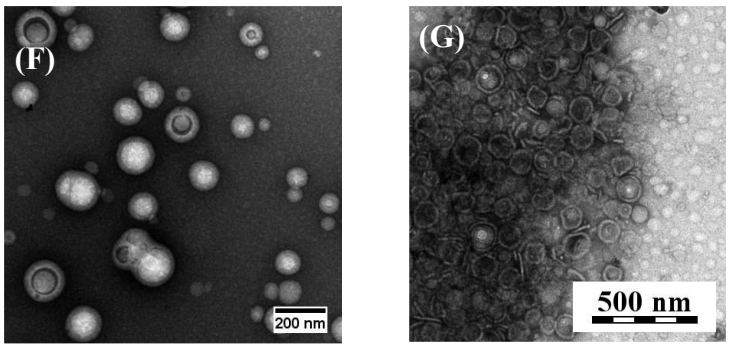

Figure 32. Microfluidic chip (A) used for the production of the polymersomes with micro-mixing chambers (B). Distributions of R_H for PHPMA$_{35}$-*b*-PDPA$_{75}$ polymersomes produced using different flow rates (C). Analogous static light scattering data ($1/I_{sc}$ *vs*. q^2) data (D). TEM images of PHPMA$_{35}$-*b*-PDPA$_{26}$ (E), PHPMA$_{35}$-*b*-PDPA$_{43}$ (F) and PHPMA$_{35}$-*b*-PDPA$_{75}$ (G) polymersomes engineered by microfluidics at aqueous/organic phase flow rate 200/100.

The significant advantage of microfluidics is highly precise control over the mixing conditions which enabled the generation of highly reproducible polymersomes across different batches, low polydispersity (PDI < 0.1), and precise control over the size.

The data presented in Table 10 and Figure 32 C show that the size of polymersomes decreases with increasing flow rate. This happens due to reduction in mixing time between phases, which results in faster aggregation kinetics and smaller particles. As the width of the focused stream is decreased by increasing the flow rate of the water streams, causing the decrease in the diffusion length between the polymer solution and the water, which leads to faster mixing between the phases and faster nucleation and aggregation occurs, therefore smaller polymersomes are produced. The TEM image of PHPMA$_{35}$-b-PDPA$_{75}$ polymersomes prepared with a flow rate ratio of 200/100 is shown in Figure 32 G and illustrates the engineering of quasi-monodisperse vesicles.

The values of the structure sensitive parameter ($\rho = R_G / R_H$), ranging from 0.94 to 1.08 obtained with DLS and SLS, also indicate the prevalence of highly hydrated objects that are compatible with hollow spheres (vesicles). The R_G values were taken from the SLS data in Figure 32 D.

Once the conditions for the preparation of the drug-free pH-sensitive polymersomes were established, the same procedure was used to prepare polymersomes containing doxorubicin and cyanine dyes for biodistribution studies and FRET. The polymeric vesicles loaded with DOX (95.0 nm) were slightly smaller in size compared to DOX-free polymersomes (101.7nm) according to DLS (Figure 33 A), however, narrow (PDI < 0.10) polydispersity was observed in both cases (Table 11). The size of obtained PS is preferable for nanomedicines that need to circulate for a long time and accumulate in tumors. [137,138] For the colloidal nanocarriers the slightly negatively charged surfaces are suitable, as higher positive or negative values are usually associated with rapid blood excretion.[139] According to ζ-potential values the polymeric vesicles are effectively shielded by the PHPMA shell through steric forces. The free-loaded and dox-loaded polymersomes of PHPMA$_{35}$-*b*-PDPA$_{75}$ were evaluated by SAXS (Figure 33 B) and imaged by cryo-TEM (Figures 33 C and D) [3].

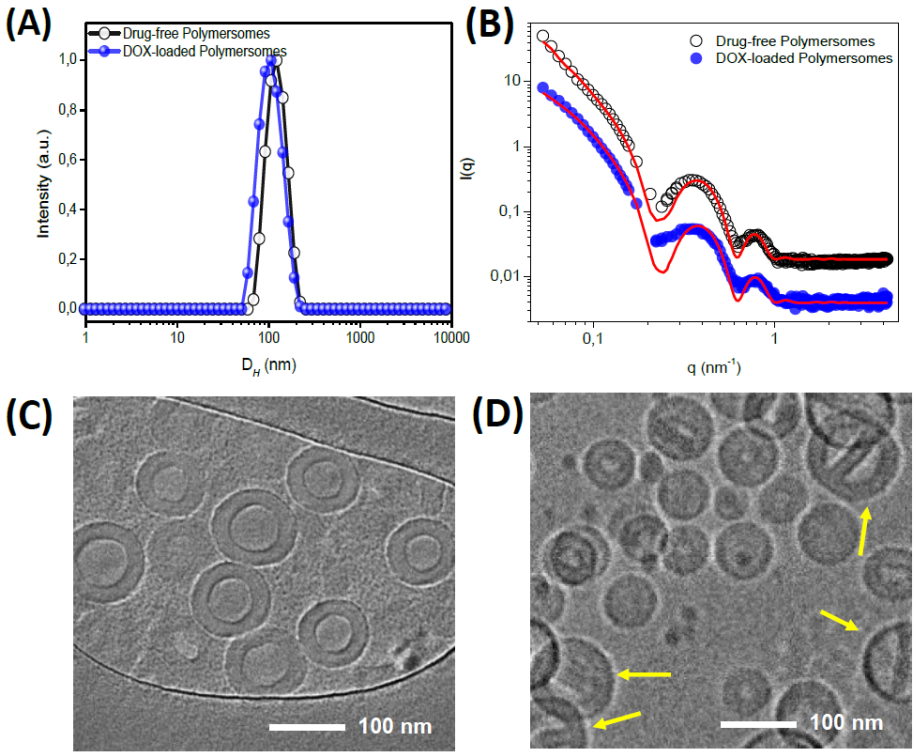

Figure 33. DOX-free and DOX-loaded PHPMA35-*b*-PDPA75 polymersomes: size distribution obtained by DLS (A) and analogous SAXS profiles (B), cryo-TEM images for DOX-free (C) and DOX-loaded (D) assemblies.

Table 11. Structural features of the prepared DOX-free and DOX-loaded polymersomes.

Entry	D_H (nm)[a]	PDI[a]	t_t (nm)[b]	t_h (nm)[b]	ζ potential (mV)[c]	LC (%)[d]	EE (%)[d]
DOX-free polymersomes	101.7	0.06	10.7	4.5	-8.8	-	-
DOX-loaded polymersomes	95.0	0.08	10.8	4.4	-3.9	9.8	53.1
Cy3-Cy5 labeled polymersomes	90.3	0.07	-	-	-10.4	-	-
Cy7-labeled polymersomes	92.2	0.05	-	-	-11.3	-	-

a) Measured by DLS; b) Measured by SAXS; c) Measured by ELS; d) Measured by HPLC.

The well-defined SAXS profiles (figure 33 B) confirm the polymeric vesicles structure. The proper fitting was possible only when bilayer vesicles shape factor was used with the thickness of the PHPMA shell in contact with water (t_h = 4.5 nm) and the thickness of the PDPA layer (t_t =

10.7 nm) as variable parameters. DOX loading had almost no effect on these dimensions (t_h = 4.4 nm and t_t = 10.8 nm, respectively). The cryo-TEM images also displayed vesicular structures with diameter~ 70-90 nm, that is in rational agreement with the size distributions acquired by DLS (Figure 33A). The data from cryo-TEM usually undersize relative to DLS, since the last one's measurements are based on intensity of light scattering in solvated state, while cryo- TEM gives number-average of diameters. Moreover, on cryo-TEM images was observed DOX crystals in the aqueous core of DOX-loaded polymersomes (Figure 33 D), that is typical for the liposomal formulations containing DOX. [140,141]

In order to supplement the assembly-disassembly investigations FRET measurements were performed. The FRET refers to non-radiative energy transfer process between an excited-state fluorescent donor (Cy3) and a ground-state acceptor (Cy5). The aim of this study was to investigate the self-assembly/disassembly process in different pH conditions according to the FRET principle. The copper-free click chemistry was used for covalent attachment of cyanine dye pairs cyanine 3-DBCO (Cy3-DBCO) and cyanine 5-DBCO (Cy5-DBCO) to the block copolymer and microfluidics was used for the polymersomes using a mixture 80:10:10 m/m/m of PHPMA$_{35}$-*b*-PDPA$_{75}$, Cy3-PHPMA$_{35}$-*b*-PDPA$_{75}$ and Cy5-PHPMA$_{35}$-*b*-PDPA$_{75}$. A schematic representation of the click chemistry reaction between the Cy3 and Cy5 dyes with the azide groups on the surface of the polymersomes represented is in Figure 34 A. The coupling and formation of dual fluorescent Cy3-Cy5 polymersomes was evaluated by Fluorescence Lifetime Correlation Spectroscopy (FLCS) measurements (Figure 34 B, C). The diffusion time values obtained (τ_D = 3.69 ms for the Cy3 channel and τ_D = 3.53 ms for the Cy5 channel) are very similar, demonstrating that both dyes were successfully conjugated to the block copolymer chains and are thus incorporated in the self-assembled structure.

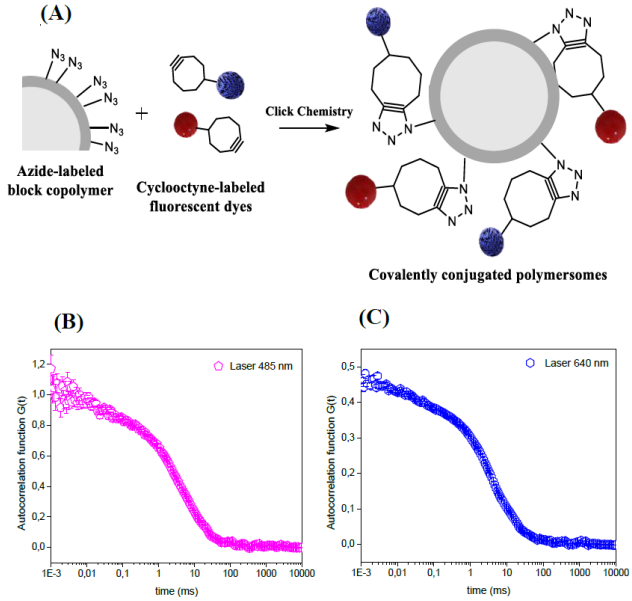

Figure 34. Representation of the click chemistry reaction between Cy3, Cy5 and the block copolymer (A), fluorescence correlation spectroscopy data for Cy3-Cy5-PHPMA35-*b*-PDPA75 polymersomes collected in Cy3-channel (λ_{ex} = 485 nm and λ_{em} = 505 nm) (B) and Cy5-channel (λ_{ex} = 640 nm and λ_{em} = 655 nm) (C).

FRET efficiency was calculated using Equation 10, the distributions are shown in Figure 35.

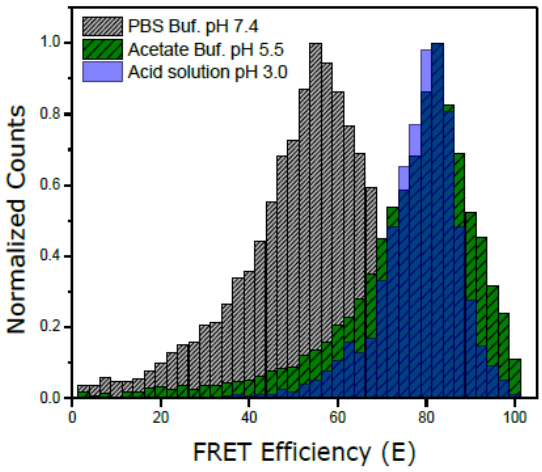

Figure 35. FRET efficiency histograms of Cy3-Cy5-polymersomes incubated in phosphate buffered saline pH 7.4 (gray bars), acetate buffer pH 5.5 (green bars) and acid solution pH ~ 3.0 (blue bars).

The FRET efficiency of Cy3-Cy5-polymersomes at pH 7.4 was E = 53.5 ± 0.2 and when assemblies were subjected to pH 5.5 and 3.0 it increased to 80.0 ± 0.1 and 80.2 ± 0.1 respectively. These values certainly reflect changes in the structure of the polymersomes mediated by various pH environmental conditions. The changes in both τ_{DA} and τ_D caused by disassembly of polymersomes, due to protonation of PDPA at pH < pKa ~ 6.8, with possible subsequent reorganization of free chains in which highly hydrophobic dyes Cyanine 3-DBCO and Cyanine 5-DBCO are sheltered in order to avoid the contact with the polar solvent. In such self-organized nonpolar environment within free block copolymer chain the inter dye distance is considerably reduced, thus increasing the FRET efficiency. The obtained data indicate that pH-dependent behavior of $PHPMA_{35}$-*b*-$PDPA_{75}$ polymersomes can be exploited for the delivery of therapeutic agents into sites of action with specific slightly acidic microenvironment.

4.4 *In Vitro* Evaluations of DOX-Loaded Polymersomes

The DOX loading content (LC) and encapsulation efficiency (EE) were determined by HPLC. The quantities were determined by using an analytical curve with a linear response in the range 0.001 - 0.5 mg. mL^{-1}. The values were calculated using the following equations:

$$LC\ (\%) = \frac{\text{DOX amount in PSs}}{\text{Mass of PSs}}\ X\ 100 \qquad (11)$$

$$\text{EE}\ (\%) = \frac{\text{DOX amount in PSs}}{\text{DOX Feeding}} X\ 100 \qquad (12)$$

The loading content of DOX into polymersomes and the encapsulation efficiency were found to be 9.8 % and 53.1 %, respectively (Table 11). After that, the DOX release profiles were tested in simulated physiological conditions (pH 7.4), pathophysiological conditions (pH ~ 6.5) and the acid environment of endosomes and lysosomes (pH ~ 5.5); the data are presented in Figure 36 A. The DOX release rate is much faster at slightly acidic environments, due to protonation of the PDPA block, with release of ~ 70-80 % of the encapsulated DOX within 24 h and 80-90 % after 48 h. At physiological pH = 7.4 DOX-loaded polymersomes demonstrate stability with 22 % of DOX release at first 24 h. This study indicates that at pH > pKa, pH-responsive polymersomes are stable and capable of transporting anticancer drugs into the bloodstream without significant drug leakage.

Further, polymersomes were used for cellular uptake and cytotoxicity experiments, with EL4 lymphoma and Jurkat cells. The equivalent amount of free DOX additionally was used in cell studies as a standard comparison.

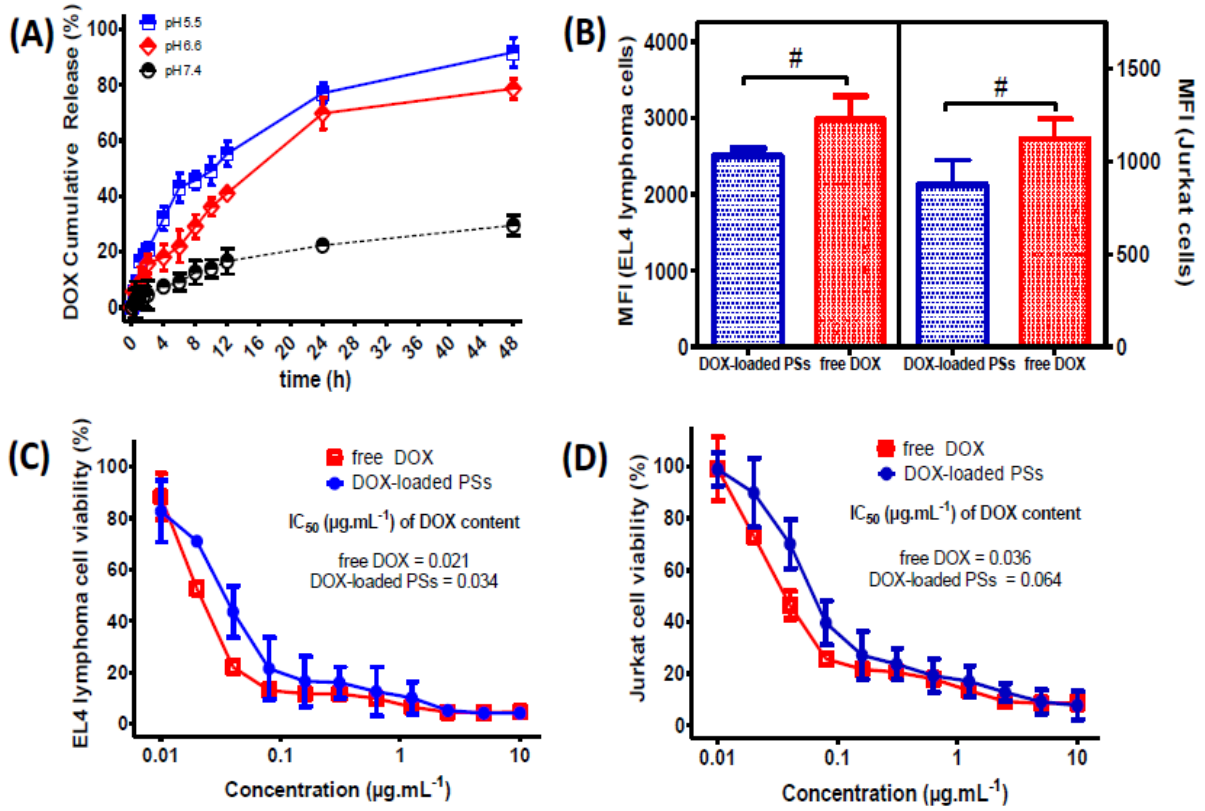

Figure 36. Cumulative DOX release from $PHPMA_{35}$-*b*-$PDPA_{75}$ polymersomes at different pH (A); Cellular uptake of free DOX and DOX-loaded assemblies as determined by flow cytometry (MFI per 10,000 events) after 2h incubation time with EL4 lymphoma and Jurkat cells (B); EL4 lymphoma (C) and Jurkat (D) cell viability after 72 h of contact with free DOX and DOX-loaded polymersomes. # in B represents non-significant differences ($p < 0.05$).

DOX cellular uptake was assessed using its intrinsic fluorescence intensity. The findings show that regardless of whether DOX is encapsulated or not, the amount of DOX uptaken by cells is similar. However, presumably only free DOX can be internalized by cells via the diffusion pathway, whereas PS loaded with DOX may be internalized by endocytosis due to their size. The *in vitro* anticancer performance of DOX-loaded polymersomes was then evaluated in both cell lines and compared with free DOX. The IC_{50} values for EL4 lymphoma cells are 0.034 and 0.021 $\mu g.mL^{-1}$ for DOX-loaded assemblies and free DOX and 0.064 and 0.036 $\mu g.mL^{-1}$, respectively for Jurkat cells, resulting in an efficient cytotoxic effect. The slightly lower IC_{50} values for free DOX may be related to its ability to diffuse across cell membranes [142] for Jurkat cells. The relatively identical values demonstrate that the assemblies effectively carry the chemotherapeutic drug to both cell types, resulting effective cytotoxicity.

4.5 Biodistribution of PHPMA$_{35}$-*b*-PDPA$_{75}$ Polymersomes in Nude Mice:

Due to low molecular weight (543 $g.mol^{-1}$) and amphiphilic character, DOX is known to accumulate preferentially in highly vascularized organs [143]. Accumulation of DOX with following oxidation damage usually leads to an increased rate of apoptosis in cardiac myocytes and consequent cardiotoxicity. [144] The fluorescent dye DBCO-Cyanine7 (Cy7), which can be detected in deep tissues *in vivo*, was used in the biodistribution assays. [145] The self-assembled vesicles were made using a 1:1 w/w of PHPMA$_{35}$-*b*-PDPA$_{75}$ and Cy7-PHPMA$_{35}$-*b*-PDPA$_{75}$ with no changes of the final size and polydispersity (D_H = 92.9 nm; PDI = 0.05). Figure 37 shows a diagram of the Cy7-labeled polymersome and the chemical structure of the block copolymer coupled to the Cy7-DBCO dye.

The female athymic nude foxnl$_{nu}$ mice were chosen for the assay due to lack of body hair as a result of reduced number of T cells caused by the deterioration or absence of thymus. Mice treated with free Cy-DBCO in saline or Cy7-labeled polymersomes, were scanned utilizing a Bruker In vivo Xtreme instrument combining optical and X-ray small animal imaging system at different time points.

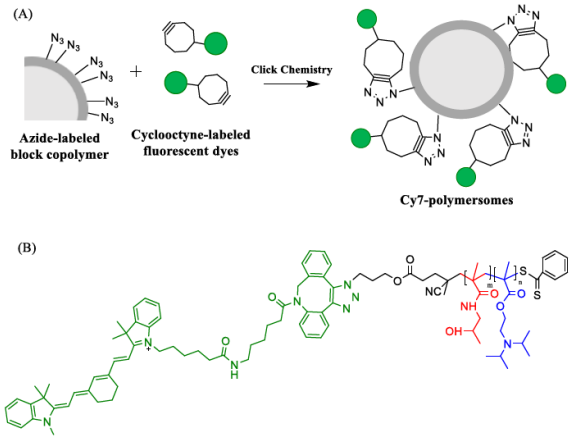

Figure 37. Representation of the click chemistry reaction between Cy7 and block copolymer PHPMA$_{35}$-*b*-PDPA$_{75}$ (A) and chemical structure of Cy7- PHPMA$_{35}$-*b*-PDPA$_{75}$.

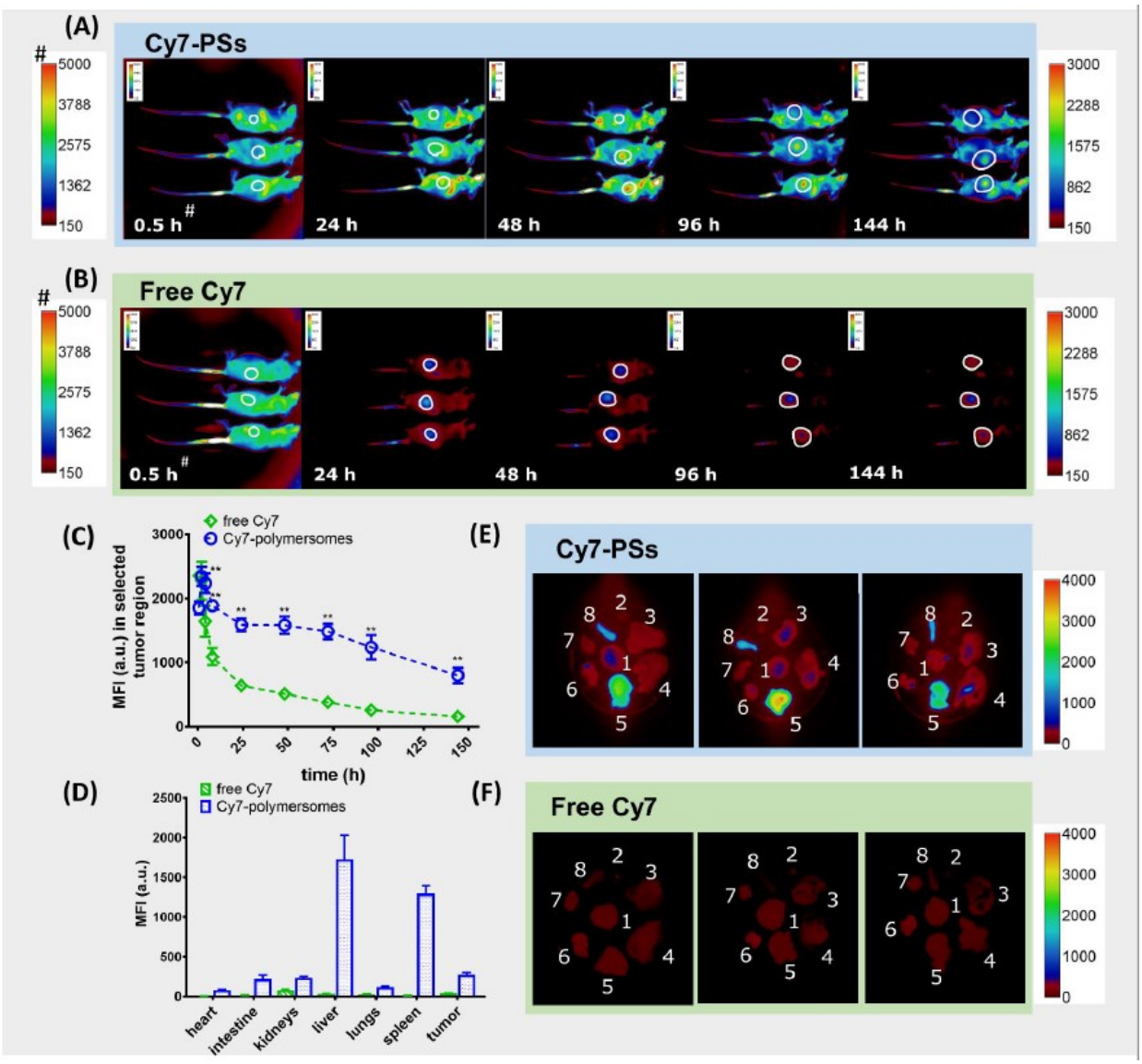

Figure 38. *In vivo* biodistribution analysis of Cy7-polymersomes (A) and free DBCO-Cy7 dye (B) as a function of time (the white circles assigns the tumor area) in mice bearing EL4 T lymphoma tumors; Mean fluorescence intensity (MFI) as function of time monitored *in vivo* at tumor region of nude mice bearing EL4 T lymphoma tumor (C); *ex vivo* Cy7-polymersomes accumulation in different organs and in EL4 T lymphoma tumors after 7 days of administration (D); *ex vivo* images of organs (1: tumor; 2: heart; 3: small intestine; 4: large intestine and cecum; 5: liver; 6: kidneys; 7: lungs; 8: spleen) after 7 days of administration of Cy7-polymersomes (E) and free DBCO-Cy7 dye (F). ** indicates statistical significance $p < 0.05$ between groups provided by one-way ANOVA; n = 3 mice/group.

After the injection of free Cy7 and Cy7-PHPMA$_{35}$-*b*-PDPA$_{75}$ fluorescence intensity remains similar for 0.5 h, but the signal for the free dye fades significantly more quickly and almost completely disappears after 24 h. Moreover, Cy7-PHPMA$_{35}$-*b*-PDPA$_{75}$ polymersomes are able to circulate in the bloodstream for at least 7 days after injection as evidenced by fluorescent

signal from tumor region (Figure 38 C). This data corresponds to the literature about regarding polymersomes circulation half-life that is at least 48 hours, which is much longer than free DOX (30 min - 3 h). [143,146] Animals was sacrificed at 144h by cervical dislocation, and their organs were imaged *ex vivo* for biodistribution analysis.

The highest amounts of Cy7 levels were found in the liver and spleen (Figure 38 D), but increased accumulation is also observed in the tumor region. Probably, the colloidal carriers' long blood circulation time permits them to accumulate in the tumor location. The lowest amount was found in the heart, implying that cardiotoxic effects should be reduced. Block copolymer nanoparticles are typically seen in high concentrations in the liver and spleen. [147,148]

4.6 In Vivo Antitumor Activity

For the in vivo therapeutic experiments, we selected female black C57BL/6J mice with EL4 lymphoma tumors that were treated with DOX-loaded polymersomes. Figure 39 shows the tumor volume, body weight change, and survival rate.

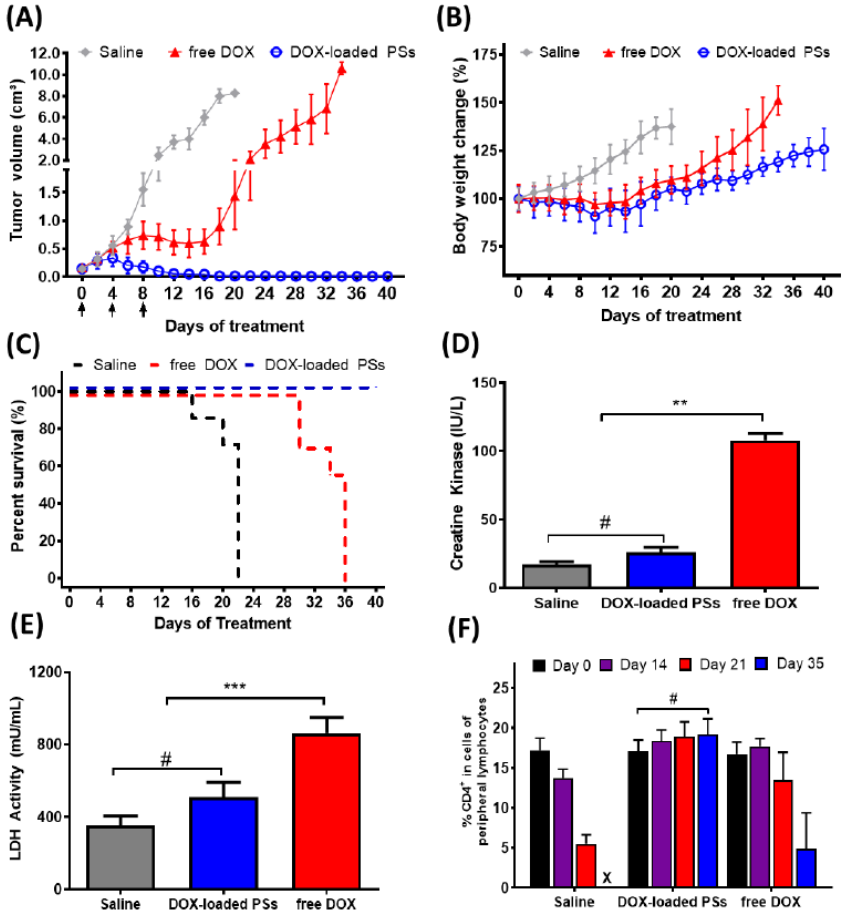

Figure 39. Tumor volume (A), body weight change % (B), and Kaplan-Meier survival plot (C) as a function of time for mice treated with saline, DOX-loaded PSs and free DOX at 5 mg.kg^{-1} DOX or equivalent according to the legends (the data are given as mean ± SD; n=7). The arrows indicate the administrations. Lactate dehydrogenase - LDH (D) and serum creatine kinase - CK (E) levels

after free DOX and DOX-loaded PSs administration (third injection) in mice bearing EL4 lymphoma tumors (the data are given as mean ± SD). Quantification of CD4+ cells in peripheral blood during the chemotherapeutic treatment using free DOX and DOX-loaded PSs (F). # non-significant difference ($p < 0.05$); ** statistically significant difference ($p < 0.05$); *** statistically significant difference ($p < 0.005$). Polymersomes were denoted as PSs.

In the group with untreated mice (saline) EL4 lymphoma tumor uncontrollably and rapidly grow in volume, resulting in death of the entire group within 22 days (Figure 39 C). Treatment with free DOX does not lead to a reduction in tumor volume, and considering the short the half-life of free DOX [143,146] the fast clearance of the therapeutic agent is probably associated with the rapid tumor growth. Treatment with free DOX, on the other hand, increased survival time by 10-14 days. The presence of ulcerated and necrotic tumors was observed in the control group (saline) and the group treated with free DOX. On the contrary, a significant suppression of tumor growth was observed when mice received treatment with the DOX-loaded polymersomes.

Due to quicker tumor growth, the body weight increased significantly in the control and free DOX-treated groups, whereas body weight was maintained in the group treated by DOX-loaded $PHPMA_{35}$-*b*-$PDPA_{75}$ vesicles during the first 20 days.

The animals looked healthy and regained weight thereafter. Most importantly, the survival rate in the treated group was maintained at 100% without deaths within the experiment's timeframe (40 days), confirming the efficacy of the DOX-loaded pH-responsive assemblies in reducing tumor growth and prolonging the survival time of the mice. This outstanding result can probably be attributed to the longer circulation time of the nanomedicines compared to free DOX, as shown in the data presented in Figure 38, as well as the pH-responsiveness of PDPA, which enables triggered and rapid release of DOX in a slightly acidic environment. In addition, hair loss was observed in the flank caudal region in the groups treated with free DOX. Hair loss is one of the side effects of chemotherapeutic treatments with doxorubicin. Fortunately, in the groups treated with DOX-loaded vesicles mice did not experience hair loss.

To assess in vivo toxicity, blood samples were taken after the third injection (day 8) and CK and LDH levels were measured (Figure 39 D, E). Cardiotoxicity is one of the key drawbacks of therapeutic treatments based on DOX.[120] Quantification of these specific enzymes (LDH and CK) released by cardiac myocytes when they are damaged is important to identify cardiotoxic effects. The data presented in Figures 39 D and 39 E show significantly higher CK and LDH levels in plasma of the free DOX treated group, indicating cardiotoxic effects. When DOX was encapsulated into the polymersomes, the levels were noticeably lower.

Finally, of CD4+ cells were quantified by flow cytometry during chemotherapeutic treatment. Figure 39 F depicts the number of CD4+ cells found in mice administered with saline, free DOX, or DOX-loaded vesicles. CD4+ cells are involved with the generation of T helper cells; hence they play an important function in the immune system. The level of CD4+ cells in untreated mice (saline) was remarkably low, less than 7% after 21 days of treatment. During the first two weeks of treatment, the number of CD4+ cells in mice treated with free DOX remained stable. Thereafter, it decreases, leading to a loss of therapeutic response presumably related to the

clearance of free DOX, which subsequently leads to an increase in tumor volume, as shown in Figure 39 A. On the other hand, treatment with the pH-responsive DOX-loaded polymersomes leads to an increase in the percentage of CD4+ cells during the experimental period (40 days), suggesting that anti-tumor T-cell immunity also supports tumor suppression.

These results highlight the potential of DOX delivery into solid tumors using a novel pH-sensitive platform. We exploited the known low local pH of tumor sites to create a pH-responsive nanoplatform potentially capable of delivering drugs preferentially to such specific regions. The adopted strategy improved treatment efficacy and reduced notorious side effects. It is expected that the results will have implications for the success of DOX-based chemotherapies in the future.

5. Synthesis of different ROS-responsive polymers based on hydrophilic PHPMA and hydrophobic phenylboronic acid pinacol ester methacrylates with following characterization and degradation studies. Production of ROS-responsive monodisperse polymersomes by microfluidic flow-focusing method, with subsequent in vitro and in vivo experiments.

Taking into consideration our previous experience with polymersomes sensitive to pH-cellular imbalances, we designed another polymersome system that is sensitive to other feature of tumor microenvironment such as elevated levels of reactive oxygen species (ROS).

This feature of TME has led to greater interest in recent decades towards the development of novel PSs for medical applications, such as enzymatic nanoreactors and drug delivery systems. [149,150] Such proposed “smart” PSs have been able to release their payloads or show reduced sizes under the presence of reactive oxygen species (ROS) in cancer cells. [151] ROS, such as hydrogen peroxide (H_2O_2), are a component of the cellular signaling pathways that are necessary for the growth, development, and fitness of living organisms. [152,153] However, imbalances in H_2O_2 production lead to oxidative stress and inflammatory events, which damage tissue and organ systems and are correlated with the onset and advancement of various diseases, including cancer. Hence, the design of PSs able to be responsive to these inherent features of the TME has been proposed as a promising approach for cancer treatment, [154,155] however, they have been far less explored. Herein, we developed a simple PS platform that allows for the specific delivery of bioactive cargo such as doxorubicin (DOX) at the inherent ROS levels typically found in the TME. Well-defined BCs were used to prepare oxidative-reductive PSs for the delivery of DOX in response to varied ROS concentrations and were synthesized by using the appropriate nitrogen or oxygen spacers based on boronic acid monomeric units (Scheme 3).

Under the envisaged targeted site-specific ROS-rich environment, an oxygen derivative can undergo complete self-immolative degradation resulting in a final hydrophilic polymer, while partial degradation occurs from the nitrogen derivative, resulting in a relatively less hydrophilic polymer containing phenols (Scheme 3A and 3B). As a stealth biocompatible hydrophilic shell assuring colloidal stability in aqueous medium and long circulation, we have chosen the well-known multivalent polymer poly(*N*-(2-hydroxypropyl)methacrylamide) (PHPMA) (Scheme 3A, blue). The ROS-responsive BC backbone was envisaged based on pinacol-type boronic ester protecting groups (Scheme 3A green and 3B red). Among the oxidative-responsive moieties, boronic acids and boronic esters undergo oxidative-triggered hydrolysis in the presence of biologically relevant levels of H_2O_2, making these compounds candidates for ROS-induced polymer decomposition. The pinacol-type boronic ester groups have been shown to be the most ROS-selective and sensitive probes to detect H_2O_2 at physiological concentrations with high specificity. [156–159] At physiologically relevant H_2O_2 concentrations (100 μM – 1 mM of H_2O_2), [160] arylboronic esters are oxidized to phenols, which then undergo a quinone methide rearrangement leading to a strong hydrophilization of the particular polymer block (discussed hereafter) and subsequent PS disassembly and cargo release (Scheme 3C).

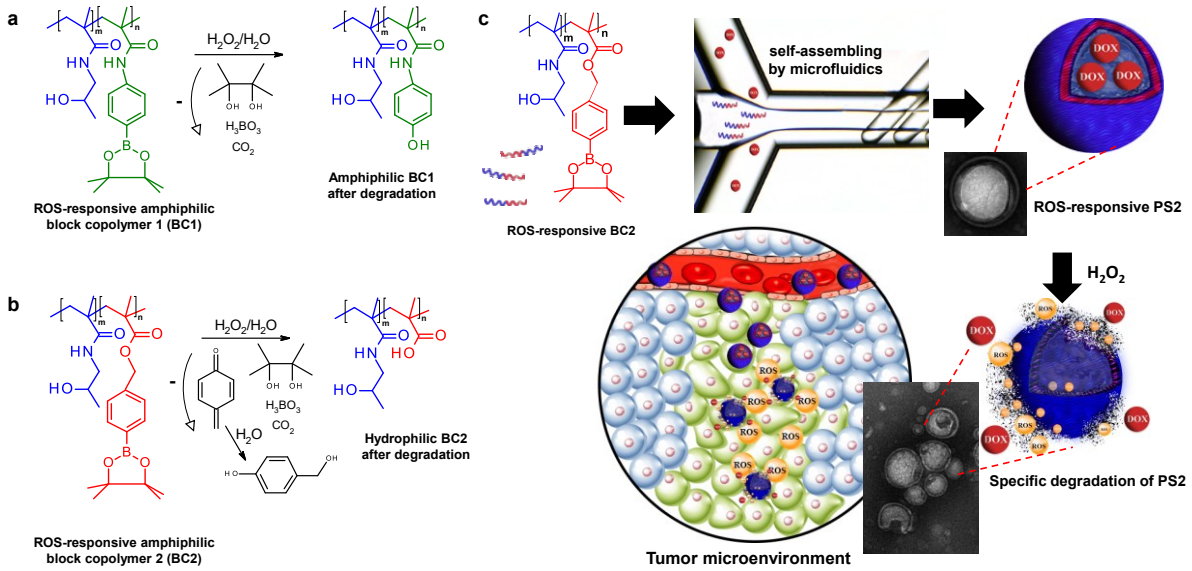

Scheme 3. Spacer design chemistry envisaged BC1 (a) and BC2 (b) and their respective mechanism of ROS-triggered degradation by H_2O_2. HPMA in blue, nitrogen-containing boronic spacer ("amphiphilic" - partially hydrophilic, BC1) in green and oxygen-containing boronic spacer (fully hydrophilic, BC2) in red. (c) MF manufacturing of doxorubicin-loaded PS2 from BC2 and the ROS degradation under H_2O_2. Cargo chemotherapeutic doxorubicin release is shown in red.

5.1 Synthesis of the ROS-Responsive Building Blocks

In a simple way, the first block of PHPMA bearing azide functional groups was synthesized (see chapter 4.2) the HPMA monomer and a modified chain transfer agent (CTA) by the reversible addition-fragmentation chain transfer (RAFT) polymerization and was used as a macro chain transfer agent (PHPMA mCTA azide, Mn = 3600 g·mol^{-1}, M_w/ Mn = 1.08). The introduction of the clickable azide groups to the ends of the PHPMA BC will allow further PS functionalization, such as with fluorescent dyes or antibodies for imaging and selective targeting, respectively. Subsequently, the 4-aminophenyl boronic acid pinacol ester (compound 1, Figure 40) was reacted with methacryloyl chloride to generate the methacrylamide pinacol ester-protected ROS monomer 1 (Scheme 3B and Figure 40). 4-(Hydroxymethyl)phenylboronic acid pinacol ester (compound 2, Figure 40) was methacryloylated to generate the methacrylate pinacol ester-protected ROS monomer 2 (Scheme 3C and Figure 40).

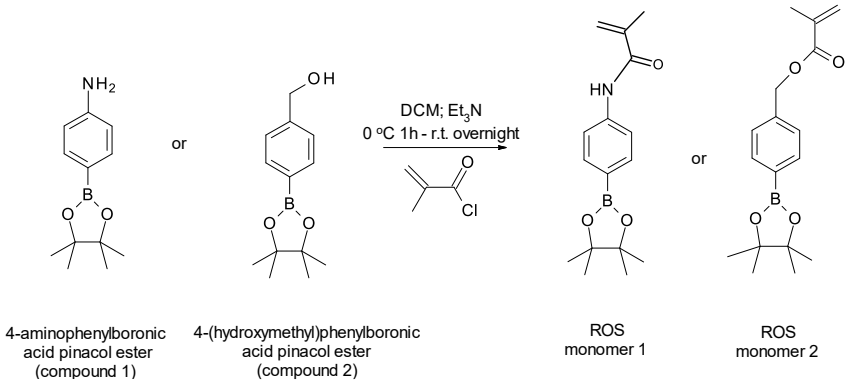

Figure 40. Molecular structures of the 4-amino phenyl boronic acid pinacol ester (compound 1) and the 4-hydroxyphenylboronic acid pinacol ester (compound 2) and synthetic route for the preparation of their respective methacrylate monomers, ROS monomer 1 and 2.

Furthermore, the ROS methacrylic monomers were copolymerized with the PHPMA mCTA azide to generate the ROS-responsive amphiphilic BC1 (Scheme 3 A, Figure 41 A) and ROS-responsive amphiphilic BC2 (Scheme 3b, Figure 41 B).

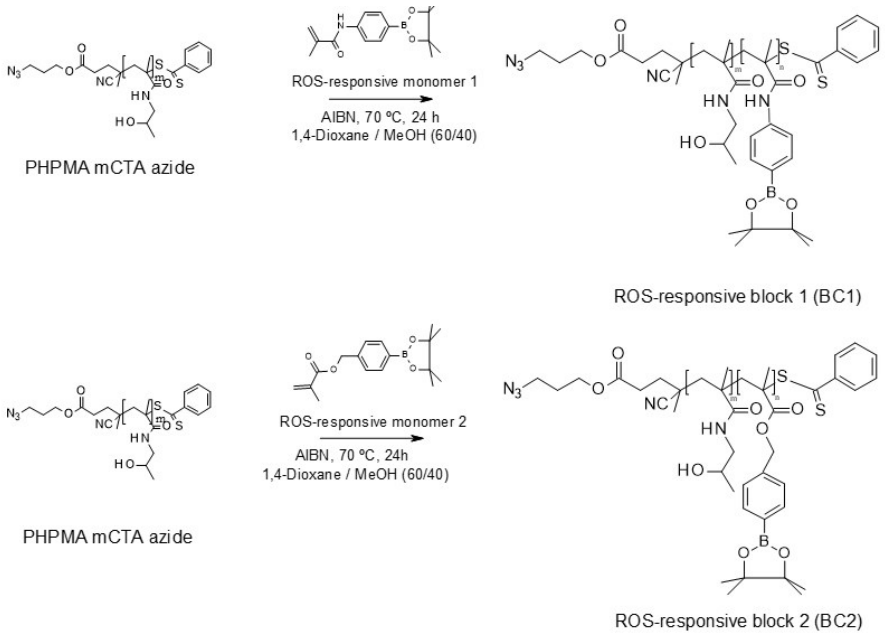

Figure 41. Synthetic route and molecular structures for the newly synthesized ROS-responsive block copolymers 1 (BC1) (b) and 2 (BC2) (c).

The BCs were successfully synthetized by the accurate RAFT polymerization technique with similar M_w and desirable polydispersity (Table 12). We targeted the synthesis of BC with the appropriate hydrophilic/hydrophobic weight ratios (ϕ = volume fraction of the hydrophilic block of the BC = 10 ~ 40 %)[149] (Table 12) for the preparation of the PS enabling the solubilization of DOX in the PS interior. Successful BC synthesis was confirmed by ^{1}H NMR (Figure 42) and size exclusion chromatography (SEC) analysis. No important differences in M_w were observed for the BCs. The *Mn* of the synthetized BC1 was ~ 20.3 kDa with reasonable dispersity M_w/ *Mn* ≈ 1.09 and these values were *Mn* ~ 21.5 kDa with a dispersity of M_w/ *Mn* ≈ 1.13 for BC2 as determined by SEC (Table 12). The ^{1}H NMR spectrum of the BC showed the characteristic signals for protons belonging to the repeating units of the monomers.

Table 12. Synthesis parameters and molecular weight data of the polymers prepared *via* RAFT polymerization.

Sample	$[M]_0/[CTA]_0/[I]_0$	Time (h)	Conversion (%)[a]	*Mn*, th[b] (g·mol)$^{-1}$	*Mn*, SEC[c] (g·mol)$^{-1}$	*Đ*[c] (M_w/ *Mn*)	ϕ[g] (%)
$PHPMA_{25}$	100/2/1[e]	16h	46	7200	3600	1.08	-
BC1	100/2/1[f]	24h	86	30200	20300	1.09	18
BC2	100/2/1[f]	24h	89	28700	21500	1.13	17

[a] Determined by ^{1}H NMR in D_2O; [b] Theoretical $Mn = [M]_0/[CTA]_0 \times \text{conversion} \times M_{w\,\text{monomer}} + M_{w\,\text{CTA}}$;

[c] Determined by SEC in DMF using PMMA as standard; [d] Determined by SEC in MeOH/acetate buffer pH 6.5, 80/20 vol. %; [e] conditions: *tert*-butanol, $[M]_0$ = 1.5 M, 70 °C; [f]conditions: 1,4-dioxane/MeOH, 60/40 vol. %, $[M]_0$ = 3 M, 70 °C; [g] Volume fraction of the hydrophilic block (SEC);

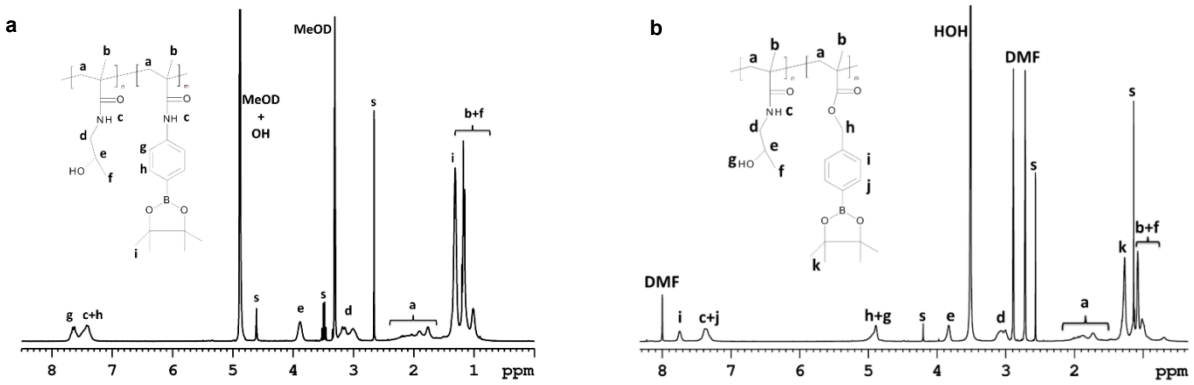

Figure 42. ^{1}H NMR spectra of the synthesized ROS-responsive BC1 (a) in MeOD-d4 and BC2 (b) in DMF- d7.

5.2 Deprotection of the ROS-Responsive Building Blocks

After BC characterization, their degradation was evaluated with ^{1}H NMR under 1 mM and 10 mM H_2O_2.[159,160] Figure 44 shows high-resolution ^{1}H NMR spectra of BC in deuterated PBS recorded 5 min and 24 h after the addition of 1 mM and 10 mM H_2O_2. Comparison between the spectra was recorded in solvents suitable for both blocks (MeOD, d_7-DMF, Figure 42) and D_2O. Figure 44 A-C (5 min, bottom) depicts weak and broad signals from the hydrophobic block and strong signals from the hydrophilic PHPMA block for both BC1 (Figure 44 A) and BC2 (Figure 44 B and C) prior to H_2O_2 addition. These results demonstrate that the protons corresponding to the hydrophobic block are restricted in mobility (not observed in spectra), whereas the protons of the PHPMA block corresponding to the hydrophilic-like portion of the BC are clearly visible. However, different behaviors after the addition of H_2O_2 were observed for BC1 (Figure 44 A, top) and BC2 (Figure 44 B and C, top). After exposure to H_2O_2, the aryl boronic ester groups of BC1 were oxidized and subsequently hydrolyzed, displaying the stable intermediate 4-amino-phenol that does not undergo the quinone methide rearrangement, whereas for BC2, the aryl boronic ester groups are oxidized and hydrolyzed, displaying an intermediate phenol that in water quickly turns to p-hydroxymethylphenol (Scheme 3b and Figure 44 B and C). The ^{1}H NMR spectra show that the side chains of BC1 (Figure 44 A) are partially degradable with 1 mM or 10 mM H_2O_2; however, the side chains of BC2 degraded into small molecules and oligomers in a time- and concentration-dependent manner (Figure 44 B, C top). For BC2, it is clearly observed that the broad peaks in ^{1}H NMR related to the BCs are replaced by the sharp peaks of the low-molecular-weight degraded side groups, showing self-immolative degradation triggered by H_2O_2. Polymer degradation proceeds more extensively with increasing incubation time or H_2O_2 concentration for BC2, as observed by following the time dependence ^{1}H NMR degradation as evaluated from the integral intensities of the appearance of the *p*-hydroxymethyl phenol group (Figure 44 D), as well as the disappearance of the pinacol-protected groups, both of which are products of the degradation of BC2 by H_2O_2 (Scheme 3 B). We further evaluated the H_2O_2 scavenging ability of the BCs. In a typical experiment, 1 mg of BC1 and BC2 were added to 1 mL of different H_2O_2 concentrations (200 and 100 μM H_2O_2), and after 3 h of incubation, the

concentration of H_2O_2 in the supernatants was determined by the Amplex Red Hydrogen Peroxide/Peroxidase Assay. [161] As shown in Figure 43, both BCs are reactive with H_2O_2 to a similar extent. The FDA-approved poly(lactic) acid-*block*-poly(ethylene) oxide (PLA-*b*-PEO) BC was used as a control (Figure 43, gray column). The ability of the BCs to react with H_2O_2 in a similar way is most likely due to the similar amount of pinacol-protected boronic groups in both BCs (Table 12). Furthermore, it is important to highlight that both BCs showed responsiveness to physiologically relevant levels of H_2O_2 ($\lesssim$ 1 mM).[153,160]

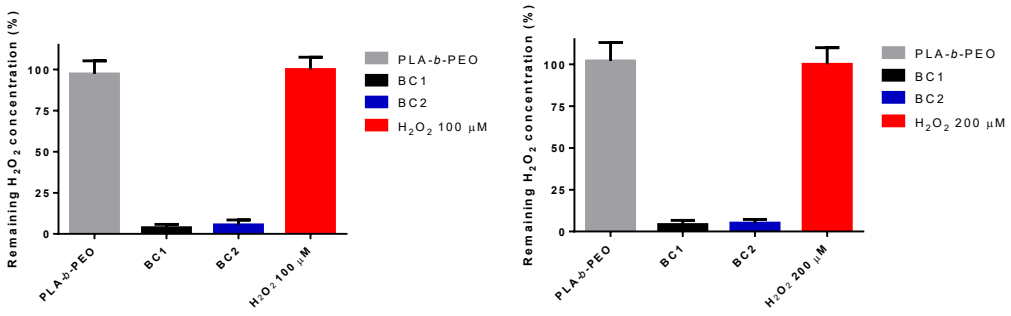

Figure 43. H_2O_2 scavenging ability of the BCs measured by Amplex Red reagent under 100 (a) and 200 (b) µM of H_2O_2.

5.3 Preparation of the ROS-Responsive Polymersomes via microfluidics

The junction of the hydrophilic PHPMA and the hydrophobic boronic-based monomer in a specific ratio and with the desired molecular weight can generate self-assembled PSs in aqueous solution.[2,149,162,163] To assemble the BCs into reliable PSs for the delivery of DOX, we utilized the elegant microfluidics technique .[2,3] The BC (concentration ~ 5 $mg \cdot mL^{-1}$) was dissolved in tetrahydrofuran/methanol (80/20). The polymer solution was pumped through the middle channel, and PBS buffer at pH 7.4 (containing DOX; 20 % *wt*/*wt* related to BC) was pumped through the side channels using two independent pumps controlled *via* PC software. The flow rates were 200 $\mu L \cdot min^{-1}$ for the water phase and 100 $\mu L \cdot min^{-1}$ for the organic phase, resulting in flow ratios of 2:1 (v/v). The resulting PSs were collected in vials and dialyzed against PBS overnight to remove the organic solvent. Spherical and uniform PSs were obtained from both BCs after dialysis and were evaluated in detail by dynamic (DLS), static (SLS) electrophoretic (ELS) light scattering, transmission electron microscopy (TEM) and cryogenic TEM (cryo-TEM). The size distribution has only one component corresponding to the spherical PSs in PBS solution with an average diameter of ~ 120 nm (PDI = 0.09) for PS1 (Figure 44 E, black circles) and ~ 132 nm (PDI = 0.10) for PS2 (Figure 44 E, blue circles) after 24 h in PBS. A slight increase in the PS diameter (~ 5 – 10 nm) and polydispersity (~ 0.1) was observed after DOX loading into the PS, however, this did not affect the PS stability and applicability. From the combination of the DLS and SLS data, important information about the colloid structure can be obtained. The obtained PS values (ρ = 1.0 to 1.08) indicate the presence of a vesicular morphology for the prepared PSs. The

estimated aggregation numbers (N_{Agg}) were also in the range of values (N_{Agg} = 250 to 2500) expected for self-assembled systems with a vesicular morphology.[164] The diameter and morphology were confirmed by TEM images. The formation of spherical and homogeneous PSs is observed for both BCs. Subsequently, the PS stability was tested under relevant H_2O_2 concentrations (~1 mM H_2O_2) as a function of time to test the ROS responsiveness. [159,160,165] Both PSs remained with unchanged diameters during 24 h incubation in PBS at pH 7.4 (Figure 44 F); however, PS degradation was observed after incubation with H_2O_2. For PS2, the scattering intensity (I_{sc}) drops almost 2-fold (Figure 44 F, blue open circles) compared with the I_{sc} in PBS conditions (Figure 44 F, blue filled circles) and PS1 in 10 mM H_2O_2 (Figure 44 F, open black circles). The more negative surface charge (ζ-potential) values after H_2O_2 incubation also evidenced the degradation of PS2 to the final carboxyl groups (Scheme 3b). The observed DLS data are in agreement with the obtained ^{1}H NMR degradation experiments mentioned above, with the degradation of BC2 = PS2 being higher than BC1 = PS1 (Figure 44). For BC2, H_2O_2-triggered polymer degradation is most likely due to the surface-eroded PS (decrease in I_{sc} of ~ 45 %) (Figure 44 F). This decrease in I_{sc} corresponded to a decrease of ~ ½ of the PS2 M_w. Subsequently, PS2 was imaged by TEM after incubation with H_2O_2 (10 mM) (Figure 44 H-I). Along incubation for 24 h, PS2 demonstrated irregularities in its morphology and shape (Figure 44 H, arrows), with PS2 vanishing after 72 h (Figure 44 I).

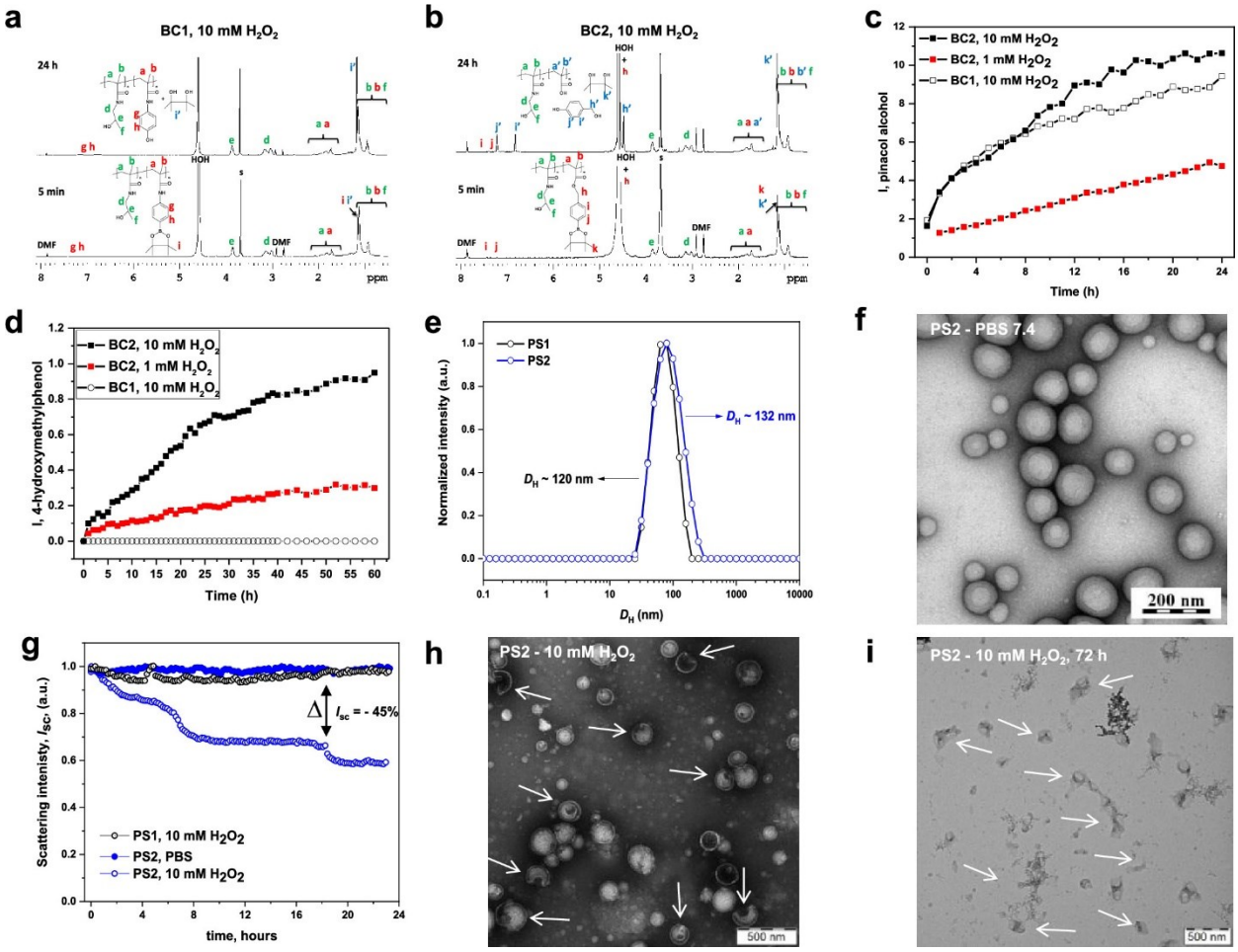

Figure 44. ^{1}H NMR spectra of BC1 (a) and BC2 (b) degradation after 5 min (bottom) and 24 h (top) of incubation with 10 mM H_2O_2 and (c) BC2 after 5 min (bottom) and 24 h (top) incubation with 1 mM H_2O_2 in d_7-DMF, deuterium PBS. (d) ^{1}H NMR integral intensities related to the appearance of the *p*-hydroxymethyl phenol group, a product of the degradation of BC2 during the 60 h of incubation with 1 mM (red squares) or 10 mM (black squares) H_2O_2. (e) Distributions of the diameter of PS1 (open black circles) and PS2 (open blue circles) in PBS pH 7.4 and (f) changes to the scattering intensity (I_{sc}) after incubation of PS2 in PBS pH 7.4 (filled blue circles) and 10 mM H_2O_2 (open blue circles) *vs* PS1 (open black circles) at 37 °C during 24 h. TEM micrographs of PS2 upon incubation in PBS pH 7.4 (g) after 24 h (h) or 72 h (i) incubation with 10 mM H_2O_2 (arrows depict the degraded or vanished PS2).

5.4 In Vitro Assays

Further, the PS degradation-triggered cargo release was studied by using DOX. Incorporation of the DOX marker (DOX is also fluorescent) provided the means to study the cellular uptake of PS and PS cytotoxicity by flow cytometry.

The DOX- loaded PS was examined with fluorescence spectroscopy measurements for 24 h upon incubation with PBS or 1 mM H_2O_2. After 24 h, the DOX release from PS1 and PS2 under simulated tumor microenvironment conditions (H_2O_2) was similar, with a slightly faster release of

DOX for PS2 during the first 9 h to 12 h (Figure 48 A later below). Both PSs released DOX twice as fast in simulated ROS-rich microenvironments than in PBS conditions, thus indicating that the observed faster ROS-dependent release could play an important role in the cytotoxicity to cancer cells.[160,165] We next evaluated the cellular uptake of DOX-loaded PS in a murine 4T1 cancer cell line. Figure 45 shows similar uptake for both PSs evaluated.

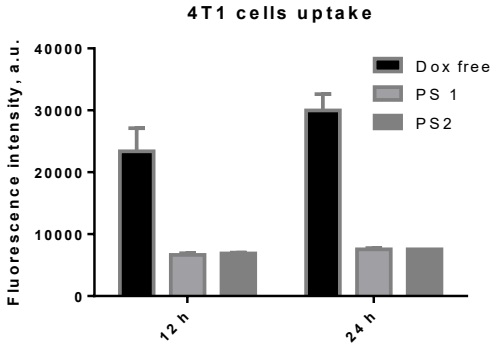

Figure 45. PS uptake and DOX-free in 4T1 tumor cell lines along 12h and 24h of incubation.

Considering that the particle uptake is generally dependent on the size of the NPs, their shape, and their surface charge, a similar uptake behavior for both PSs is expected because their surface chemistry is similar (covered by PHPMA), they are spherical in shape with similar diameters bearing a slightly negative in charge ($\zeta \approx$ - 9.34 mV for PS1 and - 11.3 mV for PS2). Subsequently, the *in vitro* therapeutic effect of the DOX-loaded PS against 4T1 cancer cells was determined by using the alamarBlue® assay at 3 different incubation times with cells (24, 48 and 72 h). Table 13 shows the dose-dependent cytotoxicity (IC_{50}) of both PSs and the DOX-free conditions. Compared with DOX-free, the DOX-loaded PSs exhibited similar cytotoxicity; however, lower cytotoxicity was observed at the same dose of DOX (Figure 46). This is most likely due to the free DOX that quickly diffuses into the nucleus. [142,166]

Table 13. IC_{50} values ($\mu g \cdot mL^{-1}$) of the PS and DOX-free in 4T1 cells along different incubation times.

Entry	24h	48h	72h
DOX-free	190	18	9
PS1	205	35	50
PS2	305	160	110

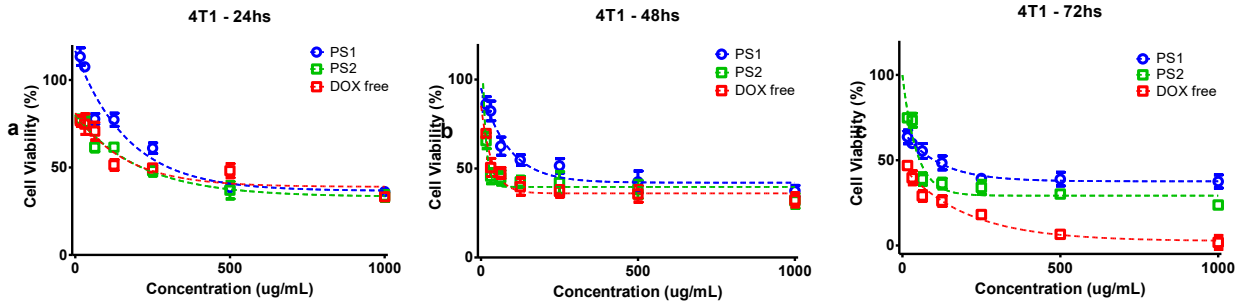

Figure 46. PS uptake and DOX-free in 4T1 tumor cell lines after 12h, 24h and 72h of incubation.

5.5 In Vivo Assays

The *in vitro* results suggest that PSs are promising for *in vivo* applications. Next, we mapped the biodistribution and accumulation of PS *in vivo* via the biofluorescent imaging of EL-4 T cell lymphoma tumor-bearing mice over 7 days with Cy7-free and Cy7-PS after intravenous injection into the tail vein of female athymic nude foxnl$_{nu}$ mice. Figure 48 B shows that the accumulation of PS is predominantly in the liver, followed by the kidneys, lungs and tumors. The Cy7-free accumulated ~2-3 times less in the tumor compared with the PS at longer incubation times, such as 3 to 7 days, which is most likely an effect of the long blood circulation promoted by the PSs (Figure 47, Figure 48C).

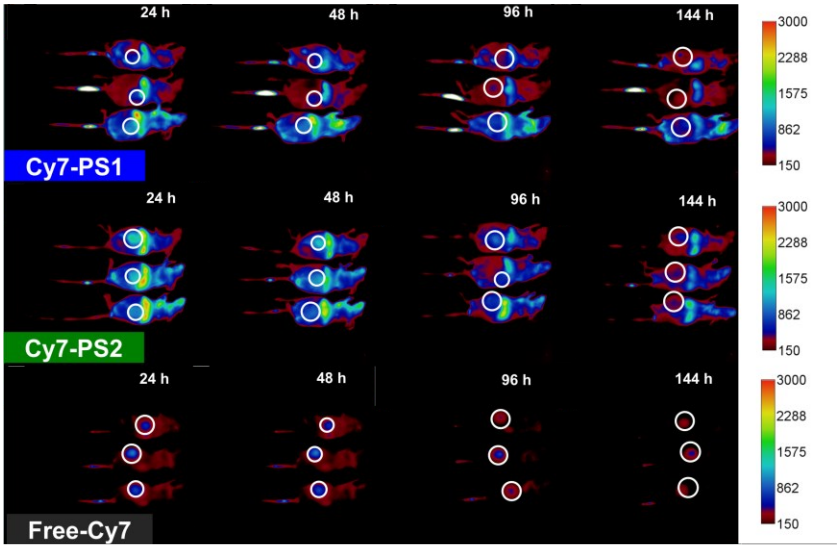

Figure 47. In vivo biodistribution analysis of Cy7-PS and free fluorescent dye DBCO-Cy7 along 144h. The mice were imaged in the right flank using Ex/Em = 750/830 nm filter pair to visualize the Cy7 dye (white circles refer to the tumor area).

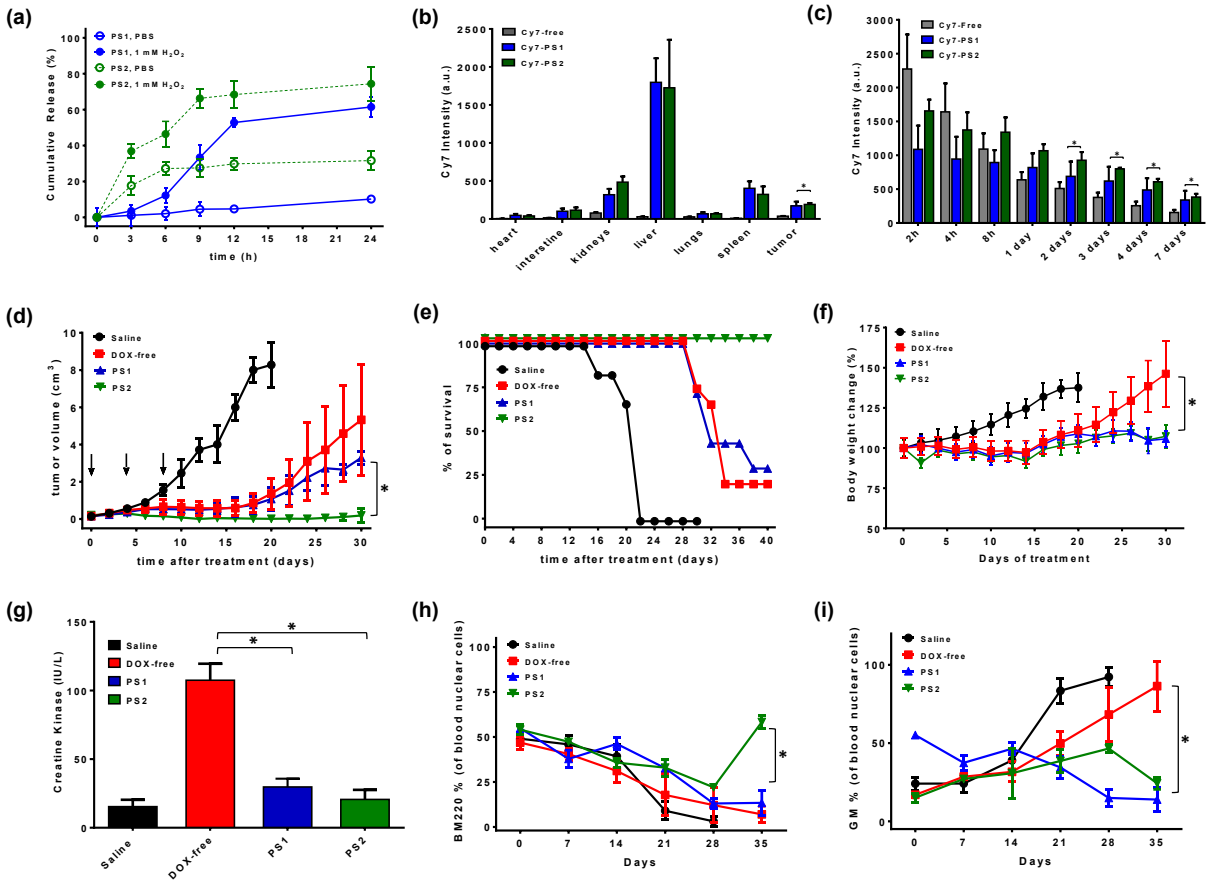

Figure 48. a) Doxorubicin cumulative release from PS in PBS buffer pH 7.4 (open blue circles - PS1; open green circles - PS2) and in 1 mM H2O2 (filled blue circles - PS1; filled green circles - PS2) over 24 h. (b) *In vivo* Cy7-PS accumulation in different organs and in EL-4 T lymphoma tumors after 7 days of PS administration and (c) the time-dependent accumulation effect of Cy7-PS in the EL-4 T lymphoma tumor vs Cy7-free administration. (d) *In vivo* effect of PS vs DOX-free and saline on the growth of T cell lymphoma EL-4, (e) Kaplan-Meier survival plot of mice after 3 × 5 mg DOX (equivalent)/kg administration and untreated control (n=4-6; black arrows indicate injections). (f) Body weight changes during PS and DOX-free treatment. (g) Serum creatine kinase levels in the blood after saline, DOX-free, PS1 and PS2 administration in mice bearing EL-4 T lymphoma. Blood cell changes, B lymphocytes (h) and granulocytes/monocytes (i) from mice during treatment with PS, Dox-free and saline. Asterisks indicate statistical significance obtained by one-way ANOVA. *P<0.01

It is important to highlight that similar accumulations of Cy7-PS1 and Cy7-PS2 were observed in the organs and especially in the tumor, which is most likely because of the similar characteristics of the PSs, such as size, shape and charge (as aforementioned).

These results suggest that PS promote the accumulation of loaded drugs in the tumor, implying improved drug delivery. In line with this, we performed *in vivo* studies of antitumor

efficacy in which PS was loaded with DOX and intravenously injected into the tail vein of mice bearing EL-4 T cell lymphoma. PS1, PS2, PBS and DOX-free were administered at doses of 5 mg DOX equivalent/kg on days 8, 12 and 16 after tumor transplantation, and tumor growth and mouse survival were monitored. Figure 48 D clearly shows more efficient suppression of tumor cell growth in mice bearing EL-4 T cell lymphoma treated with PS2. The survival time of the animals was also extended for PS1 and PS2-treated animals compared with DOX-free animals (Figure 48 E). Additionally, the side effects of the chemotherapy were substantially improved with the PSs, such as the balance of the body weight (Figure 48 F) and reduced cardiotoxicity of DOX, one of the main drawbacks of this current chemotherapeutic drug in the clinic, as observed after the decrease of serum creatine kinase levels monitored in blood (Figure 48 G) and the balanced levels of the lymphocytes (Figure 48 H), granulocytes and monocytes (Figure 48 I), monitored in mouse blood along the chemotherapeutic treatment. It is important to highlight that the *in vivo* accumulation of PS is similar for PS1 and PS2, as well as the *in vitro* uptake and cytotoxicity; however, PS2 demonstrates much better efficacy in the treatment of lymphomas *in vivo*, highlighting the chemical effect on PS efficacy.

6. pH-Responsive giant polymer vesicles prepared via PDMS microfluidics

6.1 Introduction

Giant polymersomes (PS) from amphiphilic diblock copolymers is a novel class with unique self-assembly mechanism [67,167], that possess all the properties of polymersomes such as the capability of the polymer membrane for encapsulation and release hydrophobic molecules, and use of aqueous core for the same purposes but with hydrophilic cargo. Contrary to lipid vesicles (giant and nanosized) PS are more versatile and possess better stability and mechanical properties [168]. Versatility and enhanced properties of PS comprise the control of block lengths, molecular weight, and functionalization with specific groups, utilized for creation of stimuli-responsive PS systems. Based on our previous experience with PDPA as pH-responsive polymer (see chapter 3.5 and 4) we designed an amphiphilic block copolymer with PEG as hydrophilic part, for preparation of giant stimuli-responsive polymeric vesicles (Scheme 4).

Common procedures for PS preparation are: nanoprecipitation/solvent-exchange method, film-rehydration, ultrasonication, PISA, and electroformation. The self-assemblies produced by these methods are naturally polydisperse, and have low drug-loading efficiency. [169,170]

Microfluidic technique allows precise control over PS formation with narrow monodisperse size distribution and improved encapsulation of compounds. [67] The PS in microfluidic device are prepared by dewetting of water/copolymer stabilized in organic solvent/water (W/O/W) double emulsion droplets. During evaporation of organic solvent, the copolymers assemble into a shell.

Selection of organic solvent and diblock copolymer concentration are the crucial steps in production of PS. Organic solvent must be volatile or soluble in another solvent that is volatile and suitable for complete dissolving of the diblock.

Microfluidic devices for production of PS are glass capillary devices, 3D-printed devices, and poly(dimethylsiloxane) (PDMS) systems based on soft-lithography process. Glass capillary systems have difficulties in channel design and customization. Devices which are done by 3D printing up to now have another properties limitation, such as material properties and precision of channel lengths, but it's promising candidate for future of microfluidics. PDMS devices fabricated by soft lithography can be performed with wide ranges of sophisticated channel designs with high accuracy. However, as mentioned above, PDMS can be used directly only with a limited selection of solvents: such as alcohols and oils. [171] Since PDMS has poor chemical resistance and swells in contact with many organic solvents, additional cover like glass-like sol-gel must be applied. Such sol-gel coatings like TEOS-modification produced durable glass-like layer, which significantly increased resistance of PDMS channel walls. [172]

For stable W/O/W droplets production, wetting properties of the device channels must be modified. [167,173,174] Originally PDMS is hydrophobic, so the outer post-junction channels should be covered with a hydrophilic coating. For this purpose, the PEG method was applied. [175]

Herein, we report pH-responsive giant PS prepared by W/O/W double emulsion in sol-gel coated PDMS device using volatile organic solvent (toluene).

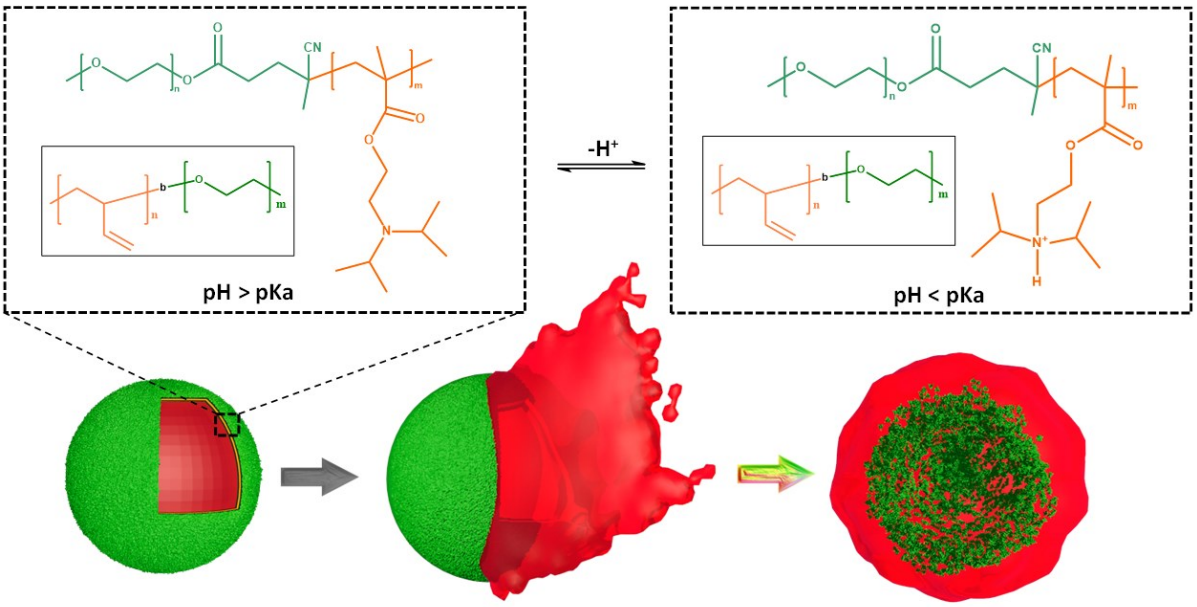

Scheme 4. Illustration scheme of pH-responsive giant vesicles triggered disruption/explosion.

6.2 Preparation of devices:

Photoresist (PR) SU-8 glass substrate was used to create a master template (Figure 49 A) by soft-lithography process. Microfluidic devices were made by pouring PDMS (Sylgard 184, Dow Corning GmbH), at a mass ratio 10:1, air bubbles were removed with vacuum in desiccator, the device was baked at 70 °C for 4 h. The PDMS blocks were then peeled off from the wafer and holes were punched out. The PDMS was then cleaned with isopropanol and dried with air. Carved PDMS blocks were then exposed to oxygen plasma for ~30 s using a MiniFlecto 2 (Plasma technology), immediately after the plasma treatment, the PDMS block was wetted by two drops of water from each side, and sandwiched with second PDMS block for silanol covalent bonding (Figure 49 B). The device was kept at RT overnight.

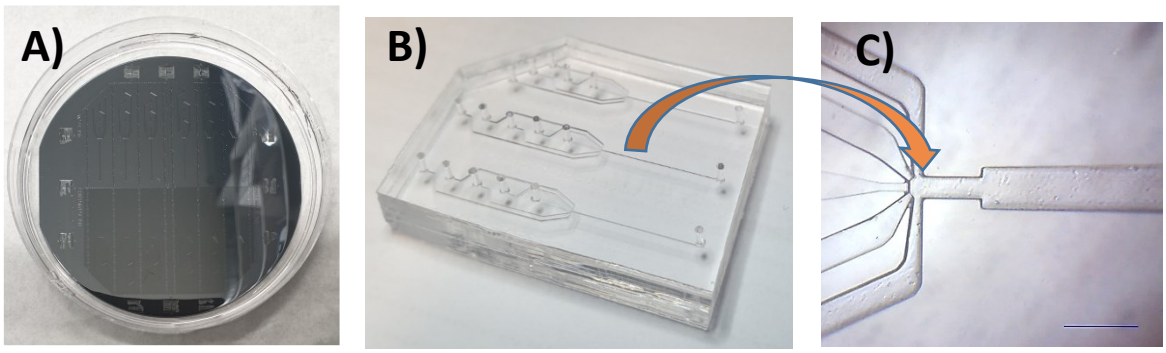

Figure 49. A) Master device; **B)** Microfluidic device; **C)** Brightfield microscope image of five-way junction geometry.

6.3 TEOS modification of microfluidic device channels.

TEOS modification was done as described by W. Mike Arnold [176]. TEOS was mixed with ethanol at ratio 1:1, device channels were filled with the solution for 15 min. The remaining solution was blown with air, and 33% *w/v* aqueous acetic acid was loaded to catalyze hydrolysis of TEOS for 3 min. Afterwards, the device was dried with air and kept at RT for 1 day.

6.4 PEG treatment of microfluidic device:

The experimental procedure was done according with C.K.Chung [175] with small changes, PEG-4600Da was dissolved in water at 0.1M concentration. Microfluidic device was treated in oxygen plasma oven for 1 min, with 80W of power. Immediately after, positive pressure was applied for selected inlet channels by using Flow-EZ 2000mbar pumps (Fluigent), and the PEG solution was applied to the outlet, the procedure continued for 30 minutes. Then outlet tube was removed, device was flushed with air, and put in oven at 115° C for 20 minutes.

6.5 Synthesis of Amphiphilic Block Copolymer PDPA-*b*-PEG:

The synthesis of the block copolymer poly[2-(diisopropylamino) ethyl methacrylate-*b*-poly(ethylene-glycol) was performed by RAFT polymerization with appropriate hydrophobic fraction towards the fabrication of stable self-assembled PS. Briefly, PEG-CTA was dissolved in 1,4-Dioxane with addition of DPA and AIBN initiator. The solution was purged with nitrogen for 30 minutes, and left to react at 70°C for 2days. The final product was purified through Sephadex LH-20 column, precipitated in cold diethyl ether with following lyophilization and analyzed by Size exclusion chromatography (SEC) and ^{1}H NMR (Figure 50).

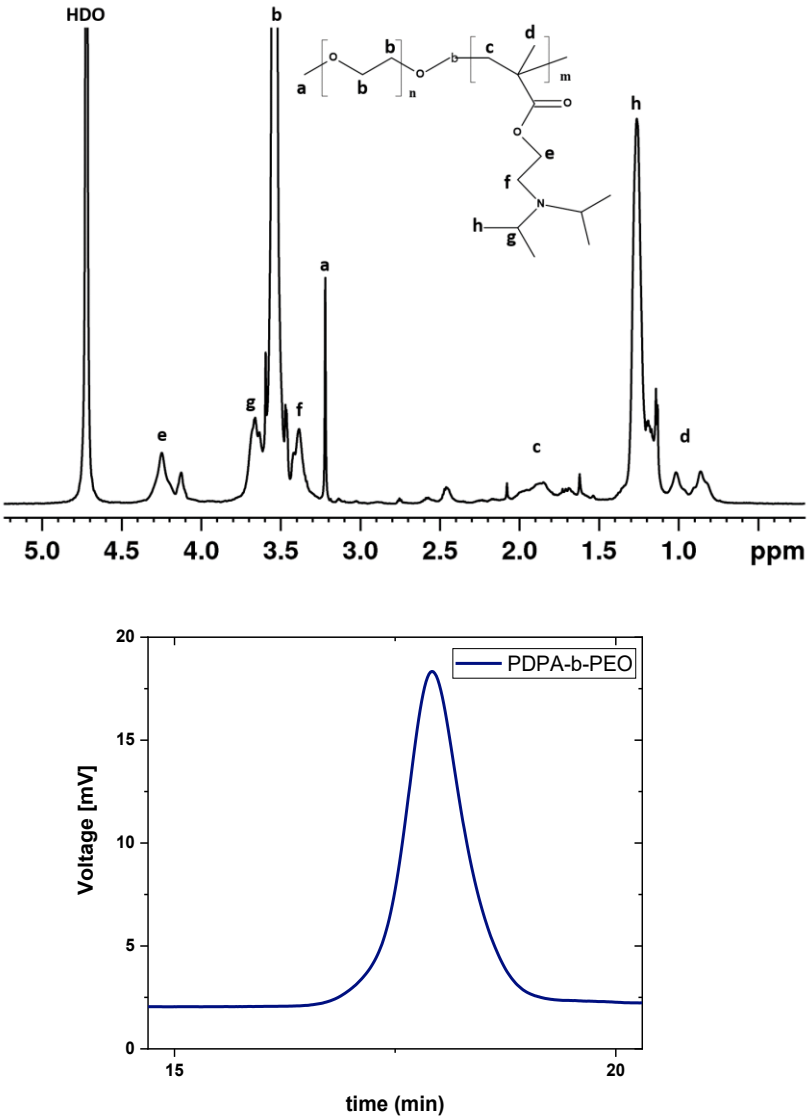

Figure 50. ^{1}H NMR and SEC of PDPA-*b*-PEG (Mn = 6257 g·mol^{-1} and $Đ$ = 1.11).

6.6 Fabrication of Double Emulsion Droplets in Microfluidic Device

Diblock copolymer 10 mg/ml poly(butadiene-*b*-ethylene oxide) (PEG_{1500}-*b*-PBD_{2500}) or 10mg/ml poly(butadiene-*b*-ethylene oxide) with 1 mg/ml poly[2-(diisopropylamino) ethyl methacrylate-*b*- poly(ethylene-glycol) ($PDPA_{4257}$-*b*-PEG_{2000}) at ratio 20:1 was dissolved in toluene as middle flow (MF), inner flow (IF) phase consists of 50 mg/ml Poloxamer188 adjusted pH to 7.4, outer flow OF consisted of 15% Glycerol which increases viscosity that leads to more stable droplet formation, and 50 mg/ml Poloxamer 188 with pH 7.4. The outlet tube with double-emulsion droplets was inserted in vial with 0.1M of Glucose solution at pH 7.4. The evaporation was followed by one day at RT. The dewetted vesicles sedimented on the bottom of the collecting vial. The obtained PS are stable for a few weeks at RT.

The device has a geometry of a five-way junction where streams simultaneously crossed in one point. One channel delivers the inner aqueous phase, two for middle organic phase, and two channels for outer aqueous phases (Figure 51).

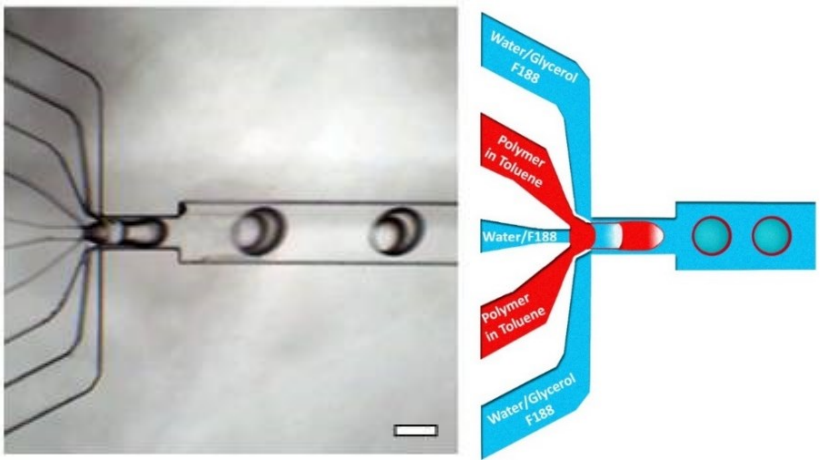

Figure 51. Microscope image and Schematic illustration of the working principle of on-chip production of giant polymer vesicles, Scale bar 100 µm;

The assembly of the giant PS is directed by the double-emulsion droplets during evaporation of the organic solvent in which the copolymer is dissolved.

As can be seen in Figure 52 after formation of the W/O/W droplet, the organic phase distributed in the wall is released into environment, resulting into a creation of a thick-shell giant polymer vesicle in 5 minutes, however, it is necessary to keep the sample overnight at RT for full organic solvent evaporation.

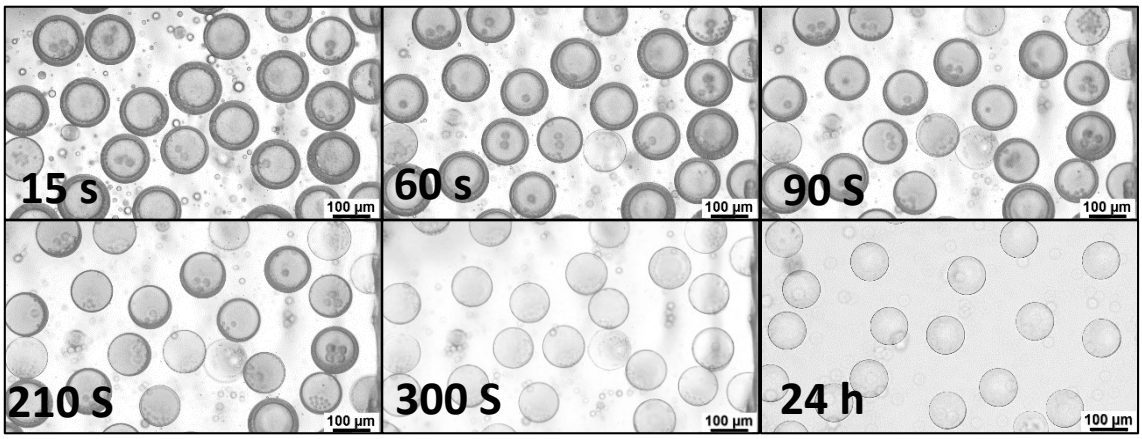

Figure 52. Bright-field microscope images of double emulsion droplets showing the dewetting process in function of time. The double emulsion drop consists of an aqueous drop surrounded by a shell of PEG_{1500}-*b*-PBD_{2500} (7.14 mg.mL^{-1}) with $PDPA_{4257}$-*b*-PEG_{2000} (0.28 mg.mL^{-1}) diblock copolymer dissolved in a toluene. The last image of the PS after complete evaporation of toluene after 24 hours is show as comparison.

By regulation of flow-rates we could achieve PS with different sizes (Figure 53). In general, by increased outer phase speed flow, the overall size decreases. By tuning the middle phase flow the thickness of the membrane can also be controlled. The resulting PS demonstrate exceptional monodispersity, and precise size control.

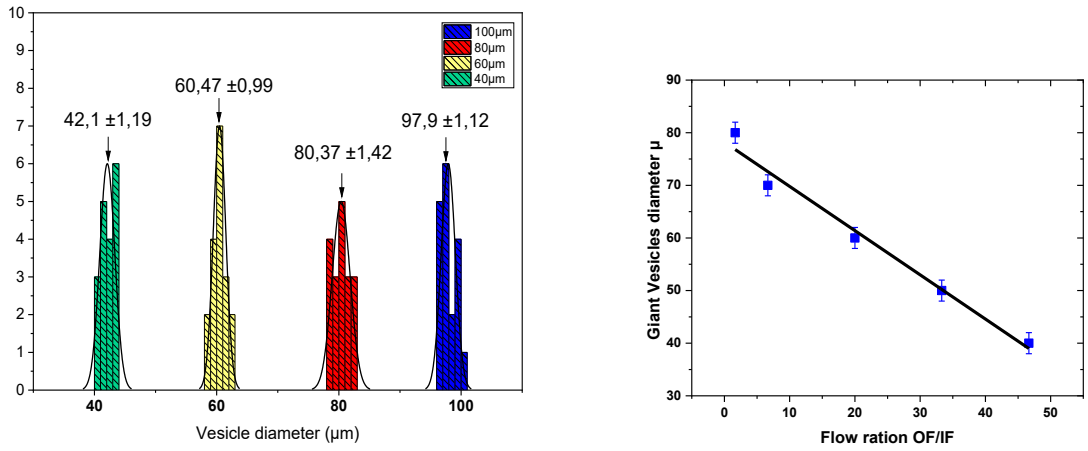

Figure 53. A) Distribution histograms showing the µm size range of Giant Polymer Vesicles (40–100 µm) with superior monodispersity for each of the populations ($n \geqslant 100$ for each population). Gaussian fits are represented by solid lines, arrows point to the mean diameters and the standard deviations (42.1±1.19, 60.47±0.99, 80,37±1.42, 97.7±1.12 µm). **B)** Giant polymer vesicles diameter versus OF flow ratio:IF flow ratio with linear fit.

The giant polymersomes loaded with Calcein and Nile Red (Figure 54) was imaged and processed by the fluorescence microscopy using an IX83 confocal laser scanning microscope

(Olympus, Tokyo, Japan) equipped with a plan S-apochromat objective (lens magnification 10x; NA 0.4; WD 3.1 mm). The excitation light at 488 nm was delivered into a diffraction-limited spot, and the emitted fluorescence was collected by a dichroic mirror DM405/488/543/635; all measurements were performed at 23 ± 1 °C.

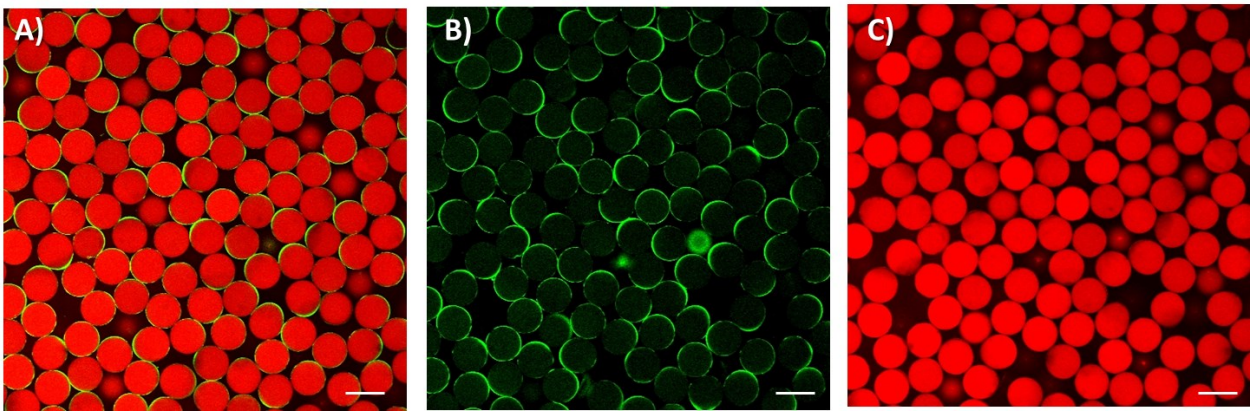

Figure 54. A) Confocal microscopy images of Giant PS loaded with Nile Red and Calcein after solvent evaporation at cross-channel; **B-C)** and single channels for each dye; Scale bar 100 µm;

6.7 Giant vesicles disruption/explosion study

Direct following of vesicles disruption/explosion was done on confocal microscopy using different buffers solutions: 0.1M PBS pH 7.4 with 0.1M of glucose and pH 6.5 – 5 by 0.1M acetate buffer containing 0.1M glucose adjusted with acetic acid. For control study the experiments were performed with non-responsive giant polymer vesicles produced from PEG_{1500}-*b*-$PBD_{2500,}$ results demonstrated complete stability at physiological pH 7.4 and as well at slightly acidic pH ranging from 6.5 to 5, as represented in Figure 55 and Figure 56A. The pH-responsive giant polymer vesicles based on PEG_{1500}-*b*-PBD_{2500} and $PDPA_{4257}$-*b*-PEG_{2000} also demonstrated full stability at pH 7.4, but undergo total disruption in 15 minutes (Figure 55 C-D). The reason of disruption is the protonation of the PDPA block for which pK_a is ~ 6.8, below this value PDPA becomes soluble in aqueous media, which in turns collapses the polymeric membrane. Moreover, in more acidic environment disruptions proceed faster, demonstrating spatial and temporal dependence (Figure 56B**).** Additionally**,** disruption of pH-responsive giant polymer vesicles with following calcein release was captured in real time and selected images over time are shown in Figure 57.

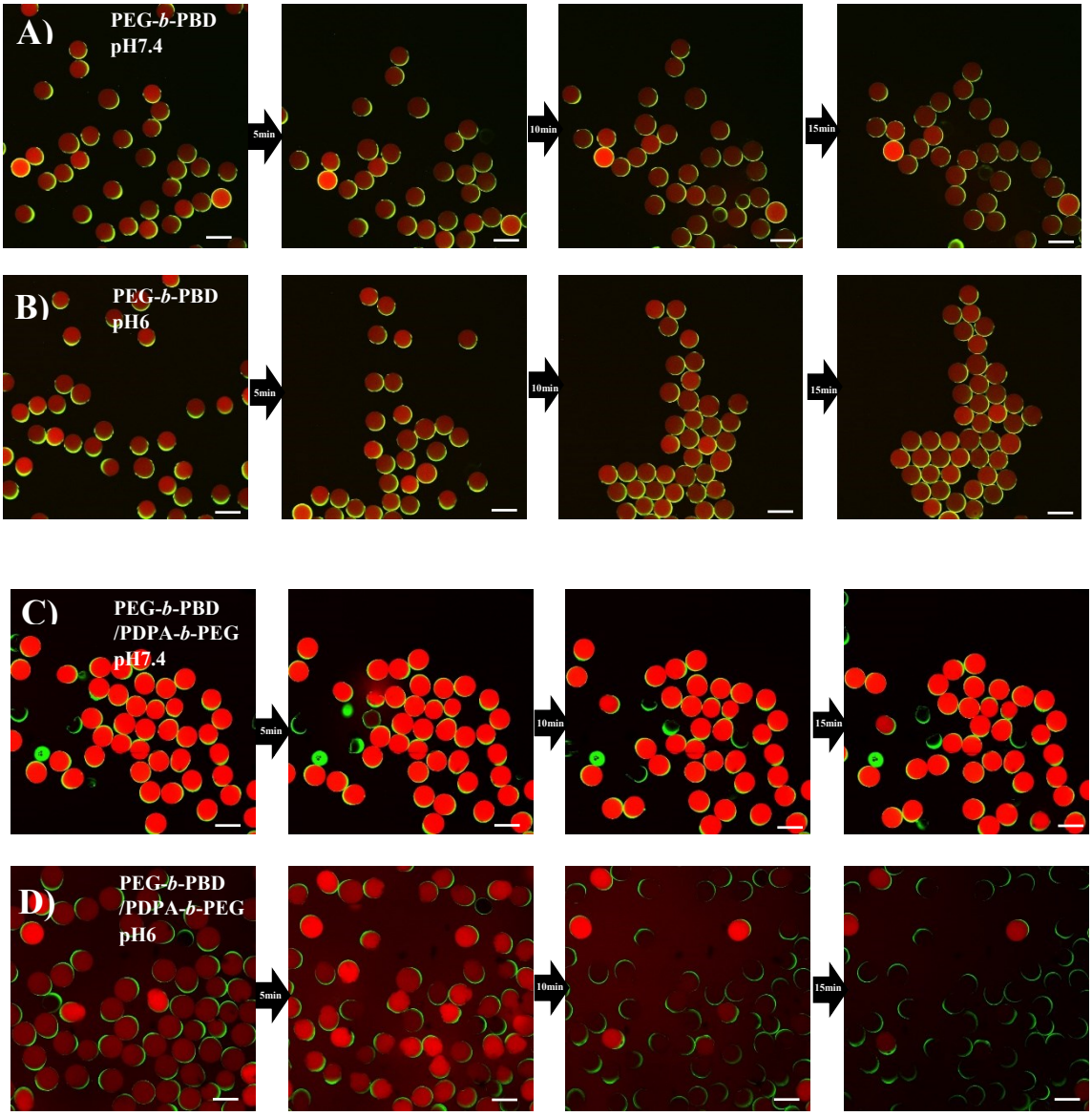

Figure 55. pH disruption (explosion) test followed by confocal microscopy within 15 minutes. A) Non-responsive PS PBD_{2500}-*b*-PEG_{1500} at pH 7.4; B) pH 6; Scale bar 100 µm. pH Degradation; C) Composition of PBD_{2500}-*b*-PEG_{1500} and 5% pH-responsive $PDPA_{4257}$-*b*-PEG_{2000} at pH 7.4; D) at pH 6; Scale bar 100 µm;

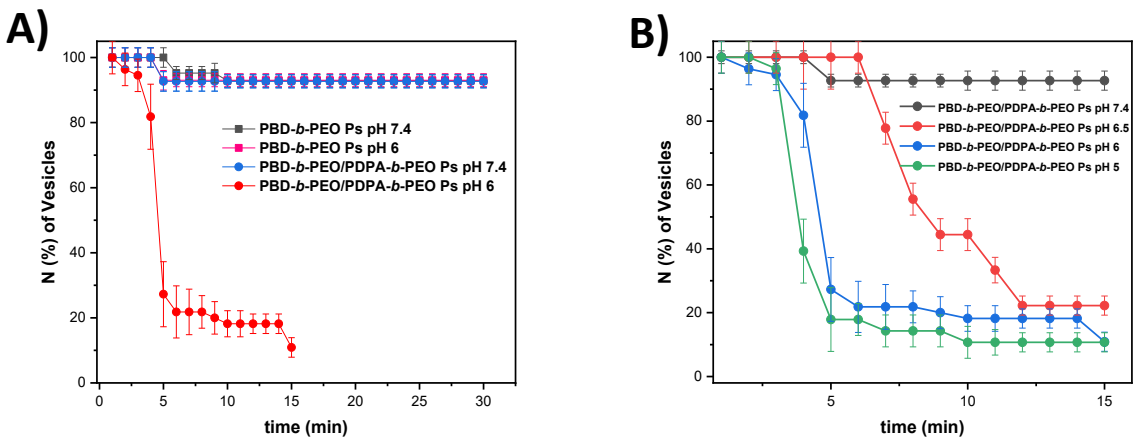

Figure 56. Time-dependent disruption/explosion of giant PS followed by confocal microscopy **A)** Non-responsive PS PBD$_{2500}$-*b*-PEG$_{1500}$ at pH 7.4 **and** pH 6; Composition of PBD$_{2500}$-*b*-PEG$_{1500}$ and 5% pH-responsive PDPA$_{4257}$-*b*-PEG$_{2000}$ at pH 7.4 at pH 6; **B)** PBD$_{2500}$-*b*-PEG$_{1500}$ and 5% PDPA$_{4257}$-*b*-PEG$_{2000}$ pH-responsive giant PS at different pH (5-7.4); The graph shows the decrease of pH-responsive PS number in pH-dependent manner.

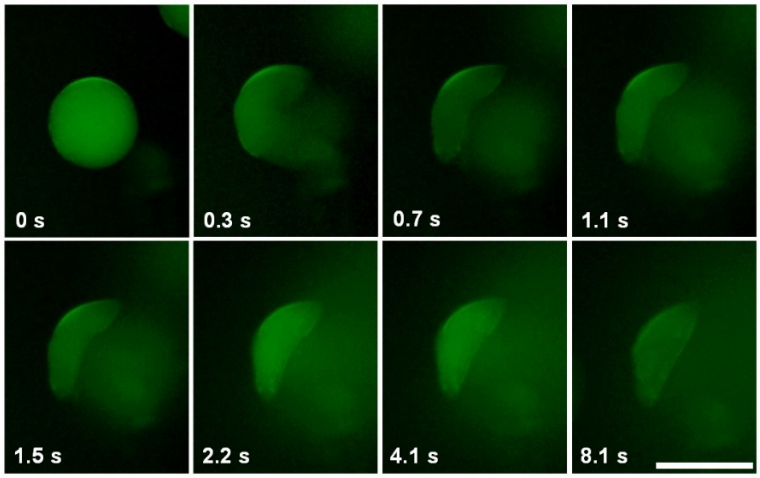

Figure 57. Time frames in seconds showing the disruption of a pH-responsive polymer vesicles and calcein release at pH 5.0. The images were obtained using the fluorescence excitation/emission of calcein (λ_{ex} = 488 nm; λ_{em} = 510-545 nm). The scale bar denotes 100 µm.

6.8 Fluorescent imaging of labeled giant polymer vesicles

In previous imaging we obtain only indirect evidences of diblock copolymer presence in giant polymer vesicles. With the aim to visualize the localization of polymers in vesicular membranes, we synthesized PBD-*b*-PEG coupled with Alexa Fluor 405 dye and triblock copolymer poly[2-(diisopropylamino)ethyl methacrylate-poly(ethylene-glycol)-poly(fluorescein o-methacrylate). The excitation and emission wavelength of Alexa 405 and fluorescein are a suitable pair for independent fluorescent imaging since they are not cross-interfered. The obtained

images clearly demonstrated that the diblocks are mutually distributed across the membrane, Rhodamine 6G was chosen as a dye for visualization of giant PS aqueous core (Figure 58).

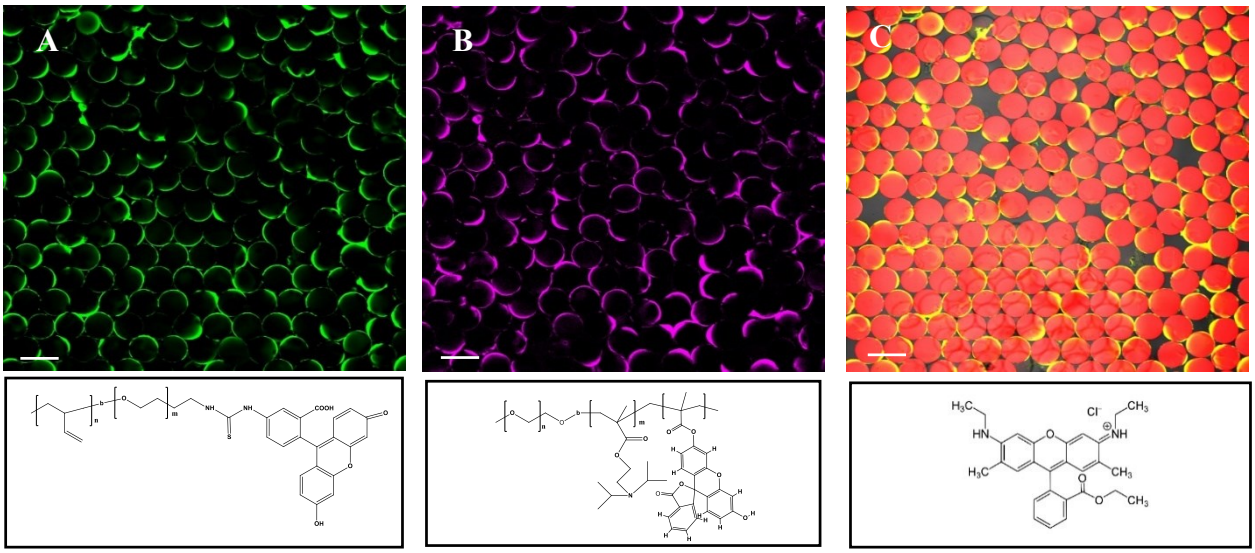

Figure 58. A) Confocal microscopy images of Giant PS **A)** PBD-*b*-PEG-Alexa 405 giant PS polymeric membrane; **B)** membrane of giant PS from PDPA-*b*-PEG-fluorescein o-methacrylate; **C)** aqueous core with Rhodamine 6G; Scale bar 100 µm;

6.9 Loading of BSA-FITC into polymeric membrane of giant PS

In order to evaluate encapsulation properties of polymeric membrane we chose albumin from bovine serum conjugated with Alexa Fluor 488 dye (BSA-FITC), the protein with relatively high M_w ~ 66.5 kDa. The BSA-FITC was pre-dissolved with DMSO and mixed with polymer in organic phase. The resulted highly monodisperse giant PS demonstrated successful loading of BSA-FITC into membrane, which was confirmed by confocal microscopy (Figure 59).

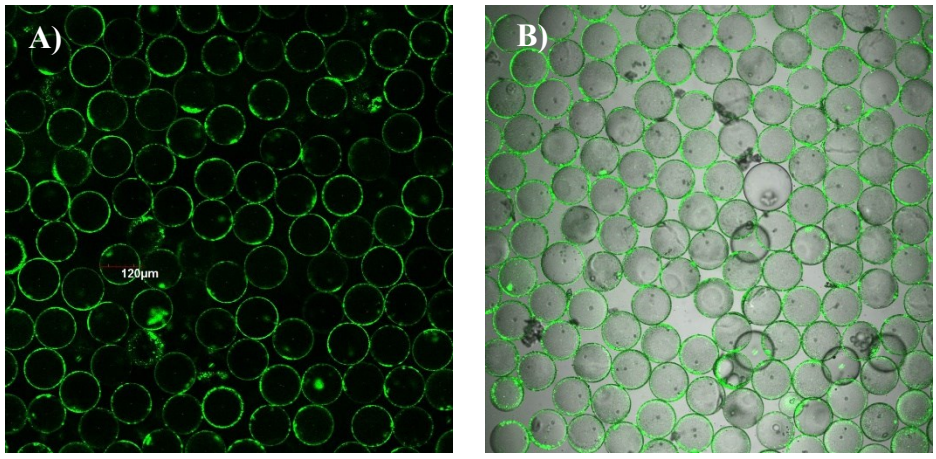

Figure 59. A) Fluorescent confocal microscopy images of Giant PS loaded with BSA-FITC in membrane wall; B) Transmittance and fluorescence cross-channel.

6.10 Cytotoxicity studies with giant PS

Cytotoxicity of giant PS was evaluated with rat mesenchymal stem cells (rMSCs). rMSCs cells were seeded onto 96-well tissue culture plates and cultured for 24-h prior to the addition of giant PS at different concentrations. Cytotoxicity of 24 h and 72 h with giant PS was quantified by MTT assay. Three replicates were used for each experimental condition. The results demonstrate great biocompatibility of giant polymersomes with rat MSC cell line and their general non-cytotoxicity (Figure 59).

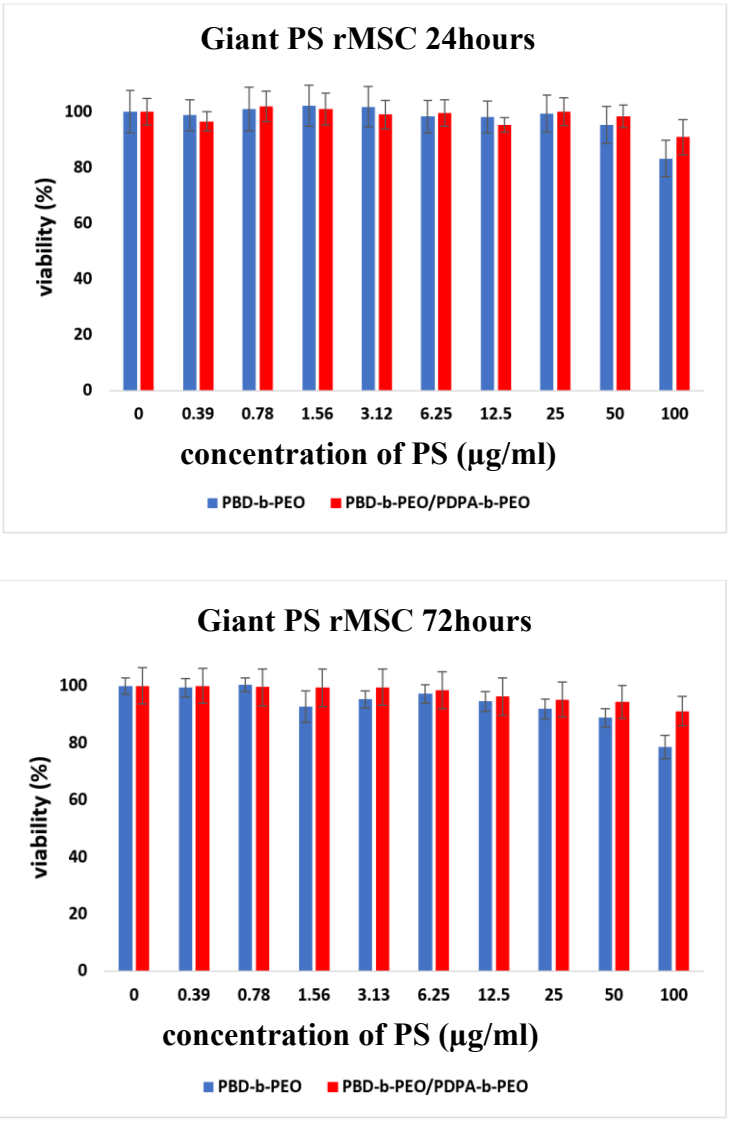

Figure 59. Cytotoxicity of giant PS in rMSC cells at 24 and 72h.

7. Conclusion

Aspects of the kinetic research of MWI-assisted RAFT polymerization were undertaken in the first work, with an emphasis on the advantages and limitations of various reaction conditions, which provide recommendations for determining the proper conditions for HPMA polymerization. With the goal of controlling molecular weights, conversions, and dispersities various CTAs, solvents, and molar ratios were investigated. The kinetic studies revealed that using an aprotic polar solvent (DMSO) resulted in poor conversions and polymerization controllability. Better reaction control was achieved with tert-BuOH as solvent at a molar ratio of $[M]_o/[CTA]_o/[I]_o$ = 100/1/0.2, however the reaction time was still relatively long (t > 12 h). In order to accelerate the reaction time and keep good control over M_w, MWI-RAFT kinetic experiments were done with water as a solvent with a composition of monomer/CTA2/initiator -100/1/0.2, resulting in a four-times faster polymerization time, higher conversion, and exceptional control. Finally, using the PHPMA-mCTA we synthesized nearly monodisperse PHPMA-*b*-bocAPMA, PHPMA-*b*-PMABH and PHPMA-*b*-PDPA by MWI-RAFT polymerization, proving the livingness of the system.

We described the synthesis of diblock copolymers with suitable hydrophilic/hydrophobic weight ratios for the preparation of pH-responsive polymersomes and their full characterization by a variety of analytical techniques (SEC, FTIR, ^{1}H NMR). Several $PHPMA_m$-*b*-$PDPA_n$ diblock copolymers were successfully synthesized by RAFT polymerization. Self-assembly of the diblock copolymers into polymeric vesicles was produced via microfluidic technology. The stimuli-responsive supramolecular self-assemblies were rationally designed to respond the extracellular tumor acidosis, and the polymersomes were further characterized by DLS, SLS, ELS, TEM and SAXS. The assembly-disassembly properties were investigated by FRET and pH titration. The pH- responsive polymersomes successfully loaded with 10% w/w DOX were prepared in a desirable size for tumor accumulation (D_H ~ 100 nm) and further investigated *in vitro* and *in vivo*. The results clearly show that the pH-switchable system is capable of releasing DOX preferentially at the desired tumor sites, with less leakage of the drug at pH 7.4 during blood circulation. The designed nanoplatform enabled effective growth inhibition of EL4 lymphoma tumor with 100% survival rate over 40 days and lower cardiotoxic effects. These features encourage the use of such assemblies as a potential platform to target damaged cells while preserving healthy environments during systemic circulation.

We have developed ROS-responsive BCs to produce PSs with tunable site-specific release of the chemotherapeutic agent DOX. We have shown that BC and PS chemistry strongly influence the degradation behavior, with a dependence on BC degradation linkage and H_2O_2 conditions. The results of this pioneering work strongly suggest that ROS-responsive PS prepared in a size- and polydispersity-controlled manner have the physicochemical and biological properties required for practical applications as nanomedicines with potential for tumor-targeting DOX delivery based on the ROS -triggered release mechanism *in vivo*.

We demonstrated the preparation of PDMS microfluidic device for the production of giant polymersomes. TEOS-modification of PDMS device was applied to create a glass-like cover layer

that significantly improves the chemical resistance, that allows to use harsh solvents as toluene and chloroform, which are volatile and compatible solvents for PS production. The hydrophilic treatment of the outer phase was achieved by PEG deposition. Stable W/O/W double emulsion PS were produced by using a five-way junction geometry microfluidic chip. Stable formation of Ps in microfluidic devices was maintained for up to a few hours. A stable and continuous production of droplets, without failures like fouling polymer on walls or clogging of the device is extremely important, for which applicable parameters were established. The non-responsive giant PS were prepared from PBD-*b*-PEG; by adding 5-10% PDPA-*b*-PEG we successfully prepared pH-responsive giant PS. The giant PS were size-tuned in the range from 30 to 200 μm. Hydrophilic and/or hydrophobic model compounds were easily encapsulated (core/shell). The pH-responsive PS demonstrated the spatial and temporal pH-controlled disruption under simulated relevant physiological conditions. The PS exhibited good biocompatibility *in vitro* (rMSC cell lines). This approach can be utilized to fabricate pH-responsive systems for several active compounds, microreactors, and artificial organelles toward cell mimicking.

8. References

[1] V. Sincari, S.L. Petrova, R. Konefał, M. Hruby, E. Jäger, Microwave-assisted RAFT polymerization of *N*-(2-hydroxypropyl) methacrylamide and its relevant copolymers, React. Funct. Polym. 162 (2021) 104875.

https://doi.org/10.1016/j.reactfunctpolym.2021.104875.

[2] L.J.C. Albuquerque, V. Sincari, A. Jäger, R. Konefał, J. Pánek, P. Černoch, E. Pavlova, P. Štěpánek, F.C. Giacomelli, E. Jäger, Microfluidic-Assisted Engineering of Quasi-Monodisperse pH-Responsive Polymersomes toward Advanced Platforms for the Intracellular Delivery of Hydrophilic Therapeutics, Langmuir. (2019) acs.langmuir.9b01009. https://doi.org/10.1021/acs.langmuir.9b01009.

[3] L.J.C. Albuquerque, V. Sincari, A. Jäger, J. Kucka, J. Humajova, J. Pankrac, P. Paral, T. Heizer, O. Janouškova, I. Davidovich, Y. Talmon, P. Pouckova, P. Štěpánek, L. Sefc, M. Hruby, F.C. Giacomelli, E. Jäger, pH-responsive polymersome-mediated delivery of doxorubicin into tumor sites enhances the therapeutic efficacy and reduces cardiotoxic effects, J. Control. Release. 332 (2021) 529–538. https://doi.org/10.1016/j.jconrel.2021.03.013.

[4] E. Jäger, V. Sincari, L.J.C. Albuquerque, A. Jäger, J. Humajova, J. Kucka, J. Pankrac, P. Paral, T. Heizer, O. Janouskova, R. Konefał, E. Pavlova, O. Sedlacek, F.C. Giacomelli, P. Pouckova, L. Sefc, P. Stepanek, M. Hruby, Reactive Oxygen Species (ROS)-Responsive Polymersomes with Site-Specific Chemotherapeutic Delivery into Tumors via Spacer Design Chemistry, Biomacromolecules. 21 (2020) 1437–1449. https://doi.org/10.1021/acs.biomac.9b01748.

[5] https://www.who.int/news-room/fact-sheets/detail/cancer.

[6] E. Lepeltier, P. Rijo, F. Rizzolio, R. Popovtzer, V. Petrikaite, Y.G. Assaraf, C. Passirani, Nanomedicine to target multidrug resistant tumors, Drug Resist. Updat. 52 (2020) 100704. https://doi.org/10.1016/j.drup.2020.100704.

[7] N.V. Rao, H. Ko, J. Lee, J.H. Park, Recent Progress and Advances in Stimuli-Responsive Polymers for Cancer Therapy, Front. Bioeng. Biotechnol. 6 (2018). https://doi.org/10.3389/fbioe.2018.00110.

[8] R.G. Thomas, S.P. Surendran, Y.Y. Jeong, Tumor Microenvironment-Stimuli Responsive Nanoparticles for Anticancer Therapy, Front. Mol. Biosci. 7 (2020). https://doi.org/10.3389/fmolb.2020.610533.

[9] E. Jäger, A. Jäger, T. Etrych, F.C. Giacomelli, P. Chytil, A. Jigounov, J.-L. Putaux, B. Říhová, K. Ulbrich, P. Štěpánek, Self-assembly of biodegradable copolyester and reactive HPMA-based polymers into nanoparticles as an alternative stealth drug delivery system, Soft Matter. 8 (2012) 9563. https://doi.org/10.1039/c2sm26150b.

[10] N.K. Green, C.W. Herbert, S.J. Hale, A.B. Hale, V. Mautner, R. Harkins, T. Hermiston, K. Ulbrich, K.D. Fisher, L.W. Seymour, Extended plasma circulation time and decreased toxicity of polymer-coated adenovirus, Gene Ther. 11 (2004) 1256–1263. https://doi.org/10.1038/sj.gt.3302295.

[11] D. Rosenblum, N. Joshi, W. Tao, J.M. Karp, D. Peer, Progress and challenges towards targeted delivery of cancer therapeutics, Nat. Commun. 9 (2018) 1410. https://doi.org/10.1038/s41467-018-03705-y.

[12] M.H. Matsumura Y, No Title, Cancer Res. 12 Pt 1 (n.d.) 6387–92.

[13] H. Maeda, H. Nakamura, J. Fang, The EPR effect for macromolecular drug delivery to solid tumors: Improvement of tumor uptake, lowering of systemic toxicity, and distinct tumor imaging in vivo, Adv. Drug Deliv. Rev. 65 (2013) 71–79. https://doi.org/10.1016/j.addr.2012.10.002.

[14] M.F. Attia, N. Anton, J. Wallyn, Z. Omran, T.F. Vandamme, An overview of active and passive targeting strategies to improve the nanocarriers efficiency to tumour sites, J. Pharm. Pharmacol. 71 (2019) 1185–1198. https://doi.org/10.1111/jphp.13098.

[15] F. Danhier, To exploit the tumor microenvironment: Since the EPR effect fails in the clinic, what is the future of nanomedicine?, J. Control. Release. 244 (2016) 108–121. https://doi.org/10.1016/j.jconrel.2016.11.015.

[16] J. Fang, W. Islam, H. Maeda, Exploiting the dynamics of the EPR effect and strategies to improve the therapeutic effects of nanomedicines by using EPR effect enhancers, Adv. Drug Deliv. Rev. 157 (2020) 142–160. https://doi.org/10.1016/j.addr.2020.06.005.

[17] S. Sindhwani, A.M. Syed, J. Ngai, B.R. Kingston, L. Maiorino, J. Rothschild, P. MacMillan, Y. Zhang, N.U. Rajesh, T. Hoang, J.L.Y. Wu, S. Wilhelm, A. Zilman, S. Gadde, A. Sulaiman, B. Ouyang, Z. Lin, L. Wang, M. Egeblad, W.C.W. Chan, The entry of nanoparticles into solid tumours, Nat. Mater. 19 (2020) 566–575. https://doi.org/10.1038/s41563-019-0566-2.

[18] J. Torres, N. Dhas, M. Longhi, M.C. García, Overcoming Biological Barriers With Block Copolymers-Based Self-Assembled Nanocarriers. Recent Advances in Delivery of Anticancer Therapeutics, Front. Pharmacol. 11 (2020). https://doi.org/10.3389/fphar.2020.593197.

[19] J. Yoo, C. Park, G. Yi, D. Lee, H. Koo, Active Targeting Strategies Using Biological Ligands for Nanoparticle Drug Delivery Systems, Cancers (Basel). 11 (2019) 640. https://doi.org/10.3390/cancers11050640.

[20] D. Liu, Cancer biomarkers for targeted therapy, Biomark. Res. 7 (2019) 25. https://doi.org/10.1186/s40364-019-0178-7.

[21] S. Awwad, U. Angkawinitwong, Overview of Antibody Drug Delivery, Pharmaceutics. 10 (2018) 83. https://doi.org/10.3390/pharmaceutics10030083.

[22] B. Bhattacharya, M.F. Mohd Omar, R. Soong, The Warburg effect and drug resistance, Br. J. Pharmacol. 173 (2016) 970–979. https://doi.org/10.1111/bph.13422.

[23] S. Kumari, A.K. Badana, M.M. G, S. G, R. Malla, Reactive Oxygen Species: A Key Constituent in Cancer Survival, Biomark. Insights. 13 (2018) 117727191875539. https://doi.org/10.1177/1177271918755391.

[24] A.D. Bangham, M.M. Standish, J.C. Watkins, Diffusion of univalent ions across the lamellae of swollen phospholipids, J. Mol. Biol. 13 (1965) 238-IN27. https://doi.org/10.1016/S0022-2836(65)80093-6.

[25] L. Maja, K. Željko, P. Mateja, Sustainable technologies for liposome preparation, J. Supercrit. Fluids. 165 (2020) 104984. https://doi.org/10.1016/j.supflu.2020.104984.

[26] M. Fathi, J. Barar, Perspective highlights on biodegradable polymeric nanosystems for targeted therapy of solid tumors, BioImpacts. 7 (2017) 49–57. https://doi.org/10.15171/bi.2017.07.

[27] I. Ekladious, Y.L. Colson, M.W. Grinstaff, Polymer–drug conjugate therapeutics: advances, insights and prospects, Nat. Rev. Drug Discov. 18 (2019) 273–294. https://doi.org/10.1038/s41573-018-0005-0.

[28] S. Manandhar, E. Sjöholm, J. Bobacka, J.M. Rosenholm, K.K. Bansal, Polymer-Drug Conjugates as Nanotheranostic Agents, J. Nanotheranostics. 2 (2021) 63–81. https://doi.org/10.3390/jnt2010005.

[29] G. Pasut, F.M. Veronese, PEG conjugates in clinical development or use as anticancer agents: An overview, Adv. Drug Deliv. Rev. 61 (2009) 1177–1188. https://doi.org/10.1016/j.addr.2009.02.010.

[30] P.A. Vasey, R. Duncan, S.B. Kaye, J. Cassidy, 929 Clinical phase I trial of PK1 (HPMA co-polymer doxorubicin), Eur. J. Cancer. 31 (1995) S193. https://doi.org/10.1016/0959-8049(95)96178-G.

[31] M.J. Vicent, F. Greco, R.I. Nicholson, A. Paul, P.C. Griffiths, R. Duncan, Polymer Therapeutics Designed for a Combination Therapy of Hormone-Dependent Cancer, Angew. Chemie Int. Ed. 44 (2005) 4061–4066. https://doi.org/10.1002/anie.200462960.

[32] H. Kostková, T. Etrych, B. Říhová, K. Ulbrich, Synergistic effect of HPMA copolymer-bound doxorubicin and dexamethasone in vivo on mouse lymphomas, J. Bioact. Compat. Polym. 26 (2011) 270–286. https://doi.org/10.1177/0883911511406326.

[33] T. Lammers, V. Subr, K. Ulbrich, P. Peschke, P.E. Huber, W.E. Hennink, G. Storm, Simultaneous delivery of doxorubicin and gemcitabine to tumors in vivo using prototypic polymeric drug carriers, Biomaterials. 30 (2009) 3466–3475. https://doi.org/10.1016/j.biomaterials.2009.02.040.

[34] H. Kostková, T. Etrych, B. Říhová, L. Kostka, L. Starovoytová, M. Kovář, K. Ulbrich, HPMA Copolymer Conjugates of DOX and Mitomycin C for Combination Therapy: Physicochemical Characterization, Cytotoxic Effects, Combination Index Analysis, and Anti-Tumor Efficacy, Macromol. Biosci. 13 (2013) 1648–1660. https://doi.org/10.1002/mabi.201300288.

[35] J. Gong, M. Chen, Y. Zheng, S. Wang, Y. Wang, Polymeric micelles drug delivery system in oncology, J. Control. Release. 159 (2012) 312–323. https://doi.org/10.1016/j.jconrel.2011.12.012.

[36] K.S. Lee, H.C. Chung, S.A. Im, Y.H. Park, C.S. Kim, S.-B. Kim, S.Y. Rha, M.Y. Lee, J. Ro, Multicenter phase II trial of Genexol-PM, a Cremophor-free, polymeric micelle formulation of paclitaxel, in patients with metastatic breast cancer, Breast Cancer Res. Treat. 108 (2008) 241–250. https://doi.org/10.1007/s10549-007-9591-y.

[37] https://clinicaltrials.gov/ct2/show/NCT00912639.

[38] H. Mukai, K. Kato, T. Esaki, S. Ohsumi, Y. Hozomi, N. Matsubara, T. Hamaguchi, Y. Matsumura, R. Goda, T. Hirai, Y. Nambu, Phase I study of NK105, a nanomicellar paclitaxel formulation, administered on a weekly schedule in patients with solid tumors, Invest. New Drugs. 34 (2016) 750–759. https://doi.org/10.1007/s10637-016-0381-4.

[39] K. Kato, K. Chin, T. Yoshikawa, K. Yamaguchi, Y. Tsuji, T. Esaki, K. Sakai, M. Kimura, T. Hamaguchi, Y. Shimada, Y. Matsumura, R. Ikeda, Phase II study of NK105, a paclitaxel-incorporating micellar nanoparticle, for previously treated advanced or recurrent gastric cancer, Invest. New Drugs. 30 (2012) 1621–1627. https://doi.org/10.1007/s10637-011-9709-2.

[40] T. Saeki, H. Mukai, J. Ro, Y.-C. Lin, Y. Fujiwara, S. Nagai, K.S. Lee, J. Watanabe, S. Ohtani, S.B. Kim, K. Kuroi, K. Tsugawa, Y. Tokuda, H. Iwata, Y.H. Park, Y. Yang, Y. Nambu, A global phase III clinical study comparing NK105 and paclitaxel in metastatic or recurrent breast cancer patients, Ann. Oncol. 28 (2017) v80–v81. https://doi.org/10.1093/annonc/mdx365.013.

[41] A. Takahashi, Y. Yamamoto, M. Yasunaga, Y. Koga, J. Kuroda, M. Takigahira, M. Harada, H. Saito, T. Hayashi, Y. Kato, T. Kinoshita, N. Ohkohchi, I. Hyodo, Y. Matsumura, NC - 6300, an epirubicin-incorporating micelle, extends the antitumor effect and reduces the cardiotoxicity of epirubicin, Cancer Sci. 104 (2013) 920–925. https://doi.org/10.1111/cas.12153.

[42] S.F. Jones, H.A. Burris, J.R. Infante, F.A. Greco, D.R. Spigel, S. Kawamura, T. Ishioka, H. Yamazaki, J.C. Bendell, A phase I study of NK012 in combination with 5-fluorouracil with or without leucovorin in patients (pts) with advanced solid tumors., J. Clin. Oncol. 30 (2012) e13076–e13076. https://doi.org/10.1200/jco.2012.30.15_suppl.e13076.

[43] https://clinicaltrials.gov/ct2/show/NCT02043288.

[44] N.P. Kamat, J.S. Katz, D.A. Hammer, Engineering Polymersome Protocells, J. Phys. Chem. Lett. 2 (2011) 1612–1623. https://doi.org/10.1021/jz200640x.

[45] J. Chiefari, Y.K. (Bill) Chong, F. Ercole, J. Krstina, J. Jeffery, T.P.T. Le, R.T.A. Mayadunne, G.F. Meijs, C.L. Moad, G. Moad, E. Rizzardo, S.H. Thang, Living Free-Radical Polymerization by Reversible Addition−Fragmentation Chain Transfer: The RAFT Process, Macromolecules. 31 (1998) 5559–5562. https://doi.org/10.1021/ma9804951.

[46] G. Moad, E. Rizzardo, S.H. Thang, End-functional polymers, thiocarbonylthio group removal/transformation and reversible addition-fragmentation-chain transfer (RAFT) polymerization, Polym. Int. 60 (2011) 9–25. https://doi.org/10.1002/pi.2988.

[47] P. Černoch, A. Jager, Z. Černochová, V. Sincari, L.J.C. Albuquerque, R. Konefal, E. Pavlova, F.C. Giacomelli, E. Jager, Engineering of pH-triggered nanoplatforms based on novel poly(2-methyl-2-oxazoline)- b -poly[2-(diisopropylamino)ethyl methacrylate] diblock copolymers with tunable morphologies for biomedical applications, Polym. Chem. 12 (2021) 2868–2880. https://doi.org/10.1039/D1PY00141H.

[48] D. Roy, A. Ullah, B.S. Sumerlin, Rapid Block Copolymer Synthesis by Microwave-Assisted RAFT Polymerization, Macromolecules. 42 (2009) 7701–7708. https://doi.org/10.1021/ma901471k.

[49] M. Teodorescu, K. Matyjaszewski, Atom Transfer Radical Polymerization of (Meth)acrylamides, Macromolecules. 32 (1999) 4826–4831. https://doi.org/10.1021/ma990175x.

[50] Č. Koňák, B. Ganchev, M. Teodorescu, K. Matyjaszewski, P. Kopečková, J. Kopeček, Poly[N -(2-hydroxypropyl)methacrylamide- block - n -butyl acrylate] micelles in water/DMF mixed solvents, Polymer (Guildf). 43 (2002) 3735–3741. https://doi.org/10.1016/S0032-3861(02)00182-9.

[51] S. Yadav, A.K. Sharma, P. Kumar, Nanoscale Self-Assembly for Therapeutic Delivery, Front. Bioeng. Biotechnol. 8 (2020). https://doi.org/10.3389/fbioe.2020.00127.

[52] A. Blanazs, S.P. Armes, A.J. Ryan, Self-Assembled Block Copolymer Aggregates: From Micelles to Vesicles and their Biological Applications, Macromol. Rapid Commun. 30 (2009) 267–277. https://doi.org/10.1002/marc.200800713.

[53] Q. He, J. Chen, J. Yan, S. Cai, H. Xiong, Y. Liu, D. Peng, M. Mo, Z. Liu, Tumor microenvironment responsive drug delivery systems, Asian J. Pharm. Sci. 15 (2020) 416–448. https://doi.org/10.1016/j.ajps.2019.08.003.

[54] R.P. Brinkhuis, T.R. Visser, F.P.J.T. Rutjes, J.C.M. van Hest, Shedding the hydrophilic mantle of polymersomes, Polym. Chem. 2 (2011) 550–552. https://doi.org/10.1039/C0PY00316F.

[55] S. Zhuo, F. Zhang, J. Yu, X. Zhang, G. Yang, X. Liu, pH-Sensitive Biomaterials for Drug Delivery, Molecules. 25 (2020) 5649. https://doi.org/10.3390/molecules25235649.

[56] C.-C. Song, F.-S. Du, Z.-C. Li, Oxidation-responsive polymers for biomedical applications, J. Mater. Chem. B. 2 (2014) 3413–3426. https://doi.org/10.1039/C3TB21725F.

[57] A. Napoli, M. Valentini, N. Tirelli, M. Müller, J.A. Hubbell, Oxidation-responsive polymeric vesicles, Nat. Mater. 3 (2004) 183–189. https://doi.org/10.1038/nmat1081.

[58] M. Geven, R. D'Arcy, Z.Y. Turhan, F. El-Mohtadi, A. Alshamsan, N. Tirelli, Sulfur-based oxidation-responsive polymers. Chemistry, (chemically selective) responsiveness and biomedical applications, Eur. Polym. J. 149 (2021) 110387. https://doi.org/10.1016/j.eurpolymj.2021.110387.

[59] N. Ma, Y. Li, H. Ren, H. Xu, Z. Li, X. Zhang, Selenium-containing block copolymers and their oxidation-responsive aggregates, Polym. Chem. 1 (2010) 1609. https://doi.org/10.1039/c0py00144a.

[60] N. Oddone, F. Boury, E. Garcion, A.M. Grabrucker, M.C. Martinez, F. Da Ros, A. Janaszewska, F. Forni, M.A. Vandelli, G. Tosi, B. Ruozi, J.T. Duskey, Synthesis, Characterization, and In Vitro Studies of an Reactive Oxygen Species (ROS)-Responsive Methoxy Polyethylene Glycol-Thioketal-Melphalan Prodrug for Glioblastoma Treatment, Front. Pharmacol. 11 (2020). https://doi.org/10.3389/fphar.2020.00574.

[61] M.S. Shim, Y. Xia, A Reactive Oxygen Species (ROS)-Responsive Polymer for Safe, Efficient, and Targeted Gene Delivery in Cancer Cells, Angew. Chemie Int. Ed. 52 (2013) 6926–6929. https://doi.org/10.1002/anie.201209633.

[62] D.S. Wilson, G. Dalmasso, L. Wang, S. V. Sitaraman, D. Merlin, N. Murthy, Orally delivered thioketal nanoparticles loaded with TNF-α–siRNA target inflammation and inhibit gene expression in the intestines, Nat. Mater. 9 (2010) 923–928. https://doi.org/10.1038/nmat2859.

[63] B.S. Swami Vetha, A.G. Adam, A. Aileru, Redox Responsive Copolyoxalate Smart Polymers for Inflammation and Other Aging-Associated Diseases, Int. J. Mol. Sci. 22 (2021) 5607. https://doi.org/10.3390/ijms22115607.

[64] C. Kang, W. Cho, M. Park, J. Kim, S. Park, D. Shin, C. Song, D. Lee, H2O2-triggered bubble generating antioxidant polymeric nanoparticles as ischemia/reperfusion targeted nanotheranostics, Biomaterials. 85 (2016) 195–203. https://doi.org/10.1016/j.biomaterials.2016.01.070.

[65] D. Lee, S. Park, S. Bae, D. Jeong, M. Park, C. Kang, W. Yoo, M.A. Samad, Q. Ke, G. Khang, P.M. Kang, Hydrogen peroxide-activatable antioxidant prodrug as a targeted therapeutic agent for ischemia-reperfusion injury, Sci. Rep. 5 (2015) 16592. https://doi.org/10.1038/srep16592.

[66] H.C. Shum, D. Lee, I. Yoon, T. Kodger, D.A. Weitz, Double Emulsion Templated Monodisperse Phospholipid Vesicles, Langmuir. 24 (2008) 7651–7653. https://doi.org/10.1021/la801833a.

[67] H.C. Shum, J.-W. Kim, D.A. Weitz, Microfluidic Fabrication of Monodisperse Biocompatible and Biodegradable Polymersomes with Controlled Permeability, J. Am. Chem. Soc. 130 (2008) 9543–9549. https://doi.org/10.1021/ja802157y.

[68] M. Abdollahi, S. Mehdipour-Ataei, F. Ziaee, Using1H-NMR spectroscopy for the kinetic study of thein situ solution free-radical copolymerization of styrene and ethyl acrylate, J.

Appl. Polym. Sci. 105 (2007) 2588–2597. https://doi.org/10.1002/app.26290.

[69] I. Krämer, H. Pasch, H. Händel, K. Albert, Chemical heterogeneity analysis of high-conversion poly[styrene-co-(ethyl acrylate)]s by NMR and on-line coupled SEC-NMR, Macromol. Chem. Phys. 200 (1999) 1734–1744. https://doi.org/10.1002/(SICI)1521-3935(19990701)200:7<1734::AID-MACP1734>3.0.CO;2-L.

[70] A.S. Brar, A. Yadav, Microstructure of glycidylmethacrylate/vinyl acetate copolymers by two-dimensional nuclear magnetic resonance spectroscopy, J. Polym. Sci. Part A Polym. Chem. 39 (2001) 4051–4060. https://doi.org/10.1002/pola.10054.

[71] Brown W, Dynamic Light Scattering: The Method and Some Applications, 16 Diffus. Spectrosc. (1993). https://doi.org/10.1016/S1359-0294(97)80032-5.

[72] H.-A. Kim, J.-K. Seo, T. Kim, B.-T. Lee, Nanometrology and Its Perspectives in Environmental Research, Environ. Health Toxicol. 29 (2014). https://doi.org/10.5620/eht.e2014016.

[73] E. Ruska, The development of the electron microscope and of electron microscopy, Biosci. Rep. 7 (1987) 607–629. https://doi.org/10.1007/BF01127674.

[74] H. Jinnai, R.J. Spontak, Transmission electron microtomography in polymer research, Polymer (Guildf). 50 (2009) 1067–1087. https://doi.org/10.1016/j.polymer.2008.12.023.

[75] L.E. Franken, E.J. Boekema, M.C.A. Stuart, Transmission Electron Microscopy as a Tool for the Characterization of Soft Materials: Application and Interpretation, Adv. Sci. 4 (2017) 1600476. https://doi.org/10.1002/advs.201600476.

[76] R.F. Thompson, M. Walker, C.A. Siebert, S.P. Muench, N.A. Ranson, An introduction to sample preparation and imaging by cryo-electron microscopy for structural biology, Methods. 100 (2016) 3–15. https://doi.org/10.1016/j.ymeth.2016.02.017.

[77] B.L. Sanchez-Gaytan, F. Fay, S. Hak, A. Alaarg, Z.A. Fayad, C. Pérez-Medina, W.J.M. Mulder, Y. Zhao, Real-Time Monitoring of Nanoparticle Formation by FRET Imaging, Angew. Chemie Int. Ed. 56 (2017) 2923–2926. https://doi.org/10.1002/anie.201611288.

[78] Y. Zhao, F. Fay, S. Hak, J. Manuel Perez-Aguilar, B.L. Sanchez-Gaytan, B. Goode, R. Duivenvoorden, C. de Lange Davies, A. Bjørkøy, H. Weinstein, Z.A. Fayad, C. Pérez-Medina, W.J.M. Mulder, Augmenting drug–carrier compatibility improves tumour nanotherapy efficacy, Nat. Commun. 7 (2016) 11221. https://doi.org/10.1038/ncomms11221.

[79] B. Gong, B.-K. Choi, J.-Y. Kim, D. Shetty, Y.H. Ko, N. Selvapalam, N.K. Lee, K. Kim, High Affinity Host–Guest FRET Pair for Single-Vesicle Content-Mixing Assay: Observation of Flickering Fusion Events, J. Am. Chem. Soc. 137 (2015) 8908–8911. https://doi.org/10.1021/jacs.5b05385.

[80] M. Vorobii, A. de los Santos Pereira, O. Pop-Georgievski, N.Y. Kostina, C. Rodriguez-Emmenegger, V. Percec, Synthesis of non-fouling poly[N-(2-hydroxypropyl)methacrylamide] brushes by photoinduced SET-LRP, Polym. Chem. 6 (2015) 4210–4220. https://doi.org/10.1039/C5PY00506J.

[81] T.T. Hoang Thi, E.H. Pilkington, D.H. Nguyen, J.S. Lee, K.D. Park, N.P. Truong, The Importance of Poly(ethylene glycol) Alternatives for Overcoming PEG Immunogenicity in Drug Delivery and Bioconjugation, Polymers (Basel). 12 (2020) 298. https://doi.org/10.3390/polym12020298.

[82] V. Raus, L. Kostka, Optimizing the Cu-RDRP of N -(2-hydroxypropyl) methacrylamide toward biomedical applications, Polym. Chem. 10 (2019) 564–568. https://doi.org/10.1039/C8PY01569D.

[83] C.W. Scales, Y.A. Vasilieva, A.J. Convertine, A.B. Lowe, C.L. McCormick, Direct, Controlled Synthesis of the Nonimmunogenic, Hydrophilic Polymer, Poly(N -(2-hydroxypropyl)methacrylamide) via RAFT in Aqueous Media, Biomacromolecules. 6 (2005) 1846–1850. https://doi.org/10.1021/bm0503017.

[84] Z. Özdemir, M. Topuzoğulları, İ.A. İşoğlu, S. Dinçer, RAFT-mediated synthesis of poly(N-(2-hydroxypropyl)methacrylamide-*b*-4-vinylpyridine) by conventional and microwave heating, Polym. Bull. 70 (2013) 2857–2872. https://doi.org/10.1007/s00289-013-0993-1.

[85] V. Šubr, L. Kostka, J. Strohalm, T. Etrych, K. Ulbrich, Synthesis of Well-Defined Semitelechelic Poly[N -(2-hydroxypropyl)methacrylamide] Polymers with Functional Group at the α-End of the Polymer Chain by RAFT Polymerization, Macromolecules. 46 (2013) 2100–2108. https://doi.org/10.1021/ma400042u.

[86] J.A. Alfurhood, H. Sun, C.P. Kabb, B.S. Tucker, J.H. Matthews, H. Luesch, B.S. Sumerlin, Poly(N-(2-hydroxypropyl)methacrylamide)–valproic acid conjugates as block copolymer nanocarriers, Polym. Chem. 8 (2017) 4983–4987. https://doi.org/10.1039/C7PY00196G.

[87] M. Barz, M. Tarantola, K. Fischer, M. Schmidt, R. Luxenhofer, A. Janshoff, P. Theato, R. Zentel, From Defined Reactive Diblock Copolymers to Functional HPMA-Based Self-Assembled Nanoaggregates, Biomacromolecules. 9 (2008) 3114–3118. https://doi.org/10.1021/bm800684b.

[88] D. Bogdal, P. Penczek, J. Pielichowski, A. Prociak, Microwave Assisted Synthesis, Crosslinking, and Processing of Polymeric Materials, in: 2003: pp. 194–263. https://doi.org/10.1007/b11051.

[89] R. Hoogenboom, U.S. Schubert, Microwave-Assisted Polymer Synthesis: Recent Developments in a Rapidly Expanding Field of Research, Macromol. Rapid Commun. 28 (2007) 368–386. https://doi.org/10.1002/marc.200600749.

[90] S. Sinnwell, H. Ritter, Recent Advances in Microwave-Assisted Polymer Synthesis, Aust. J. Chem. 60 (2007) 729. https://doi.org/10.1071/CH07219.

[91] V. Polshettiwar, R.S. Varma, eds., Aqueous Microwave Assisted Chemistry, Royal Society of Chemistry, Cambridge, 2010. https://doi.org/10.1039/9781849730990.

[92] S.L. Brown, C.M. Rayner, S. Graham, A. Cooper, S. Rannard, S. Perrier, Ultra-fast microwave enhanced reversible addition-fragmentation chain transfer (RAFT) polymerization: monomers to polymers in minutes, Chem. Commun. (2007) 2145. https://doi.org/10.1039/b703386a.

[93] S.L. Brown, C.M. Rayner, S. Perrier, Microwave-Accelerated RAFT Polymerization of

Polar Monomers, Macromol. Rapid Commun. 28 (2007) 478–483. https://doi.org/10.1002/marc.200600755.

[94] Z. An, Q. Shi, W. Tang, C.-K. Tsung, C.J. Hawker, G.D. Stucky, Facile RAFT Precipitation Polymerization for the Microwave-Assisted Synthesis of Well-Defined, Double Hydrophilic Block Copolymers and Nanostructured Hydrogels, J. Am. Chem. Soc. 129 (2007) 14493–14499. https://doi.org/10.1021/ja0756974.

[95] Y. Assem, A. Greiner, S. Agarwal, Microwave-Assisted Controlled Ring-Closing Cyclopolymerization of Diallyldimethylammonium Chloride Via the RAFT Process, Macromol. Rapid Commun. 28 (2007) 1923–1928. https://doi.org/10.1002/marc.200700377.

[96] C.T. Nguyen, Q.D. Nghiem, D.-P. Kim, J. San Chang, Y.K. Hwang, Microwave assisted synthesis of high molecular weight polyvinylsilazane via RAFT process, Polymer (Guildf). 50 (2009) 5037–5041. https://doi.org/10.1016/j.polymer.2009.08.035.

[97] K. Ulbrich, V. Šubr, J. Strohalm, D. Plocová, M. Jelínková, B. Říhová, Polymeric drugs based on conjugates of synthetic and natural macromolecules, J. Control. Release. 64 (2000) 63–79. https://doi.org/10.1016/S0168-3659(99)00141-8.

[98] Z. Xu, K. Zhang, C. Hou, D. Wang, X. Liu, X. Guan, X. Zhang, H. Zhang, A novel nanoassembled doxorubicin prodrug with a high drug loading for anticancer drug delivery, J. Mater. Chem. B. 2 (2014) 3433–3437. https://doi.org/10.1039/C4TB00128A.

[99] M. Danial, S. Telwatte, D. Tyssen, S. Cosson, G. Tachedjian, G. Moad, A. Postma, Combination anti-HIV therapy via tandem release of prodrugs from macromolecular carriers, Polym. Chem. 7 (2016) 7477–7487. https://doi.org/10.1039/C6PY01882C.

[100] M.E. Fox, F.C. Szoka, J.M.J. Fréchet, Soluble Polymer Carriers for the Treatment of Cancer: The Importance of Molecular Architecture, Acc. Chem. Res. 42 (2009) 1141–1151. https://doi.org/10.1021/ar900035f.

[101] X. Pan, F. Zhang, B. Choi, Y. Luo, X. Guo, A. Feng, S.H. Thang, Effect of solvents on the RAFT polymerization of N-(2-hydroxypropyl) methacrylamide, Eur. Polym. J. 115 (2019) 166–172. https://doi.org/10.1016/j.eurpolymj.2019.03.016.

[102] D. Dallinger, C.O. Kappe, Microwave-Assisted Synthesis in Water as Solvent, Chem. Rev. 107 (2007) 2563–2591. https://doi.org/10.1021/cr0509410.

[103] W.L.A. Brooks, B.S. Sumerlin, Microwave-Assisted RAFT Polymerization, Isr. J. Chem. 52 (2012) 256–263. https://doi.org/10.1002/ijch.201100140.

[104] J. Arredondo, P. Champagne, M.F. Cunningham, RAFT-mediated polymerisation of dialkylaminoethyl methacrylates in tert -butanol, Polym. Chem. 10 (2019) 1938–1946. https://doi.org/10.1039/C8PY01803K.

[105] S. Perrier, 50th Anniversary Perspective : RAFT Polymerization—A User Guide, Macromolecules. 50 (2017) 7433–7447. https://doi.org/10.1021/acs.macromol.7b00767.

[106] M. Lobert, R. Hoogenboom, C.-A. Fustin, J.-F. Gohy, U.S. Schubert, Amphiphilic gradient copolymers containing fluorinated 2-phenyl-2-oxazolines: Microwave-assisted one-pot

synthesis and self-assembly in water, J. Polym. Sci. Part A Polym. Chem. 46 (2008) 5859–5868. https://doi.org/10.1002/pola.22901.

[107] C. Guerrero-Sanchez, M. Lobert, R. Hoogenboom, U.S. Schubert, Microwave-Assisted Homogeneous Polymerizations in Water-Soluble Ionic Liquids: An Alternative and Green Approach for Polymer Synthesis, Macromol. Rapid Commun. 28 (2007) 456–464. https://doi.org/10.1002/marc.200600728.

[108] D.B. Thomas, A.J. Convertine, R.D. Hester, A.B. Lowe, C.L. McCormick, Hydrolytic Susceptibility of Dithioester Chain Transfer Agents and Implications in Aqueous RAFT Polymerizations, Macromolecules. 37 (2004) 1735–1741. https://doi.org/10.1021/ma035572t.

[109] A.W. York, Y. Zhang, A.C. Holley, Y. Guo, F. Huang, C.L. McCormick, Facile Synthesis of Multivalent Folate-Block Copolymer Conjugates via Aqueous RAFT Polymerization: Targeted Delivery of siRNA and Subsequent Gene Suppression, Biomacromolecules. 10 (2009) 936–943. https://doi.org/10.1021/bm8014768.

[110] L. Kostka, L. Kotrchová, V. Šubr, A. Libánská, C.A. Ferreira, I. Malátová, H.J. Lee, T.E. Barnhart, J.W. Engle, W. Cai, M. Šírová, T. Etrych, HPMA-based star polymer biomaterials with tuneable structure and biodegradability tailored for advanced drug delivery to solid tumours, Biomaterials. 235 (2020) 119728. https://doi.org/10.1016/j.biomaterials.2019.119728.

[111] T. Etrych, M. Šírová, L. Starovoytova, B. Říhová, K. Ulbrich, HPMA Copolymer Conjugates of Paclitaxel and Docetaxel with pH-Controlled Drug Release, Mol. Pharm. 7 (2010) 1015–1026. https://doi.org/10.1021/mp100119f.

[112] F.C. Giacomelli, P. Stepánek, C. Giacomelli, V. Schmidt, E. Jäger, A. Jäger, K. Ulbrich, pH-triggered block copolymer micelles based on a pH-responsive PDPA (poly[2-(diisopropylamino)ethyl methacrylate]) inner core and a PEO (poly(ethylene oxide)) outer shell as a potential tool for the cancer therapy, Soft Matter. 7 (2011) 9316. https://doi.org/10.1039/c1sm05992k.

[113] Y. Wang, K. Zhou, G. Huang, C. Hensley, X. Huang, X. Ma, T. Zhao, B.D. Sumer, R.J. DeBerardinis, J. Gao, A nanoparticle-based strategy for the imaging of a broad range of tumours by nonlinear amplification of microenvironment signals, Nat. Mater. 13 (2014) 204–212. https://doi.org/10.1038/nmat3819.

[114] Y. Li, T. Zhao, C. Wang, Z. Lin, G. Huang, B.D. Sumer, J. Gao, Molecular basis of cooperativity in pH-triggered supramolecular self-assembly, Nat. Commun. 7 (2016) 13214. https://doi.org/10.1038/ncomms13214.

[115] C. Giacomelli, L. Le Men, R. Borsali, J. Lai-Kee-Him, A. Brisson, S.P. Armes, A.L. Lewis, Phosphorylcholine-Based pH-Responsive Diblock Copolymer Micelles as Drug Delivery Vehicles: Light Scattering, Electron Microscopy, and Fluorescence Experiments, Biomacromolecules. 7 (2006) 817–828. https://doi.org/10.1021/bm0508921.

[116] J.U. Izunobi, C.L. Higginbotham, Polymer Molecular Weight Analysis by 1 H NMR Spectroscopy, J. Chem. Educ. 88 (2011) 1098–1104. https://doi.org/10.1021/ed100461v.

[117] R.L. Siegel, K.D. Miller, A. Jemal, Cancer statistics, 2019, CA. Cancer J. Clin. 69 (2019) 7–34. https://doi.org/10.3322/caac.21551.

[118] Yamauchi, Camptothecin induces DNA strand breaks and is cytotoxic in stimulated normal lymphocytes, Oncol. Rep. 25 (2011). https://doi.org/10.3892/or.2010.1100.

[119] T. Rupp, D. Zuckerman, Quality of Life, Overall Survival, and Costs of Cancer Drugs Approved Based on Surrogate Endpoints, JAMA Intern. Med. 177 (2017) 276. https://doi.org/10.1001/jamainternmed.2016.7761.

[120] S. Turakhia, C.D. Venkatakrishnan, K. Dunsmore, H. Wong, P. Kuppusamy, J.L. Zweier, G. Ilangovan, Doxorubicin-induced cardiotoxicity: direct correlation of cardiac fibroblast and H9c2 cell survival and aconitase activity with heat shock protein 27, Am. J. Physiol. Circ. Physiol. 293 (2007) H3111–H3121. https://doi.org/10.1152/ajpheart.00328.2007.

[121] L. Simón-Gracia, H. Hunt, P.D. Scodeller, J. Gaitzsch, G.B. Braun, A.-M.A. Willmore, E. Ruoslahti, G. Battaglia, T. Teesalu, Paclitaxel-Loaded Polymersomes for Enhanced Intraperitoneal Chemotherapy, Mol. Cancer Ther. 15 (2016) 670–679. https://doi.org/10.1158/1535-7163.MCT-15-0713-T.

[122] L. Guan, L. Rizzello, G. Battaglia, Polymersomes and their applications in cancer delivery and therapy, Nanomedicine. 10 (2015) 2757–2780. https://doi.org/10.2217/nnm.15.110.

[123] K.K. Upadhyay, A.K. Mishra, K. Chuttani, A. Kaul, C. Schatz, J.-F. Le Meins, A. Misra, S. Lecommandoux, The in vivo behavior and antitumor activity of doxorubicin-loaded poly(γ-benzyl l-glutamate)-block-hyaluronan polymersomes in Ehrlich ascites tumor-bearing BalB/c mice, Nanomedicine Nanotechnology, Biol. Med. 8 (2012) 71–80. https://doi.org/10.1016/j.nano.2011.05.008.

[124] C. Corbet, O. Feron, Tumour acidosis: from the passenger to the driver's seat, Nat. Rev. Cancer. 17 (2017) 577–593. https://doi.org/10.1038/nrc.2017.77.

[125] B.A. Webb, M. Chimenti, M.P. Jacobson, D.L. Barber, Dysregulated pH: a perfect storm for cancer progression, Nat. Rev. Cancer. 11 (2011) 671–677. https://doi.org/10.1038/nrc3110.

[126] L.W. Seymour, R. Duncan, J. Strohalm, J. Kope?ek, Effect of molecular weight (M_w) ofN-(2-hydroxypropyl)methacrylamide copolymers on body distribution and rate of excretion after subcutaneous, intraperitoneal, and intravenous administration to rats, J. Biomed. Mater. Res. 21 (1987) 1341–1358. https://doi.org/10.1002/jbm.820211106.

[127] P.H. Kierstead, H. Okochi, V.J. Venditto, T.C. Chuong, S. Kivimae, J.M.J. Fréchet, F.C. Szoka, The effect of polymer backbone chemistry on the induction of the accelerated blood clearance in polymer modified liposomes, J. Control. Release. 213 (2015) 1–9. https://doi.org/10.1016/j.jconrel.2015.06.023.

[128] L. Brown, S.L. McArthur, P.C. Wright, A. Lewis, G. Battaglia, Polymersome production on a microfluidic platform using pH sensitive block copolymers, Lab Chip. 10 (2010) 1922. https://doi.org/10.1039/c004036c.

[129] J. Xu, S. Zhang, A. Machado, S. Lecommandoux, O. Sandre, F. Gu, A. Colin, Controllable Microfluidic Production of Drug-Loaded PLGA Nanoparticles Using Partially Water-

Miscible Mixed Solvent Microdroplets as a Precursor, Sci. Rep. 7 (2017) 4794. https://doi.org/10.1038/s41598-017-05184-5.

[130] G. Li, H. Zheng, R. Bai, A Facile Strategy for the Preparation of Azide Polymers via Room Temperature RAFT Polymerization by Redox Initiation, Macromol. Rapid Commun. 30 (2009) 442–447. https://doi.org/10.1002/marc.200800666.

[131] V. Ladmiral, T.M. Legge, Y. Zhao, S. Perrier, "Click" Chemistry and Radical Polymerization: Potential Loss of Orthogonality, Macromolecules. 41 (2008) 6728–6732. https://doi.org/10.1021/ma8010262.

[132] P. V. Mendonça, A.C. Serra, A. V. Popov, T. Guliashvili, J.F.J. Coelho, Efficient RAFT polymerization of N-(3-aminopropyl)methacrylamide hydrochloride using unprotected "clickable" chain transfer agents, React. Funct. Polym. 81 (2014) 1–7. https://doi.org/10.1016/j.reactfunctpolym.2014.04.001.

[133] Chapter 2. Heat of Polymerization, J. Macromol. Sci. Part C Polym. Rev. 3 (1969) 339–356. https://doi.org/10.1080/15583726908545927.

[134] D. Quémener, T.P. Davis, C. Barner-Kowollik, M.H. Stenzel, RAFT and click chemistry: A versatile approach to well-defined block copolymers, Chem. Commun. (2006) 5051–5053. https://doi.org/10.1039/B611224B.

[135] L. Guan, L. Rizzello, G. Battaglia, Polymersomes and their applications in cancer delivery and therapy, Nanomedicine. 10 (2015) 2757–2780. https://doi.org/10.2217/nnm.15.110.

[136] C. LoPresti, H. Lomas, M. Massignani, T. Smart, G. Battaglia, Polymersomes: nature inspired nanometer sized compartments, J. Mater. Chem. 19 (2009) 3576. https://doi.org/10.1039/b818869f.

[137] J. Fang, H. Nakamura, H. Maeda, The EPR effect: Unique features of tumor blood vessels for drug delivery, factors involved, and limitations and augmentation of the effect, Adv. Drug Deliv. Rev. 63 (2011) 136–151. https://doi.org/10.1016/j.addr.2010.04.009.

[138] A. Nel, E. Ruoslahti, H. Meng, New Insights into "Permeability" as in the Enhanced Permeability and Retention Effect of Cancer Nanotherapeutics, ACS Nano. 11 (2017) 9567–9569. https://doi.org/10.1021/acsnano.7b07214.

[139] J.S. Lee, M. Ankone, E. Pieters, R.M. Schiffelers, W.E. Hennink, J. Feijen, Circulation kinetics and biodistribution of dual-labeled polymersomes with modulated surface charge in tumor-bearing mice: Comparison with stealth liposomes, J. Control. Release. 155 (2011) 282–288. https://doi.org/10.1016/j.jconrel.2011.07.028.

[140] X. Li, D.J. Hirsh, D. Cabral-Lilly, A. Zirkel, S.M. Gruner, A.S. Janoff, W.R. Perkins, Doxorubicin physical state in solution and inside liposomes loaded via a pH gradient, Biochim. Biophys. Acta - Biomembr. 1415 (1998) 23–40. https://doi.org/10.1016/S0005-2736(98)00175-8.

[141] P.P. Wibroe, D. Ahmadvand, M.A. Oghabian, A. Yaghmur, S.M. Moghimi, An integrated assessment of morphology, size, and complement activation of the PEGylated liposomal doxorubicin products Doxil®, Caelyx®, DOXOrubicin, and SinaDoxosome, J. Control. Release. 221 (2016) 1–8. https://doi.org/10.1016/j.jconrel.2015.11.021.

[142] C. Cui, Y.-N. Xue, M. Wu, Y. Zhang, P. Yu, L. Liu, R.-X. Zhuo, S.-W. Huang, Cellular uptake, intracellular trafficking, and antitumor efficacy of doxorubicin-loaded reduction-sensitive micelles, Biomaterials. 34 (2013) 3858–3869. https://doi.org/10.1016/j.biomaterials.2013.01.101.

[143] W.Y. Ayen, N. Kumar, In Vivo Evaluation of Doxorubicin-Loaded (PEG)3-PLA Nanopolymersomes (PolyDoxSome) Using DMBA-Induced Mammary Carcinoma Rat Model and Comparison with Marketed LipoDox™, Pharm. Res. 29 (2012) 2522–2533. https://doi.org/10.1007/s11095-012-0783-8.

[144] S.E. AL-HARTHI, O.M. ALARABI, W.S. RAMADAN, M.N. ALAAMA, H.M. AL-KREATHY, Z.A. DAMANHOURI, L.M. KHAN, A.-M.M. OSMAN, Amelioration of doxorubicin-induced cardiotoxicity by resveratrol, Mol. Med. Rep. 10 (2014) 1455–1460. https://doi.org/10.3892/mmr.2014.2384.

[145] K. Yang, S. Zhang, G. Zhang, X. Sun, S.-T. Lee, Z. Liu, Graphene in Mice: Ultrahigh In Vivo Tumor Uptake and Efficient Photothermal Therapy, Nano Lett. 10 (2010) 3318–3323. https://doi.org/10.1021/nl100996u.

[146] J. van Asperen, O. van Tellingen, F. Tijssen, A.H. Schinkel, J.H. Beijnen, Increased accumulation of doxorubicin and doxorubicinol in cardiac tissue of mice lacking mdr1a P-glycoprotein, Br. J. Cancer. 79 (1999) 108–113. https://doi.org/10.1038/sj.bjc.6690019.

[147] G. Wang, R.M. de Kruijff, D. Abou, N. Ramos, E. Mendes, L.E. Franken, H.T. Wolterbeek, A.G. Denkova, Pharmacokinetics of Polymersomes Composed of Poly(Butadiene-Ethylene Oxide); Healthy versus Tumor-Bearing Mice, J. Biomed. Nanotechnol. 12 (2016) 320–328. https://doi.org/10.1166/jbn.2016.2178.

[148] J.P. Jain, M. Jatana, A. Chakrabarti, N. Kumar, Amphotericin-B-Loaded Polymersomes Formulation (PAMBO) Based on (PEG) 3 -PLA Copolymers: An in Vivo Evaluation in a Murine Model, Mol. Pharm. 8 (2011) 204–212. https://doi.org/10.1021/mp100267k.

[149] J.S. Lee, J. Feijen, Polymersomes for drug delivery: Design, formation and characterization, J. Control. Release. 161 (2012) 473–483. https://doi.org/10.1016/j.jconrel.2011.10.005.

[150] F. Ahmed, R.I. Pakunlu, A. Brannan, F. Bates, T. Minko, D.E. Discher, Biodegradable polymersomes loaded with both paclitaxel and doxorubicin permeate and shrink tumors, inducing apoptosis in proportion to accumulated drug, J. Control. Release. 116 (2006) 150–158. https://doi.org/10.1016/j.jconrel.2006.07.012.

[151] A. Minelli, I. Bellezza, C. Conte, Z. Culig, Oxidative stress-related aging: A role for prostate cancer?, Biochim. Biophys. Acta - Rev. Cancer. 1795 (2009) 83–91. https://doi.org/10.1016/j.bbcan.2008.11.001.

[152] J.T. Hancock, R. Desikan, S.J. Neill, Role of reactive oxygen species in cell signalling pathways, Biochem. Soc. Trans. 29 (2001) 345. https://doi.org/10.1042/0300-5127:0290345.

[153] B. D'Autréaux, M.B. Toledano, ROS as signalling molecules: mechanisms that generate specificity in ROS homeostasis, Nat. Rev. Mol. Cell Biol. 8 (2007) 813–824. https://doi.org/10.1038/nrm2256.

[154] T. Thambi, J.H. Park, D.S. Lee, Stimuli-responsive polymersomes for cancer therapy, Biomater. Sci. 4 (2016) 55–69. https://doi.org/10.1039/C5BM00268K.

[155] W. Tao, Y. Liu, B. Jiang, S. Yu, W. Huang, Y. Zhou, D. Yan, A Linear-Hyperbranched Supramolecular Amphiphile and Its Self-Assembly into Vesicles with Great Ductility, J. Am. Chem. Soc. 134 (2012) 762–764. https://doi.org/10.1021/ja207924w.

[156] W. Zhao, Lighting up H 2 O 2 : The Molecule that Is a "Necessary Evil" in the Cell, Angew. Chemie Int. Ed. 48 (2009) 3022–3024. https://doi.org/10.1002/anie.200805651.

[157] B.C. Dickinson, C.J. Chang, A Targetable Fluorescent Probe for Imaging Hydrogen Peroxide in the Mitochondria of Living Cells, J. Am. Chem. Soc. 130 (2008) 9638–9639. https://doi.org/10.1021/ja802355u.

[158] V.S. Lin, B.C. Dickinson, C.J. Chang, Boronate-Based Fluorescent Probes, in: 2013: pp. 19–43. https://doi.org/10.1016/B978-0-12-405883-5.00002-8.

[159] C. de Gracia Lux, S. Joshi-Barr, T. Nguyen, E. Mahmoud, E. Schopf, N. Fomina, A. Almutairi, Biocompatible Polymeric Nanoparticles Degrade and Release Cargo in Response to Biologically Relevant Levels of Hydrogen Peroxide, J. Am. Chem. Soc. 134 (2012) 15758–15764. https://doi.org/10.1021/ja303372u.

[160] C. Wang, J. Wang, X. Zhang, S. Yu, D. Wen, Q. Hu, Y. Ye, H. Bomba, X. Hu, Z. Liu, G. Dotti, Z. Gu, In situ formed reactive oxygen species–responsive scaffold with gemcitabine and checkpoint inhibitor for combination therapy, Sci. Transl. Med. 10 (2018). https://doi.org/10.1126/scitranslmed.aan3682.

[161] X. Liang, J. Duan, X. Li, X. Zhu, Y. Chen, X. Wang, H. Sun, D. Kong, C. Li, J. Yang, Improved vaccine-induced immune responses via a ROS-triggered nanoparticle-based antigen delivery system, Nanoscale. 10 (2018) 9489–9503. https://doi.org/10.1039/C8NR00355F.

[162] C. Schatz, S. Louguet, J.-F. Le Meins, S. Lecommandoux, Polysaccharide- block - polypeptide Copolymer Vesicles: Towards Synthetic Viral Capsids, Angew. Chemie Int. Ed. 48 (2009) 2572–2575. https://doi.org/10.1002/anie.200805895.

[163] H. Che, S. Cao, J.C.M. van Hest, Feedback-Induced Temporal Control of "Breathing" Polymersomes To Create Self-Adaptive Nanoreactors, J. Am. Chem. Soc. 140 (2018) 5356–5359. https://doi.org/10.1021/jacs.8b02387.

[164] C.E. de Castro, B. Mattei, K.A. Riske, E. Jäger, A. Jäger, P. Stepánek, F.C. Giacomelli, Understanding the Structural Parameters of Biocompatible Nanoparticles Dictating Protein Fouling, Langmuir. 30 (2014) 9770–9779. https://doi.org/10.1021/la502179f.

[165] E. Jäger, A. Höcherl, O. Janoušková, A. Jäger, M. Hrubý, R. Konefał, M. Netopilik, J. Pánek, M. Šlouf, K. Ulbrich, P. Štěpánek, Fluorescent boronate-based polymer nanoparticles with reactive oxygen species (ROS)-triggered cargo release for drug-delivery applications, Nanoscale. 8 (2016) 6958–6963. https://doi.org/10.1039/C6NR00791K.

[166] X. Hu, S. Liu, Y. Huang, X. Chen, X. Jing, Biodegradable Block Copolymer-Doxorubicin Conjugates via Different Linkages: Preparation, Characterization, and In Vitro Evaluation, Biomacromolecules. 11 (2010) 2094–2102. https://doi.org/10.1021/bm100458n.

[167] J. Thiele, A.R. Abate, H.C. Shum, S. Bachtler, S. Förster, D.A. Weitz, Fabrication of Polymersomes using Double-Emulsion Templates in Glass-Coated Stamped Microfluidic Devices, Small. 6 (2010) 1723–1727. https://doi.org/10.1002/smll.201000798.

[168] E. Rideau, R. Dimova, P. Schwille, F.R. Wurm, K. Landfester, Liposomes and polymersomes: a comparative review towards cell mimicking, Chem. Soc. Rev. 47 (2018) 8572–8610. https://doi.org/10.1039/C8CS00162F.

[169] D.E. Discher, A. Eisenberg, Polymer Vesicles, Science (80-.). 297 (2002) 967–973. https://doi.org/10.1126/science.1074972.

[170] K. Kita-Tokarczyk, J. Grumelard, T. Haefele, W. Meier, Block copolymer vesicles—using concepts from polymer chemistry to mimic biomembranes, Polymer (Guildf). 46 (2005) 3540–3563. https://doi.org/10.1016/j.polymer.2005.02.083.

[171] J.N. Lee, C. Park, G.M. Whitesides, Solvent Compatibility of Poly(dimethylsiloxane)-Based Microfluidic Devices, Anal. Chem. 75 (2003) 6544–6554. https://doi.org/10.1021/ac0346712.

[172] M. Aymerich, A. Gómez-Varela, E. Álvarez, M. Flores-Arias, Study of Different Sol-Gel Coatings to Enhance the Lifetime of PDMS Devices: Evaluation of Their Biocompatibility, Materials (Basel). 9 (2016) 728. https://doi.org/10.3390/ma9090728.

[173] T. Trantidou, Y. Elani, E. Parsons, O. Ces, Hydrophilic surface modification of PDMS for droplet microfluidics using a simple, quick, and robust method via PVA deposition, Microsystems Nanoeng. 3 (2017) 16091. https://doi.org/10.1038/micronano.2016.91.

[174] S. Deshpande, Y. Caspi, A.E.C. Meijering, C. Dekker, Octanol-assisted liposome assembly on chip, Nat. Commun. 7 (2016) 10447. https://doi.org/10.1038/ncomms10447.

[175] H.P. Long, C.C. Lai, C.K. Chung, Polyethylene glycol coating for hydrophilicity enhancement of polydimethylsiloxane self-driven microfluidic chip, Surf. Coatings Technol. 320 (2017) 315–319. https://doi.org/10.1016/j.surfcoat.2016.12.059.

[176] J.H.L. Beal, A. Bubendorfer, T. Kemmitt, I. Hoek, W. Mike Arnold, A rapid, inexpensive surface treatment for enhanced functionality of polydimethylsiloxane microfluidic channels, Biomicrofluidics. 6 (2012) 036503. https://doi.org/10.1063/1.4740232.